STEP INDUCED SEPARATION OF A TURBULENT BOUNDARY LAYER

PART I. EXPERIMENTS IN SUPERSONIC FLOW

PART II. A MODEL FOR INCOMPRESSIBLE FLOW IN A CHANNEL

Thesis by

Robert Lee Gran

In Partial Fulfillment of the Requirements

For the Degree of

Doctor of Philosophy

California Institute of Technology

Pasadena, California

1970

(Submitted December 9, 1969)

ACKNOWLEDGMENTS

In addition to the appreciation due to the fellow students and faculty with whom the author has had contact here at the California Institute of Technology, the author is especially grateful to:

the National Science Foundation and the California Institute of Technology who provided financial support during the course of the author's graduate study;

the staff of the Aeronautics department machine shop, especially Messrs. G. Carlson and E. Dahl, for their invaluable assistance in fabricating the experimental apparatus;

Messrs. S. Roman, J. Van Dijk, P. Baloga and the staff of the Hydrodynamics Laboratory for their assistance in conducting the experiments;

Mrs. Virginia Conner for her excellent and tireless typing of this manuscript; and

Professor Wilhelm Behrens for his patient assistance in the acquisition of some of the data.

The author would also like to thank Professors Edward Zukoski and Toshi Kubota who have provided the stimulation, direction and discussion necessary for the completion of this work.

In recognition of their forebearance and encouragement throughout these difficult years and without which it may not have been possible, this thesis is dedicated to my wife, Jean and my children, Jerri and John.

ABSTRACT

This thesis is concerned with the separation of a two-dimensional turbulent boundary layer caused by a forward facing step. The two major flow regimes considered here are in the realms of supersonic flow and incompressible flow in a channel.

For the case of supersonic turbulent boundary layer separation, a series of experiments were conducted. The upstream pressure field for step sizes in the range from 5% to 150% of the local boundary layer thickness was determined and correlated with "large" step data. The separated shear layer was found to be approaching a constant pressure and self-similar flow in a distance of around 6-10 initial boundary layer thicknesses. Fluctuation measurements were conducted near the similar flow region. In addition, the low-frequency unsteady behavior associated with the separation phenomenon was examined and is presumed to be caused by a standing wave acoustic in the subsonic separated region.

For the incompressible flow over a step in a channel, an inviscid model utilizing free streamline theory and based on experimental observations was constructed and solved with the aim of predicting the upstream flow field. Although the solution is not in "closed form" (two experimental parameters are required) it does show that the far upstream pressure field is predominately fixed by the flow geometry as opposed to viscous effects such as the Reynolds number or step height-to-boundary layer thickness ratio. Close to the step these effects do, however, become important and are unaccounted for here. The effect of finite blockage ratio (step height-to-channel height ratio) is shown to be substantial for quite modest values (greater than 2%). The precise

values of the two experimental parameters are not required for accurate prediction of the upstream influence.

TABLE OF CONTENTS

TABLE OF CONTENTS (Cont'd)

PART I. EXPERIMENTS IN SUPERSONIC FLOW

List of Figures - Part I

List of Figures - Part I (Cont.)

List of Symbols - Part I

a	local speed of sound $\equiv \sqrt{\gamma RT}$, or $k_w/k_T(\ell/d)^2$
a_1	Mach number parameter $\equiv 1 + \frac{\gamma-1}{2} M^2$
b	$\equiv Nu_T - \frac{i^2 r_r \alpha_r}{\pi \bar{k}_T}$
c	$\equiv \frac{i^2 r_r}{\pi k_T \bar{\eta} \bar{T}_r} [1 + \alpha_r(\eta T_T - T_r)]$
C_1, C_2	constants defined in Appendix I-A
$C(f)$	compensating amplifier gain
C_f	local skin friction coefficient $\equiv \tau_w / \frac{1}{2} \rho_e u_e^2$
C_p	specific heat at constant pressure
C_v	specific heat at constant volume
d	hot-wire diameter or $\overline{Nu}_T$-b
e	hot-wire output voltage
E	amplifier output voltage
f	frequency
f^*	reduced frequency
F	function defined in section I. 5. 1
$G(f)$	hot-wire amplifier frequency response
G_0	zero frequency gain of hot-wire amplifier
h	heat transfer coefficient
i	hot-wire current or $\sqrt{-1}$
k	thermal conductivity or derivative of wire resistance with respect to Joule heating
K	characteristic time $\equiv \frac{\rho_w c_w d^2}{4 \bar{k}_T}$
ℓ	hot-wire length

L	length of separated cavity
$L(x)$	similarity scale length
m	$\partial(\ell n k)/\partial \ell n\, T$ for air ($m \approx .786$ at 300°K)
M	Local Mach number = u/a
M_A	compensating amplifier time constant
M_t	hot-wire time constant
n	$\partial(\ell n\, \mu)/\partial \ell n\, T$; for air @300°K $n \approx 0.665$
Nu	Nusselt Number
p	pressure
Δp	difference in static pressure
$\dot{q}$	heat transfer rate
r, r^*	sensitivity ratio or resistance of hot-wire per unit length
R	Correlation coefficient
R_M	measured wire resistance
Re	Reynolds number
S_α	fluctuations in subscripted quantity
t	time
T	temperature
u, v, w	fluid velocity
x, y, z	orthogonal coordinate system
x_0	beginning of interaction region
α	$\left[\frac{Nu_T\, k_T}{k_w} - \frac{i^2 r_r \alpha_r}{\pi k_w}\right]\left(\frac{\ell}{d}\right)^2 = b/a$
γ	ratio of specific heats $\equiv C_p/C_v$
δ	local shear layer thickness
δ_D	distance from wall to dividing streamline

δ^* displacement thickness of shear layer

η recovery factor $\equiv T_{aw}/T_T$

θ momentum thickness of shear layer

Θ virtual ideal hot-wire output

μ fluid viscosity

π non-dimensional pressure $\equiv \frac{1}{\gamma}(p-p_0)/p_0$

ρ fluid density

σ non-dimensional entropy $\equiv (s-s_0)/C_p$

τ wire overheat parameter $\equiv (T_w-T_{aw})/T_{aw}$

τ_T non-dimensional temperature $= T/T_T$

τ_w wall shear stress

Subscripts

a adiabatic condition

e local edge value

i ideal (massless) wire output

m measured value

o free stream or conditions ahead of interaction

p plateau value

r reference quantity

s wire support

T total or stagnation condition

w wire

Superscripts

$*$ dividing streamline value or non-dimensional quantity

$(\tilde{\ })$ root-mean-square value

$(\bar{\ })$	average value with respect to time
$(\ )'$	instantaneous fluctuating value

I. 1 Introduction

One of the major areas of present-day research in the fluid mechanics of compressible turbulent boundary layers is that flow regime where there is a strong interaction between the boundary layer and the outer inviscid portion of the flow. The term strong interaction is taken here to mean that the outer flow cannot be computed, even to lowest order, by neglect of the turbulent boundary layer. A typical example of this type of interaction is afforded by the separation of the boundary layer caused either by convex surfaces such as exist at the base region of a body or due to an adverse pressure gradient caused by an impinging shock wave or surface mounted obstacle.

The usual situation encountered by the engineer in the design of structures in contact with supersonic flows is how to predict or prevent separation due to its generally adverse effects. For instance, at high angles of attack, airfoils tend to "stall" which markedly affects their lift and drag characteristics. Also, in overexpanded rocket nozzles the turbulent boundary layer can separate resulting in uncontrolled thrust vectoring. The effects of separation need not always be adverse as evidenced by the use of spoilers or injected streams for controlled thrust vectoring and the applications of fluidic devices which depend to some extent on separation for their success.

In any situation where separation might occur, the designer would like to be able to predict its occurrence and its effects such as extent of the region and the changes in surface pressures and heat transfer rates so as to more efficiently design his product.

The subject of this paper, the separation of a supersonic turbulent boundary layer caused by a forward facing step, has received much attention over the past 15 years or so. The reason for this is because it has been shown that details near the separation point and within the separated region are relatively independent of the mechanism which causes it; this result is sometimes referred to as the "free-interaction" hypothesis.[1] Thus the flow field over the geometrically simple forward facing step is very much like that caused by, say, impinging shock waves or other wall mounted obstacles.

This subject has been extensively investigated for many years with particular attention paid to wall pressure distributions and photographic coverage of the flow field starting with the work of Chapman, Kuehn, and Larson[1] and continues to the present day. It is not the purpose of this thesis to give a detailed account of all this work inasmuch as this has already been completed,[35] and furthermore, the scaling parameters of the length of the interaction and pressure distribution are empirically well known from the recent review article by Zukoski.[16] In light of all this existing data, the question of what else can be learned from additional experiments naturally arises.

To begin with, the correlation of existing data in step induced separation has really only been done for step sizes at least 50% larger than the local undisturbed boundary layer thickness. Although some data for step sizes smaller than this does exist, it was felt that further experimental work would supplement this data and might permit the extension of the previously mentioned scaling parameters to the

smaller step size interaction.

The nonsteady pressure field associated with turbulent boundary layer separation has become more important in recent years because of the fact that structures are operated in flows with quite high dynamic pressures. This unsteady behavior was recognized many years ago,[1, 3] but not until recent times have any quantitative measurements been conducted. The recent interest in noise problems, both radiated away from flight vehicles and transmitted through to their interiors, has intensified research in this area along with the possibilities of structural fatigue failure.

To date, the existing experimental data in this regard has been aimed mostly at the measurement of fluctuating pressure levels[13, 14] and some measurement of the correlation distances and spectra.[15] The usefulness of this data is restricted, however, because the mechanism which causes these high fluctuating pressure levels is not well understood (typically, the R.M.S. pressure in a separated layer is 10 to 20 times that of a flat plate R. M. S pressure level[13]). One reason for this lack of understanding is that the effect of Mach number alone has been investigated, but as yet the effect of step height (or equivalently the length of the separated region) has not been studied. Thus, it was felt that an investigation of the effect of step height at a constant Mach number might provide the clue to the unsteady mechanism.

The third area of interest regarding supersonic turbulent boundary layer separation that has not received much attention is the detailed characteristics of the shear layer as to the development of both the velocity profile and the turbulent energy distribution. More

specifically, it was desired to assess the effect of the recirculating or reversed flow region on the development of the separated shear layer to a similarity type of behavior which was suspected first from the observed linear growth rates as seen in Schlieren photographs.

This is not an academic point, however, in light of the attempts to describe the turbulent separation problem from a theoretical standpoint.[21, 23] One feature of some of these solutions is that in some fashion the concept of similarity in the mean shear flow is used either directly as in the equivalent jet hypothesis,[21] or indirectly as in some of the integral methods. Thus it becomes important to determine first whether or not the separated shear layer ever becomes similar, and in the event that it does, to determine the extent of the transition distance for similarity to be achieved.

The purpose of this paper is to report on experimental investigations on the three aforementioned areas related to the separation of a supersonic turbulent boundary-layer caused by a forward facing step. Recapitulating, these areas are the wall pressure distribution for step sizes smaller than the local undisturbed boundary layer thickness, the measurement of the unsteady behavior associated with this phenomena leading to a model for the mechanism which causes it, and the approach of the separated shear layer to a conical or similar flow behavior.

I. 2 General Description of Experiments

I. 2. 1 Wind Tunnel Facilities

The experiments reported herein were all conducted in the Supersonic Wind Tunnel of the Graduate Aeronautical Laboratories, California Institute of Technology (GALCIT). The test section for this tunnel is 2 inches high by $2\frac{1}{2}$ inches wide and operates at a nominal free stream Mach number of 2. 6. All experiments were carried out with stagnation conditions of 74. 2 cm Hg (± 0. 5 cm) total pressure and 78°F (± 3°F) total temperature. The boundary layers on the tunnel wall and in the test section varied in thickness from about 0. 15 inch to 0. 23 inch depending on the distance from the throat, and they were tripped upstream of the throat to ensure that they would be turbulent. Verification that the boundary layers were turbulent was obtained from velocity profiles and from hot-wire fluctuation measurements.

The wind tunnel was run in a closed cycle mode with all air passed through a dryer of activated alumina to remove moisture which was reactivated after each day. Despite these efforts low humidity air could not be obtained, the lowest dew point reading being around 14°F as measured in the plenum chamber. Because of the moisture in the air, a condensation shock was always observed (by means of a Schlieren system) in the expanding portion of the nozzle and could be measured by means of static pressure orifices located in the nozzle. This condensation shock altered the stagnation conditions for the test section to a total pressure of about 64 cm Hg, a total temperature of around 80°F, and test section Mach No. of

2.46 ± 0.03. All test results reported here were obtained with a dew point of 14° F (± 4° F) although no marked changes in flow field could be detected when runs were made at higher dew points (30° F to 45° F) other than a higher static pressure level in the test section (up from 4.0 cm Hg. to 4.3 cm Hg.) and a slight reduction in test section Mach number.

Fluctuation measurements in free stream (to be described in Section I.4.5.3) showed that the tunnel free stream conditions are very steady and fluctuations in free stream are most likely due to very weak pressure waves radiated by the turbulent boundary layer although special precautions to damp upstream fluctuations in the plenum chamber were not made. Total temperature fluctuations were measured at 0.08% R.M.S. which is extremely low and in fact may be lower than can be accurately determined from the hot-wire set. The total temperature fluctuations are most likely due to variations caused by motion of the condensation shock. Mass flow per unit area fluctuations in the free stream were measured to be about 0.4%.

Heat transfer effects were considered negligible since the total temperature and wall temperatures were within 9° F of each other over operating periods of several hours as determined in an independent investigation by Sigal.[2] Total temperature measurements were not made in this series of experiments.

I.2.2 Models

The models employed in these tests were a series of forward facing normal steps ranging in thickness from 0.010 inch to 0.32 inch. All steps smaller than 0.18 inch spanned the width of the tunnel

and all steps were attached to the test section by means of two especially constructed bolts with very thin heads to reduce interference effects. For the larger steps (greater than 0.08 inch) reliefs were provided in the step to accomodate the bolt heads. The three largest steps (0.18, 0.24, and 0.32 inches) were 2 inches wide and were run both with and without splitter plates (see Figure I-1) to eliminate sidewall boundary layer interactions as much as possible. To prevent leakage under the step, vacuum grease was applied to the step bottom surface to seal the crack between step and wall.

The test section itself was constructed from a 1.2 inch thick aluminum block and 64 static pressure orifices were drilled in it over a distance of 3 inches along the centerline of the tunnel and at several locations in the transverse direction (for drawing and detail see Figure I-1). Mounting holes for the steps were provided at several locations so that the steps could be placed to avoid the impingement of various waves in the tunnel.

After operation of the tunnel for a period of about one hour an oil film could be seen quite clearly on the sidewalls and also a bead of oil near the separation point. The straightness of this oil bead was used to determine the uniformity of the flow. Generally, for the smaller steps (less than 0.18 inch) this oil line looked very straight over the middle half of the tunnel. Near the side walls interaction with the sidewall boundary layers could be seen but seemed to have little effect on the resultant flow. For larger steps (0.18 inch and larger) significant departures from two-dimensionality could be seen. It was for this reason that the splitter plates were constructed and their use

eliminated this three-dimensionality for the 0.18 inch step and the 0.24 inch step. The situation for the 0.32 inch step was even more aggravated and as a result only restricted data for this step is presented here. Moreover, with the 0.32 inch step the tunnel was very difficult to start and the resultant flow was visually unsteady and appeared on the verge of choking the tunnel.

I.2.3 Instrumentation

I.2.3.1 Pitot Tube and Static Pressure Tube

The Pitot probe and static pressure probe used in these experiments are shown in Figure I-2. The Pitot tube tip was constructed from 0.065 inch o.d. stainless steel tubing with a tip flattened and ground to 0.008 inch by 0.08 inch wide with an opening of approximately 0.004 inch. The rather sharp bends shown were fabricated to facilitate readings in front of the step. The tip was also bent up about 10° from the horizontal to account for the fact that the flow angle behind the shock wave was of this order. Measurements made with this probe and several others gave identical results.

The static pressure tube was fabricated from 0.043 inch o.d. stainless steel tubing with the tip sealed and sharpened to a cone of approximately 8° semi-vertex angle. Four 0.014 inch holes were drilled through the probe about 10 probe diameters from the end of the conical section. The static pressure probe was also inclined at about 12° from horizontal as with the Pitot tube. Stiffeners constructed from brass were soldered to the probe to eliminate vibration problems. An independent investigation by Igawa[26] showed that the effect of angle of attack for this probe was less than that of several

other designs considered. The angle of attack effect on the measured static pressure for this probe is shown in Figure I-2 along with a drawing of the probe.

The Pitot pressure and/or static pressure were measured using a Statham pressure transducer (PA-208TC-50084; 0-10 psia) which had a linear calibration. The probe position was determined from a 40-turn Helipot (Model E). The electrical outputs from both the pressure transducer and the Helipot were connected directly to a Mosely X-Y recorder and the drive rate of the probe was slow enough to eliminate pressure lags in the system. Due to the previously mentioned oil film, an electrical device for determining probe contact with the wall proved to be erratic but it was found that this could be determined visually to within ±0.005 inch by observing the probe and its reflection off of the test section surface.

I. 2. 3. 2. Wall Static Pressures

Wall static pressures were measured by means of a series of 64 static pressure taps drilled into the test section as shown in Figure I-1. The pressure taps were mostly 0.014 inch diameter for 0.030 inch depth where the hole opened up to 0.042 inch diameter. A series of 0.006 inch diameter pressure taps were also drilled in a small area. These pressures were measured by means of a mercury manometer which permitted a reading of ± 0.05 cm Hg. For the free stream static pressure level in the test section this corresponds to an error of less than 2%.

I. 2. 3. 3. Hot-Wire Instrumentation

The hot-wire probes employed in these tests were originally

fabricated by Fernandez[7] and were altered to suit the needs of the present experiment. To the probes were soldered 0.0001 inch Platinum, 10% Rhodium wires (manufactured by the Sigmund Cohn Corp.). The hot-wires generally were about 0.005 inch long resulting in a length to diameter ratio of about 50, several tests were conducted with 0.012 inch long wires to insure against end effect errors.

In the original set of experiments even longer wires were used (up to 0.025 inch), however with these it was noticed that a resonant oscillation occurred in the output spectrum and was always in the frequency band of interest (1-320 KC). These oscillations were most likely due to a phenomenon known as "strain-gaging,"[8] i.e. changes in wire resistance due to a fluctuating strain in the wire itself. This would give quite large errors in the measurement of total mean-square voltage output especially in regions of low signal as in the free stream. Standard methods of damping this vibration suggested by other authors[9, 10] could not be exploited because of the small length of wires used. The only other alternative then was to decrease the wire length which in turn increases the natural frequency of vibration. For the lengths of wire employed here, no noticeable oscillation occurred in the frequency band 1-500 KC.

The electronic instrumentation consisted of a Shapiro-Edwards constant current hot-wire anemometer set and has been described previously by Behrens.[11] Briefly, the hot-wire set consists of; a constant current supply capable of wire currents from 0 to 100 ma. and steady within 1% over eight hour periods, a bridge circuit for measuring the resistance of the wire plus lead cable accurate to

within 0.01 ohm, an amplifier capable of a zero frequency gain of up to 52,000 and includes a separate compensating amplifier that corrects for the attenuation of higher frequencies,[28] a 5:1 turn input transformer that permits a five fold gain in signal and has low noise, and finally a square wave generator that enables the hot-wire time constant to be measured and is valuable in calibration.

Auxilliary equipment used in conjunction with the hot-wire set included a Hewlett-Packard Oscilloscope, Model 120B, a Panoramic Ultra Sonic Wave Analyzer, a Ballantine True RMS Meter, a Hewlett-Packard Wave Analyzer, Model SB-76Z, a Philco Ford Intermittency Meter, Model ADP-11, a Tektronix split beam oscilloscope (Type 549), and a Monsanto frequency counter, Model 100A .

An exterior circuit was constructed and attached to the hot-wire set in order to measure the wire current and voltage drop across the lead line and wire. The current was determined by the voltage drop across a 10 ohm (1/20%) resistor and was measured by a Fairchild integrating digital voltmeter, Model 7100, along with the voltage drop across the lead line. The measurement of current was made to within 0.01 ma. (less than 0.1%) and voltage drop to within 0.1 mv. (less than 1%). This method was favored over using the bridge circuit because of convenience and a smaller effect on the circuit.

When it was desired to make quantitative fluctuation measurements it was learned that the hot-wire amplifier had not been accurately calibrated as to gain and frequency response. This was accomplished and the amplifier characteristics are shown in Figures I-29 and I-30.

The total mean square voltage was usually measured by means of a thermocouple circuit included in the hot-wire set or by employing the R. M. S. meter and was uncorrected for frequency response. The error introduced by this procedure should be small inasmuch as most of the fluctuation energy is in the range 0-300 KC and the frequency response is down only 30% at this frequency. The output from the thermocouple circuit was connected directly to a Mosely X-Y plotter along with probe position from the 40-turn Helipot.

I. 3 Data Reduction Procedures and Experimental Difficulties

1. 3. 1 Pitot Probe and Static Pressure Probe Measurements

Pitot tube data was reduced using the measured static pressure and the Rayleigh Pitot tube formula to calculate the resultant Mach number distribution. Corrections for Pitot tube angle of attack and local turbulence were not accounted for inasmuch as the error introduced from these effects is probably as large as that from Reynolds number effects and calibration limits on the pressure transducer. These Mach number profiles were then used to compute velocity profiles using the assumption that the shear flow is iso-energetic, i. e. the total temperature is constant throughout the whole flow field. Since both the tunnel and plenum were at room temperature this assumption is reasonable, although measurements were not made to verify this.

Integral properties could not be computed from the velocity profiles because detailed measurements in the recirculating region were not possible since the dynamic pressure is low and the turbulence level is quite high. For this reason also, the streamlines for the outer portion of the flow were computed by identifying a streamline in the inviscid flow (using oblique shock relations[27]) and integrating the local mass flux distribution, $\rho u/\rho_e u_e$, toward the wall.

For the measurement of static pressure, some interpretation of a typical traverse like that of Figure I-9 is necessary in order to explain the various interference problems. From the geometry of the static pressure probe (Figure I-2), it is seen that the measuring orifices are located about 0. 5 inch from the tip. As mentioned earlier, the probe was aligned with the separated flow to within 1°. During the

traverse, the tip of the probe would intersect the shock wave when sufficiently far from the wall, and this interaction would cause an abnormal reading of static pressure. This region of the traverse is indicated in the figure.

Upon bringing the probe closer to the edge of the shear layer, an increase in indicated static pressure above the mean level of about 0.3 cm Hg. was observed. This same phenomena was observed by Igawa[26] in a separate investigation as the probe approached a flat plate boundary layer. Discussion of this matter has led to the explanation that the weak compression wave from the tip was reflecting off of the turbulent interface and impinging on the orifice area. Rough geometrical construction has verified this behavior. Once the probe is immersed in the shear layer, the above described behavior disappears and the pressure level appears relatively constant. The fact that the static pressure as measured by the probe was about 5% lower than the wall static pressure was attributed to probe error inasmuch as this particular probe was not calibrated in a known free stream. In any event, the effect of this on the velocity profiles is very slight except quite near the wall where the Pitot tube data is suspect because of angle-of-attack errors.

I. 3. 2 Hot-Wire Measurements

I. 3. 2. 1 Qualitative Studies

For qualitative measurement of fluctuations the hot-wires were always operated at rather high currents (25-35 ma.). From the physical characteristics of the flow field and the wire the maximum allowable current was on the order of 42 ma. and this was incidentally verified with several of the longer wires, i. e. at currents of around

40-45 ma. the wires "burned out" or failed structurally due to high temperature. For shorter wires this never occurred because of the high energy loss to the probe tips. The reason why such high current levels were used even for qualitative measurement is that it was suspected that fluctuations in mass flow per unit area would be more intense than fluctuations in total temperature and a "hot" wire is relatively more sensitive to mass flow fluctuations than a "cold" wire. At zero current the wire is operating essentially as a recovery factor probe and is relatively insensitive to velocity and density fluctuations. As the wire temperature is increased through increased current, the sensitivity to mass flow fluctuations increases to around 40% of the sensitivity to total temperature fluctuations at around 35 ma.

It is also of interest to note that the qualitative data measured with the hot-wire was taken with a rather long wire ($\ell/d \approx 200$) and the "strain gaging" behavior noted earlier was readily apparent in the spectra in the same manner as depicted by Demetriades.[8] Because of the fact that measurements of the fluctuation modes (i. e. velocity, density, total temperature, etc.) was desired, considerably shorter wires ($\ell/d \sim 50\text{-}100$) were employed in subsequent tests. Although this did in fact remove strong hot-wire oscillations from the frequency range of interest (1-500 KC) it was at the expense of a lower signal-to-noise ratio. It is felt that the wires used with $\ell/d \sim O(50)$ are really too short for this reason and also because end-losses (heat conduction to wire supports) appreciably affect the operation of the hot-wire and the resultant data reduction. Several measurements of fluctuations with a hot-wire of $\ell/d \approx 125$ were reduced and the change

in final results was well within experimental scatter, however the various overheats of wire temperature were much easier to set and calculate due to the reduction in end losses.

When making measurements of the shock motion frequency, a square wave type of signal was found from the hot-wire when it was placed within the limits of motion as shown in the upper drawing of Figure I-15. Direct measurement of this signal was not possible because the freestream noise levels triggered the counter and gave abnormally high readings. To filter out the noise, yet keep the square wave character of the signal, the Philco-Ford Intermittency meter was employed. By observing both the original hot-wire signal and the intermittency meter output on a dual beam storage scope the meter trigger level could be adjusted so that the meter output was considered "most representative" of the original signal. A typical intermittency meter output is shown in the lower drawing of Figure I-15 and is plotted in the same time scale as the original hot-wire signal. Since this was a subjective measurement it was repeated several times as a qualitative check and also other people were asked to go through this procedure as a final check. The intermittency meter output was then fed to a frequency counter for the measurement of the square wave frequency. The results of this were fairly consistent and are believed to be within 10%.

For determining the oscillation mode of the shock two hot-wire probes were employed, the second inserted through a sidewall and supported by an existing traversing mechanism which was modified to be compatible with the supersonic tunnel. The probe holder was

cantilevered from the traverse mechanism a distance of about one foot and because of this stiffness problems were encountered. This was overcome to some degree by jamming the probe holder against the traverse mechanism and repeatable measurements could be made.

This second probe could be moved in the "y" and "z" directions (see Figure I-1) and the shock position determined by observing the "square-wave" type of signal. The first probe could be moved in the "x and y" directions and the shock location determined similarly. The correlation measurements of shock position were computed by measuring the mean square values of each of the signals plus the sum and difference of the two signals (which could easily be done at the input of the hot wire amplifier). The correlation coefficient was then defined by

$$R(x'y') = \frac{\overline{e_1(x, z)\, e_2(x + x',\ z + z')}}{\sqrt{\overline{e_1^2}\ \overline{e_2^2}}}$$

$$= \frac{\overline{(e_1+e_2)^2} - \overline{(e_1-e_2)^2}}{4\sqrt{\overline{e_1^2} \cdot \overline{e_2^2}}} \qquad \text{(I-1)}$$

where x', z' are the distances between the two probes in the plane of the shock wave. This method of measuring correlation coefficients is not optimum for low correlations because, as can be seen from equation I-1, the differences of two large numbers are being taken and the relative error in these becomes appreciable when considered in size to the small remainder. A direct reading correlation meter was unavailable and the above procedure was the only one that could be used.

I. 3. 2. 2 Quantitative Hot-wire Studies

When it was desired to use the hot-wire as a means of making unsteady measurements in velocity, density, etc. it was first necessary to relate the voltage output of the amplifier to the various fluctuating quantities in the flow field. This is accomplished by first determining the response of an ideal (massless) hot-wire to each of the various modes of fluctuation. These response characteristics are termed sensitivity coefficients and have been evaluated by a number of authors[9], [10] for wires of infinite length.

Since relatively short wires were employed in these tests, the effect of heat conduction to the wire supports had to be considered in the derivation of the sensitivity coefficients. This has recently been completed for subsonic and supersonic flows by Behrens[12] and since it is as yet unpublished and because the importance of accounting for finite length has previously been neglected, an abridged derivation of the hot-wire response characteristics is given in Appendix I-A. Full credit for this must be given to Dr. Behrens and the contribution by the present author is in the area of having checked the results and applied the calculated formulae to a real physical situation.

The sensitivity coefficients as derived in Appendix I-A are shown to be functions of the local mean flow conditions and the wire operating current. The former is evaluated by knowledge of the local Mach number and Reynolds number ($Re_T = \frac{\rho u d}{\mu_T}$ where μ_T is the fluid viscosity at the stagnation temperature) both of which are calculated from the Pitot pressure and static pressure measurements and employing relatively simple formula using NACA Report 1135.[27]

The wire operating current, in addition to appearing explicitly in the sensitivity coefficients, also appears implicitly through the wire overheat parameter $\overline{\tau}_m$. A method for computing $\overline{\tau}_m$ from knowledge of the wire current $\overline{i}$, adiabatic (zero current) wire resistance, R_{aw}, and slope of the wire resistance, R_w vs. Joule heating ($i^2 R_w$) wire calibration is also given in Appendix I-A.

Since it is not possible to measure the output of a fictitious ideal wire as derived in Appendix I-A but instead only the hot-wire amplifier output can be measured, it is necessary to relate these two quantities. This is accomplished in Appendix I-B and is subject to the assumption that $(2\pi f M_t)^2 >> 1$ where f is the frequency of fluctuation and M_t is the hot wire time constant. This assumption is quite reasonable for frequencies greater than 2-3 Kc and is also employed in the derivation of the sensitivity coefficients.

In order to separate the modes of fluctuation the hot-wire response equation as derived in Appendix I-A is used

$$e_i' = -S_\rho \rho' - S_u u' + S_{T_T} \tau_T' \qquad \text{(I-2)}$$

where e_i' is the response of an ideal (massless) hot-wire, S_ρ, S_u, and S_{T_T} are the sensitivity coefficients to density, velocity, and total temperature fluctuations respectively and ρ', u' and τ_T' are the fluctuations in density, velocity, and total temperature normalized by their local mean values. In practice, it is not advantageous to make instantaneous measurements of the fluctuating quantities as in equation I-2 but rather the statistical properties such as mean-square values are more desirable. In squaring and time averaging equation

I-2, six unknown quantities then result such as the mean-square values of density, velocity, and total temperature and the three correlations between each of these. These could be separated by operating at a minimum of six different wire currents which in turn would give six different sets of sensitivity coefficients and the resultant simultaneous equations solved. In order to reduce the amount of labor in this measurement, however, several assumptions were employed.

For the inviscid flow fluctuation measurements, both ahead of and behind the separation shock wave, the Mach number is fairly high. Because of this, the sensitivity coefficients to density and velocity fluctuations are approximately equal (at M = 1.95 for example these two differed by only 5%). Thus the mean square hot-wire equation I-2 may be written taking $S_{\dot{m}} \approx S_{\rho} \approx S_{u}$ as

$$\Theta^2(r) \equiv \overline{e_i'^2}/S_{T_T}^2 = \overline{\tau_T'^2} - 2r\,\tilde{\tau}_T\,\tilde{\dot{m}}\,R_{\dot{m}T_T} + r^2\overline{m'^2} \qquad \text{(I-3)}$$

where r is the sensitivity ratio $\equiv S_{\dot{m}}/S_{T_T}$

$\tilde{\tau}_T$ and $\tilde{\dot{m}}$ are the root-mean square fluctuations to total temperature and mass flow per unit area, respectively,

and $R_{\dot{m}T_T}$ is the correlation coefficient of mass flow and total temperature fluctuation $\equiv \overline{m'\tau_T'}/(\tilde{\tau}_T\tilde{\dot{m}})(-1 \leq R_{\dot{m}\tau_T} \leq 1)$.

The measurements by the hot-wire then gives the value of $\overline{e_i'^2}$ and the two sensitivity coefficients S_{T_T} and $S_{\dot{m}}$. A "fluctuation diagram"[9] or a plot of $\sqrt{\overline{e_i'^2}/S_{T_T}^2}$ vs r was constructed and the values of $\overline{\tau_T'^2}$, $\overline{\dot{m}'^2}$, and $R_{\dot{m}T_T}$ determined from a best-fit hyperbola in the manner after Kovásznay.[9]

For the measurements within the shear layer the procedure used above is no longer applicable since the local Mach number can be well below the free stream values. The standard assumption[8, 25] used to reduce the data is that the pressure fluctuations within the shear layer are negligible compared to those in density and local static temperature. This is entirely equivalent to assuming that variations in vorticity and entropy are much greater than the potential variations caused by pressure waves. To rewrite the hot-wire response so as to explicitly display the pressure fluctuations is a relatively simple derivation[12] which results in

$$e_i' = S_u^* u' + S_\sigma \sigma' + S_\pi \pi' \qquad \text{(I-4)}$$

where $\sigma' \equiv \Delta s/C_p$ (entropy fluctuation)

$\pi' = \Delta p/\gamma\overline{p}$ (pressure fluctuation)

and

$$\begin{aligned} S_u^* &= \frac{2(a_1-1)}{a_1} S_{T_T} - S_u \\ S_\sigma &= S_\rho + \frac{1}{a_1} S_{T_T} \\ S_\pi &= \frac{\gamma-1}{a_1} S_{T_T} - S_\rho \\ a_1 &= 1 + \frac{\gamma-1}{2} M^2 \end{aligned} \qquad \text{(I-5)}$$

With the assumption that the pressure variations are negligible or, more precisely, that $S_\pi^2 \overline{\pi'^2} \ll S_u^{*2} \overline{u'^2}, S_\sigma^2 \overline{\sigma'^2}$, then equation I-4 becomes upon squaring and time averaging

$$\overline{e_i'^2}/S_\sigma^2 = \overline{\sigma'^2} + 2\, r^* \tilde{\sigma}\, \tilde{u} R_{\sigma u} + r^{*2} \overline{u'^2} \qquad \text{(I-6)}$$

where $r^* \equiv S_u^*/S_\sigma$

$R_{\sigma u} \equiv \overline{\sigma' u'}/\tilde{\sigma}\,\tilde{u}$

$\tilde{\sigma}$ and $\tilde{u}$ are the root-mean-square fluctuations in entropy and velocity

It is also easily shown that the other fluctuating quantities are related to σ', u', and π' by

$$\tau_T' = \frac{1}{a_1}\{\sigma' + (\gamma-1)\pi' + 2(a_1-1)u'\}$$

$$\rho' = \pi' - \sigma' \qquad \text{(I-7)}$$

$$T' = \sigma' + (\gamma-1)\pi' \quad .$$

Hence, with pressure disturbances neglected, the quantities σ' and u' are tantamount to density and vorticity fluctuations respectively. Moreover, the root mean square values of the quantities given in equation I-7 are related to $\overline{\sigma'^2}$, $\overline{u'^2}$, and $R_{\sigma u}$ by easily derived formulae. The level of pressure fluctuations can be estimated from known experimental data and its neglect checked after data reduction.

For the particular test conducted here, a series of only three wire currents were used mainly due to a lack of time. This quite naturally makes the curve fitting of a hyperbola to the fluctuation diagram obtained from equation I-6 rather difficult. The data did suggest that the correlation coefficient, $R_{\sigma u}$, was very near to a value of -1. The plausibility of this was verified through the measurements of Demetriades[8] ($R_{\sigma u} \approx -0.9$) and Laufer and Vrebalovich[30] ($R_{\sigma u} \approx -1$). This was then taken as an assumption and the

data reduced from straight line curve fits to the fluctuation diagram. The total temperature and mass flow fluctuations were then computed from

$$\tilde{\tau}_T = \frac{1}{a_1} \left| \tilde{\sigma} - 2(a_1 - 1)\tilde{u} \right|$$
$$\tilde{\dot{m}} = \left[\tilde{\sigma} + \tilde{u} \right] \qquad \text{(I-8)}$$

which are commensurate with equations I-7 and the above stated assumptions.

I. 4 Experimental Results

I. 4. 1 Resultant Flow Fields

Schlieren photographs were taken generally during most tests to first get a crude idea of the flow field characteristics. A pictorial representation of the flow over the 0. 24 inch step is shown in Figure I-3 and is a compilation of Schlieren photographs, Pitot tube measurements, and hot-wire traverses. Also shown is the wall pressure distribution for this flow field. This step was taken as representative of all steps tested and the differences for these cases will be discussed as the need arises. The general features of the flow as illustrated by the 0. 24 inch step will first be discussed.

As the flow approaches the step face from upstream the slow moving fluid particles in the boundary layer do not possess enough momentum to negotiate the necessary pressure rise to go over the step. As a result of this, these slow moving fluid particles begin to decelerate and thus cause a deflection of the streamlines in the supersonic portion of the boundary layer which generates a series of closely spaced compression wavelets originating near the wall and which coalesce into the separation shock outside of the boundary layer. The deflection of the streamlines as they pass through the compression waves and shock wave amounts to about 12° to 13°. The low momentum fluid in the boundary layer gains the necessary energy to pass through this region of steep pressure rise by a complicated mixing process with the faster moving fluid particles, thus the slow moving particles also undergo a deflection of 12° to 13° and the boundary layer separates from the wall. The length of this region from the

start of interaction to the separation point is around two initial boundary layer thicknesses.

The wall pressure level in this region increases rapidly from the start of interaction up to about the separation point where the pressure rise tends to level off as illustrated in the pressure distribution shown in Figure I-3. Having separated, the shear flow continues downstream at about the same inclination of 12° to 13° thus passing over a roughly triangular shaped region of low energy fluid which is termed the recirculating region or separation bubble. By virtue of the turning angle of the shear flow this recirculating region is around four step heights in length and is comprised of fluid particles that become entrained in the lower portion of the shear layer, impinge on the step face, and are returned along the wall in front of the step in a direction opposite to the main flow until they again become entrained. The reversed flow velocity in the recirculating region is on the order of 40% of the external flow velocity.[13, 16] The static wall pressure in this region increases from the separation point slightly to a first peak at around two step heights from the step face and is known as the plateau pressure. The static pressure nearer to the step remains close to this plateau pressure value until very close to the step face where another sharp rise is encountered.

After passing over the separation bubble, the shear flow and external flow turns back parallel to the original flow direction beginning at the corner of the step. This results in an expansion fan which originates near the step corner and radiates outward into the inviscid flow until it interacts with the separation shock wave.

The outer edge of the shear layer in the separated region makes an angle of about 16° to 17° with the original flow direction and thus the shear layer grows at an angle of around 3° to 4°. The streamlines in the shear layer are closely aligned with those in the inviscid region including the dividing streamline.

For the upstream Mach number tested here ($M_0 \approx 2.46$) the inviscid flow behind the shock wave is still supersonic at about $M_e = 1.95$ and the static pressure jump associated with the shock wave agrees closely with the aforementioned plateau pressure. The dividing streamline was found to be slightly supersonic over most of the separation bubble at around a Mach number of 1.10.

The above flow field description is generally applicable to step sizes greater than or equal to the initial boundary layer thickness, δ_0, and agrees quite well with the basic flow features and scaling parameters as described by Zukoski.[16]

For the smaller step sizes ($h/\delta_0 \leqslant 1$), the extent of the inviscid flow between the separation shock and the expansion wave decreases until the interaction between these two occurs within the boundary layer at around a step height of 50% of the initial boundary layer thickness. Until this point is reached, however, the strength of the shock wave remains constant and the plateau pressure decreases somewhat due to the shortening of the mixing region along the dividing streamline.

For step heights less than 50% of the initial boundary layer thickness the flow can no longer be divided into the two areas discussed above as these tend to overlap. The general features such as the shock

wave, separation bubble, and expansion fan described above still can be observed even for steps as small as 5% of the initial boundary layer thickness.

Pitot tube surveys were conducted at various stations in the flat-plate boundary layer ahead of the interaction and within the separated region for the larger step sizes in order to determine the velocity profiles. A typical Pitot tube survey is shown in Figure I-8 for the separated region and the particular flow field characteristics such as the shock wave and shear layer are easily discerned and indicated in the figure. Surveys at other flow stations exhibit a similar behavior except for the initial interaction region. These Pitot tube profiles were not shown, however, because they are adequately represented by surveys conducted by Bogdonoff.[3]

Static pressure surveys were also conducted at the various stations with a representative traverse shown in Figure I-9. The interpretation of this traverse is given in detail in Section I. 3. 1 of this thesis.

For the qualitative measurement of turbulence intensity hot-wire traverses were also conducted at various stations in the separated region for the larger steps. Again, these traverses were all similar in character once downstream of the initial interaction region and a representative output is shown in Figure I-11 where the characteristics of the flow field are again distinct and indicated in the figure. The local shear layer thickness was determined from these hot-wire traces by employing the slope-intercept method as indicated on Figure I-11. The results obtained by the method were in good

agreement with the thickness as estimated from the velocity profiles.

For the typical Pitot tube traverse shown in Figure I-8 note that the shock wave is not detected as a sudden jump but rather as a rapid transition from the upstream level to that behind the shock wave. This is also apparent in the Pitot surveys conducted by Bogdonoff.[3] This behavior had previously been accounted for by assuming there is an interaction between the separation shock wave and the bow shock in front of the Pitot tube. With the preliminary hot-wire surveys this same phenomenon was also observed as shown in Figure I-11 and again the transition from upstream to downstream is spread over approximately the same region. Furthermore, when the hot-wire was placed in this area and the output observed on an oscilloscope, a distinct square wave behavior was seen and is depicted in the upper drawing of Figure I-15. The only interpretation that can explain this is that the shock wave is oscillating about its mean position and the square wave is the result of the abrupt changes in heat transfer to the fluid ahead of and behind the shock. This square wave signal was observed with all steps tested and with several different hot-wire probes.

When the separation shock was observed in the Schlieren system it appeared as a blurred region of approximately the same width as described above. A series of spark Schlieren pictures (about 5 μsec duration) were taken to see if the above motion could be detected visually. These gave essentially the same appearance as with the continuous Schlieren observations. Thus, it appears as though the shock wave motion is not correlated across the width of

the tunnel. Detailed measurements of the shock motion are presented in Section I. 4. 5.

I. 4. 2 Wall Pressure Measurements

A wealth of experimental data is available for the mean wall pressure distributions in front of forward facing steps for step heights greater than or equal to the initial boundary layer thickness. The majority of this work has been reviewed recently by Zukoski.[16] However, it was felt that for step sizes less than a boundary layer thickness that the existing wall pressure data should be supplemented and the effect of step height in certain scaling parameters determined.

The mean wall pressure data for a series of forward facing steps ranging in height from 0. 01 inch ($h/\delta_0 \approx 0.048$) to 0. 32 inch ($h/\delta_0 \approx 1.5$) were measured and are presented in Figure I-4 where the fractional change in wall pressure, $\frac{\Delta p}{p_0} \equiv \frac{p-p_0}{p_0}$, is plotted against distance from the step face. The uniformity of the pressure data in the spanwise direction, although not shown, was quite good except near the start of the interaction region where the pressure gradients are steep. This spanwise uniformity was usually within about 5% of the mean level and considerable improvement was observed when splitter plates were employed.

Details of the pressure distributions near the step face for the larger step sizes is not shown for clarity and because all were very similar to that shown for the 0. 18 inch step.

The pressure distribution for the 0. 32 inch step, both with and without splitter plates, is shown only for comparative purposes because of the non-uniformity of the entire flow field as discussed

previously.

For the larger step sizes, say $0.12'' \leq h < 0.32''$, the location of the separation pressure ratio, $\Delta p_s / p_0 \approx 0.93$,[16] is in good agreement with known correlations. For steps smaller than this, significant departures from this value are evident, which incidentally corresponds to the disappearance of a plateau pressure region.

I. 4. 3 Velocity Profiles and Qualitative Hot-wire Measurements

In several of the theoretical attempts to treat the separation of supersonic turbulent boundary layers various assumptions regarding the character of the shear layer are made such as the "equivalent jet" hypothesis of Paynter.[21] Moreover, there is presently some interest in treating the separation problem by moment methods[23] which utilize several integral properties of the flow (e. g. displacement thickness and momentum thickness, among others) and one way of approximating these is to employ certain classes of similarity solutions.

In both of these cases, there is some question of their validity near the interaction region where the boundary layer undergoes the transition to a separated shear flow. In addition, it was not clear that as the separated shear layer moved far downstream of the interaction region whether the influence of the wall and the recirculating flow could prevent the approach to a similar type flow (similarity is implicit in the "equivalent jet" hypothesis). Thus, because of these doubts, detailed surveys of the separated shear layer by means of the Pitot tube and the hot-wire anemometer were conducted.

The approaching boundary layer velocity profile is presented in Figure I-7 where the velocity ratio u/u_e is plotted against distance from the wall. The boundary layer thickness in the test section area is taken as 0.21 inch and the momentum thickness calculated from the velocity profile is about 0.014 inch. The two characteristic Reynolds numbers for the initial boundary layer are then

$$\begin{aligned} Re_{\delta_0} &\approx 4.35 \times 10^4 \\ Re_{\theta_0} &\approx 2.4 \times 10^3 \end{aligned} \qquad \text{(I-9)}$$

(using the relations given in NACA Report 1135[27]).

In the separated flow region the velocity profiles for the 0.24 inch step are shown in Figure I-10 where the velocity ratio u/u_e is plotted against y/δ and δ is the local shear layer thickness measured from the wall and determined from the hot-wire measurements as mentioned earlier. These profiles are shown for five stations downstream of the beginning of interaction as measured in initial boundary layer thicknesses. Also included in Figure I-10 is the approximate dividing streamline velocity. Velocity profiles for stations closer to the beginning of interaction than 2.67 boundary layer thicknesses are not presented because accurate data on the local static pressure could not be ascertained. The last two survey stations ($\frac{x_0-x}{\delta_0} = 4.90$ and 5.64) are shown only partially because the step prevented probing closer to the wall. Likewise, velocity measurements in the reversed flow regime were not measured due to the difficulties discussed previously. The velocity at the outer edge of the shear layer, u_e, was constant to within 1% for each of the stations shown.

Also, for the separated shear layer, profiles of the turbulence intensity were taken for the 0.24 inch step by use of the hot-wire anemometer and are shown in Figure I-12. The hot-wire output is normalized by a reference output (equal in this case to the maximum output value) and is shown for four stations downstream of the interaction and also for the approaching boundary layer and plotted against the fraction of layer thickness y/δ (the local value of δ was determined from these and other hot-wire profiles). Again the profiles do not extend to the wall because of the presence of the step.

Spectral measurements of the hot-wire signal for several stations were also made at the peak signal location and are shown in Figure I-14. The individual spectra were normalized in a manner that more clearly illustrates the differences at the low frequency end of the spectrum. It was reasoned that in the short space from separation to the step face the smaller or dissipative eddy scale would not change markedly whereas the larger eddies are the most effective in changing the gross behavior of the shear flow, e.g. the velocity profile. Moreover, the unsteady phenomena associated with the separation bubble itself (see Section I.4.5) is at low frequency (less than 12 KC) and thus has very little effect on the higher frequency components. The normalization itself was conducted by equating the energy levels in the 1 KC band width centered at 200 KC for each of the spectra. This procedure, while admittedly arbitrary, does illustrate the differences between the unseparated flow and the separated flow better than other arbitrary methods.[8]

The spectra shown in Figure I-14 are uncorrected for amplifier response but do include compensation for the real wire attenuation (thermal lag). As can be seen from the amplifier characteristics shown in Figure I-29, the neglect of amplifier attenuation has little or no effect for frequencies lower than 100 KC which is where essentially all of the spectral changes occur.

I. 4. 4 Shear Layer Fluctuation Measurement

Since it was suspected that the shear layer was in some sense approaching similarity (see Section I. 5. 2) it was decided to utilize the capabilities of the hot-wire anemometer to measure the fluctuations in density, velocity, mass flux, and total temperature near the similar region. This was done in order to make more meaningful the qualitative studies presented earlier and to see if any significant differences existed between the separated shear layer and other turbulent flows such as a flat plate boundary layer.

Fluctuation measurements were conducted at only one streamwise station in the separated shear layer. This station was 5. 6 initial boundary layer thicknesses downstream of the start of interaction and was, for this step size (0. 24 inch) and initial boundary layer thickness (0. 21 inch), the closest station to an equilibrium similar flow as determined in Section I. 5. 2.

The data taken in this series of tests was reduced in accordance with the assumptions and derivations outlined in Section I. 3. 2. 2. In order to more clearly establish the magnitude of the hot-wire properties defined in that section the measured adiabatic wire resistance and the slope of the measured wire resistance vs. wire Joule

heating are shown in the upper drawing of Figure I-19. The changes in measured adiabatic wire resistance and the above mentioned slope are due to the variations in Nusselt number and recovery factor across the shear layer.

Also shown in Figure I-19 is the variation in several of the sensitivity coefficients across the shear layer for one of the three mean wire currents employed. As can easily be seen, the magnitudes of the various coefficients are rather low because of the very short wires used; the total temperature sensitivity coefficient is only 32.4 mv. per 100% level of fluctuation and decreases some 40% through the shear layer.

The root-mean-square fluctuation magnitudes of the streamwise velocity and local static temperature are shown in Figure I-20 plotted, as before, against the fraction of the local shear layer thickness. These static temperature fluctuations are rather high reaching a maximum value of 12.1% within the layer. The velocity fluctuations, on the other hand, are considerably lower reaching a maximum of some 5% within the layer and appear to be increasing as the wall is approached. The root-mean-square magnitudes of the fluctuations in total temperature and mass flow per unit area shown in Figure I-21 were calculated from the above by using equations I-8. It should be recalled that the wire response to pressure fluctuations was assumed negligible and that the correlation coefficient between static temperature and streamwise velocity fluctuations was assumed to be -1 as justified in Section I.3.2.2.

The assumption regarding the neglect of pressure fluctuations can be checked at this point using the R. M. S. pressure coefficient fluctuation ($\tilde{C}_p \equiv \frac{\tilde{p}}{\frac{1}{2}\rho_0 u_0^2}$) of around 2.5% as found by Coe[14] within the separated region over a wide range of Mach number ($1.5 \leq M_0 \leq 2.5$). The ideal hot-wire response is given approximately by (cf. Eq. I-4)

$$\tilde{e}_i = \left[S_\sigma^2 \tilde{\sigma}^2 - 2 S_\sigma S_u \tilde{\sigma}\tilde{u} + S_u^2 \tilde{u}^2 + S_\pi^2 \tilde{\pi}^2 + \cdots \right]^{\frac{1}{2}} \qquad \text{(I-10)}$$

The term representing the pressure wave response only becomes appreciable near the wall and at the measuring position nearest the wall the four terms shown within the bracket had values of $2.14(mv)^2$, $0.88(mv)^2$, $0.09(mv)^2$, and $0.008(mv)^2$. Thus, the neglect of the wire response to pressure waves is indeed justifiable.

Spectra of the hot-wire signals were taken at three locations in the profile for each of the three operating currents used. Near the outer edge of the layer the spectral signal was very erratic which is not unexpected because of the intermittent character of the flow. The remaining two positions where spectra were taken, one near the maximum signal location and the other near the inner edge ($y/\delta \approx 0.6$), did not differ much in character for a given operating condition. The spectra for the three wire currents (overheats) are displayed in Figure I-22 where the fluctuation intensity as a function of frequency is plotted in arbitrary units but without the normalization employed previously. These spectra are also corrected for amplifier attenuation which was very small except at the high frequencies where the signal is small thus giving confidence to the mean square measurements that were uncorrected for amplifier attenuation.

These spectra could again be reduced by modes since the sensitivity coefficients are independent of frequency (see Appendix I-A), but this was not done because of the scant amount of data taken (Demetriades,[8] for example, used a series of eleven wire currents to spectrally separate the modes). It should be noticed from the three spectra taken that not only does the signal level increase with wire current but also the shapes of the three spectra are different, especially in the lower frequencies as was found by Kistler[25] for a supersonic flat plate boundary layer. As mentioned earlier, a "cold" wire is responsive mainly to total temperature variations, thus the lowest current setting is close in shape to the total temperature spectra. For the higher current setting the hot-wire becomes more responsive to mass-flow fluctuations. Thus, qualitatively, the spectra of mass-flow fluctuations increases as the frequency decreases as opposed to total temperature spectra which has a peak near 25-50 KC.

The slight "bump" in the spectra near a frequency of 60 KC shown in Figure I-22 is an example of the "strain gaging" phenomena alluded to previously. In this particular case the effect of this bump on the mean square signal is entirely negligible. In the data taken in the qualitative hot wire measurements a much more pronounced bump was present in the spectra in the range 240 KC to 320 KC (not shown in Figure I-14). The magnitude of this was as high as the turbulence signal itself although the energy contained in this (area under spectral curve) was at most 20% of the turbulent signal energy.

I. 4. 5 Shock Motion Studies

One of the most interesting observations made during the hot-wire surveys was that the separation shock wave was not fixed with respect to the step but rather oscillated over a small region about its mean position. The output signal of the hot-wire when placed within the shock motion limits closely resembled a square wave, the top and bottom of which correspond to the shock wave being either upstream or downstream of the wire position. A typical example of this output is shown in the upper drawing of Figure I-15 which was traced directly from an oscilloscope photograph.

The detection of shock motion by means of a hot-wire was first reported by Kovasznay[9] for the case of the leading edge shock from a flat plate. The observation and measurement of the motion of the shock caused by turbulent boundary layer separation in front of a forward facing step was originally due to Kistler[13] who utilized wall pressure fluctuation data. Although limited in scope, Kistler did find that the origin of the shock oscillated about its mean position with a characteristic frequency and over a range of about one boundary layer thickness. Wall pressure spectral measurements conducted in the separated region by Speaker and Ailman[15] show several distinct oscillation frequencies, but the reasons for this oscillation were not given.

With the square-wave behavior of the hot-wire signal when placed in the limits of shock motion it was felt that the effect of the step size on the unsteady behavior could be assessed more easily than by conducting wall pressure fluctuation measurements.

Before presenting the measurements of the shock-motion it should be shown that this motion in most part was not due to some upstream influence, but was in fact a result of the separated shear layer with its attendant subsonic cavity. These upstream causes, if they did exist, would be due to some unsteadiness in the tunnel free stream or to the displacement of the shock origin by large eddies in the approaching boundary layer.

The free stream fluctuation measurements obtained in the course of these experiments were shown to be very small in magnitude and the result primarily of the radiated noise from the turbulent boundary layer. In order to insure that the shock motion was not caused by free-stream fluctuations two auxilliary experiments were conducted; the first was the frequency measurement of the oscillation of one of the weak compression waves in the tunnel which emerged from the opposite wall; and the second was the frequency and amplitude measurement of an oblique shock of about the same strength as the separation shock and was produced by a wedge placed in the free stream. Both of these frequencies were in the range 11-12 KC and were checked several times using the procedure described in Section I. 3. 2. 1. This value was higher than the frequency measurements made on the separated shock waves and furthermore the separated shock frequency was found to be dependent upon the step height which further excludes the free stream fluctuation influence.

The influence of the approaching boundary layer can be shown negligible by the following argument: if the displacement of the shock wave were in fact caused by the largest eddies within the boundary

layer, then the characteristic frequency associated with this would be on the order of U'/ℓ where U' is the propagation velocity of these eddies ($U' \approx 0.6\, u_e$ [13]) and ℓ is the characteristic length of the eddies (ℓ is of the order of a boundary layer thickness). Thus, this characteristic frequency is about $0.6\, u_e/\delta_0$ and for the conditions of this experiment has a value of 110 KC which is an order of magnitude greater than the measured frequency of shock motion. Thus it is safe to disregard both upstream fluctuations as the direct cause of the shock motion.

I. 4. 5. 1 Amplitude of Shock Motion

The amplitude of shock motion was the easiest of the unsteady characteristics to measure requiring only traverses through the shock and recording the mean square hot-wire output. This was done for four step heights ranging from 0. 08" to 0. 32" (or $h/\delta_0 \approx 0.38$ to 1. 52) and it was first observed that for each step the amplitude of motion was very close to being independent of position along the shock wave (a slight increase in amplitude was observed very near the edge of the boundary layer which is due to the fact that the compression waves from the separation had not yet coalesced into a well defined shock). The immediate conclusion from this measurement is that the shock motion is not "hinged" at the separation point but rather it moves either as a plane surface or with waves propagated along the shock wave.

Typical mean square hot-wire output traverses through the shock wave for two step sizes are shown in Figure I-23 where the output is plotted as a function of distance normal to the shock wave mean position. Note that the shock motion is over a limited range of less

than 0.06 inch and that the amplitude varies with the step height. Also plotted in these figures is the probability that the shock wave, at any given time, is located upstream of the position y' and is denoted by $P(y')$. This probability distribution was computed from the mean square output data from

$$\overline{E'^2}/\overline{E'^2}_{max} = 4P(y)\,[1-P(y)] \qquad (I-10)$$

which is easily derived by considering the wire output as a square wave with the duration of the upper segment being $P(y)$ (the period is taken as 1) and computing the resultant mean square value.

The variation of shock amplitude (as determined by a slope-intercept method to the computed $P(y)$ curve) with step height is shown in Figure I-24. Also included in this figure is the amplitude measurement for the shock wave caused by 13° wedge placed in the free stream. As explained earlier, the data for the 0.32 inch step is considered questionable and is shown by "?". From this figure, it appears that the amplitude of shock motion increases more or less linearly with step height up to a step height of around 0.16 inches where the amplitude becomes relatively independent of step height as depicted by the curve drawn on the figure.

I.4.5.2 Frequency of Shock Oscillation

Utilizing the square wave behavior of the hot-wire output the oscillation frequencies of the separation shock waves were measured in the manner described in Section I.3.2.1. This was done for four step sizes ranging from 0.08 inch to 0.32 inch.

The oscillation frequency as measured several times was not

a constant value as may or may not be expected, but rather was spread over a frequency band about a peak or mean value. Because of this, the frequency was measured over one second intervals many times and the results plotted in histogram form as depicted for the 0.24 inch step in Figure I-25. The low number of measurements is because the data had to be recorded manually but nevertheless a distinct peak occurred in the histogram for each step size.

During the data reduction of these frequency measurements, it was noticed that the peak frequency was very nearly inversely proportional to the step height. This being the case, one possible cause of the shock motion is an acoustic oscillation in the reversed flow subsonic cavity. This acoustic oscillation would, if valid, require that the resonant frequency be inversely proportional to the cavity length and proportional to the acoustic propagation speed. Since the reversed flow velocity in the separation bubble is quite low ($M \leq 0.2$[3]) the acoustic propagation speed is then close to the speed of sound at the stagnation temperature, a_T. If a Strouhal number, or reduced frequency, is defined then by $f^* \equiv fL/a_T$ where L is the cavity length, and the data plotted in this form for the various step sizes as is done in Figure I-26, it is seen to be remarkably constant at a value of 0.256 except for the 0.32 inch step data (indicated by a "?") which is believed erroneous because of the tunnel choking problems mentioned earlier.

I.4.5.3 Free Stream Fluctuation Measurements

An attempt to get more definitive information concerning the shock motion was made by making inviscid flow fluctuation measurements ahead of and behind the separation shock wave. The reasoning

behind this was that because of the shock motion, the levels of fluctuation in both total temperature and mass flux would increase downstream of the shock. The total temperature fluctuations would then be directly related to the R. M. S. shock velocity (the variations in mass flux would also, but to a lesser degree, because of the noise radiated from the separated shear layer). Unfortunately, this experiment was not entirely successful from a spectral viewpoint mainly because of the low signal levels. In spite of this, these measurements did provide a check on the previous shock frequency and amplitude measurements, and also were invaluable in formulating a model for the unsteady behavior.

In the course of this experiment, the free stream fluctuations were measured and the data points were plotted on a fluctuation diagram as outlined in Section I. 3. 2. 2 and are shown in Figure I-16. The fluctuation levels determined in this manner give values of 0. 08% for R. M. S. total temperature fluctuations and 0. 55% for R. M. S. mass flux variations with approximately zero correlation between the two.

For the inviscid flow fluctuations behind the separation shock caused by the 0. 08 inch step, the data was taken and is shown in Figure I-17 again in fluctuation diagram form. It should be noted that two sets of measurements are presented here for two different wire lengths and the comparison between the two is very good. From a least squares curve fit to this data the R. M. S. total temperature fluctuations were 0. 41% and the R. M. S. mass flux variations were 1. 66% with a correlation coefficient of 0. 73.

These levels correspond very well to those that would be computed from the measurements of the shock motion amplitude and frequency and utilizing simple unsteady oblique shock relations. The R. M. S. variations from the calculation gives 0. 45% for total temperature and 3. 6% for mass flux with a correlation coefficient of 1. The difference in mass flux variations and correlation coefficients is most likely due to pressure waves radiated from and through the separated shear layer.

In addition to the levels of fluctuation, the spectra of the hot-wire signal behind the 0. 08 inch step shock wave was also measured and is shown in Figure I-18. The frequency for this figure is normalized by the value f_o which is the mean oscillation frequency determined from the shock motion measurements ($f_o = 0.256\ a_T/L$). As can easily be seen, distinct peaks in the spectrum occur in the neighborhood of $f/f_o = 1$ and $f/f_o \approx 3$. Also plotted in Figure I-18 is the spectra of the wall pressure fluctuations just downstream of separation as determined by Speaker and Ailman[15] and the correspondence between these is quite good especially considering that these were taken at different free stream Mach numbers. This also indicates how the shock motion is related to the motion within the separated region. It should be mentioned that the curve representing the data of Speaker and Ailman[15] more closely approximates the actual data taken by them than the smoothed curve they used to fit the data.

I. 4. 5. 4 Shape of the Shock Motion

In view of the fact that the separation shock wave was found to oscillate about its average position, some information regarding

the manner in which it moved was desired to explain the blurred appearance even in spark Schlieren photographs. This blurring could be due either to warping of the shock surface in a direction transverse to the flow or due to waves possibly propagated from the separation region and along the shock surface in the streamwise direction. This could only be done in a statistical sense, however, and thus the measurement of the shock wave motion correlation was done by utilizing two hot-wire probes and computing the correlation between the two raw square-wave signals in the manner outlined in Section I. 3. 2. 1.

The transverse correlation measurement was done for three step sizes (each with splitter plates attached) and the results are indicated in the left hand drawing of Figure I-27 where the correlation coefficient $R(0, Z', 0)$ is plotted as a function of the distance between probes in the spanwise direction Z'. The results indicate that the form of the oscillation is relatively independent of step size and that the motion of the shock is more or less random in the spanwise direction with a correlation coefficient that decreases approximately exponentially with probe separation, i. e. $R(0, Z', 0) \approx e^{-Z'/a}$, where $a \approx 0.2$ inch. Since the wind tunnel is 2 1/2 inches wide, this explains why the shock wave appears as a blurred region in Schlieren photographs and also why motion of the shock cannot be detected by high speed motion pictures. It is not known how the correlation distance of about 0. 2 inch would change if the Mach number or boundary layer thickness were changed other than that this distance of about one boundary layer thickness is of the same order as found by Speaker and Ailman for spanwise pressure fluctuation correlations at $M_0 \approx 3.5$.

The streamwise correlation coefficient was measured for only one step size and is shown in the right hand drawing of Figure I-27 where the correlation coefficient $R(x', 0.36 \text{ inch}; 0)$ is plotted as a function of the probe separation distance in the streamwise direction along the shock wave, x' (note that the probes are separated by 0.36 inch in the transverse direction in order to eliminate interference problems). The results of this measurement indicate that the length of the waves propagating along the shock in the streamwise direction are very long – at least much greater than the scale of the experiment.

I. 5 Discussion of Results

I. 5. 1 Mean Wall Pressures

Before discussing the results of the data obtained here it is useful first to briefly consider several features of the pressure distributions for flows over large steps in order to more clearly display the effect of step size. In addition to the length scales of the flow mentioned in Section I. 4. 1 which are known to be independent of Mach number,[16] it is also well known that for fully developed turbulent boundary layers the flow field is virtually independent of Reynolds number[16] (for the range $10^4 < Re_{\delta_0} < 10^6$). The plateau pressure ratio as defined in Section I. 4. 1 has been determined by Zukoski[16] to be adequately represented by

$$\frac{\Delta p_P}{p_0} \approx 0.55\, M_0 \qquad (I-11)$$

where Δp is the difference between the plateau pressure, p_P and the initial static pressure ahead of the interaction, p_0, and M_0 is the free stream Mach number (Plateau pressures up to 5% higher than those predicted by the above expression have been reported by Hahn,[17] who employed step heights on the order of 4 to 8 initial boundary layer thickness). The steep pressure rise at the start of the interaction has also been shown to scale with the initial boundary layer thickness and the rate of increase in pressure in this region is given by,[16]

$$\left.\frac{\partial p}{\partial x}\right|_{max} \approx 0.5\, \frac{\Delta p_P}{\delta_0} \qquad (I-12)$$

where δ_0 is the initial undisturbed boundary layer thickness. Using equation I-11 to explicitly display the Mach number dependence on

pressure gradient, equation I-12 becomes

$$\left.\frac{\partial(\Delta p/p_0)}{\partial(x/\delta_0)}\right|_{max} \approx 0.275\ M_0 \qquad \text{(I-13)}$$

Bear in mind that the results presented above were ascertained for step heights greater than the initial boundary layer thickness and it was desired to determine experimentally the dependence of step height on the above expressions.

The wall pressure distributions for a series of step sizes from 0.01 inch thick to 0.32 inch thick (or for $0.048 \leq h/\delta_0 \leq 1.52$) were measured and are shown in Figure I-4. There are several general features that are immediately apparent from this drawing; first, the absolute extent of the pressure field in front of the step increases with the step height as expected; second, the appearance of a plateau pressure, as such, is not visible for step sizes less than 0.08 inch but rather rises monotonically to a peak pressure at the step face; third, the peak pressure, or plateau pressure for the larger steps, increases with step size becoming asymptotic to a maximum value which is very close to the value predicted by equation I-10; and fourth, the initial pressure rise appears to have a slope which is more or less independent of the step size.

The appearance of a plateau pressure for steps larger than 0.08 inch also coincided with the appearance of an inviscid flow region between the separation shock wave and the expansion fan caused by the turning of flow at the step corner whereas for smaller step sizes the interaction of these two occurred within the boundary layer. Moreover, the length of the separation zone for large step sizes (4.1 step

heights[16]) gives a constant separation pressure for steps greater than 0.12 inch that is in good agreement with the value suggested by Zukoski[16] at this Mach number. This implies that the length scale for the separation zone given above is valid for steps as small as, say, 50% of the initial boundary layer. This is roughly the same as is implied by other measurements[3], [5] at different Mach numbers but sufficient data is not available to generalize this result to all Mach numbers.

The value of the peak pressure, or plateau pressure, may be shown from a dimensional analysis to be a function only of Mach number and step height-to-boundary layer thickness ratio if Reynolds number effects are ignored. It was felt that equation I-11 might adequately account for the Mach number dependence for, as mentioned earlier, as h/δ_0 becomes much larger than unity the effect of step height on plateau pressure becomes negligible. This would imply then that the plateau pressure rise might be given by

$$\frac{\Delta p}{p_0}\ (M_0,\ h/\delta_0) \approx 0.55\ M_0 \cdot F(h/\delta_0) \quad . \tag{I-14}$$

With this in mind, the plateau-pressure ratio normalized by the quantity $0.55\ M_0$ was plotted against h/δ_0 for the data taken here and is shown in Figure I-5. The results of investigations by Bogdonoff[3], [5] at free stream Mach numbers of 3.85 and 3.0 along with some unpublished data by Czarnecki[18] at Mach numbers of 1.61 and 3.0 are also shown. Within experimental scatter, the results of this plot are seen to be fairly independent of Mach number. Thus, the assumption of equation I-14 for the plateau pressure is verified experimentally and

the dependence on h/δ_0 is determined. This relation is certainly not valid for extremely small steps, say $h/\delta_0 \leqslant 0.05$, where undoubtedly Reynolds number effects become important, but should give consistent results for steps larger than this.

The initial pressure rise associated with flow over a normal step appears to be independent of step size and agrees quite well with the maximum slope as predicted in equation I-11. Also see Figure I-6; here the data for several step sizes has been replotted against the variable $(x_0-x)/\delta_0$ where x_0 is the start of the interaction. Furthermore, the pressure distribution for a 13° wedge mounted on the wall (which somewhat models the flow over the separation bubble) is also plotted on this figure and it agrees closely with the other data. Note; this wedge angle did not separate the flow which is in agreement with the incipient separation data in front of compression corners.[20]

It should be mentioned that the observation that the initial pressure gradient is independent of step height is in agreement with the unpublished data of Czarnecki[18] but contradictory to the findings of Bogdonoff, et. al.[3],[5] The latter data shows a steep rise in maximum pressure gradient as the step height to boundary layer thickness ratio is reduced; in fact, for $h/\delta_0 \approx 0.5$, the maximum pressure gradient data of Bogdonoff is twice that for $h/\delta_0 > 1$. This level of increase was certainly not observed here over the range of h/δ_0 tested $(0.05 \leqslant h/\delta_0 \leqslant 1.52)$.

In Section I.4.5 it was shown that the separation shock wave and also the separation point oscillate about their mean positions with an amplitude that depends upon the step size. Furthermore, this

amplitude of motion decreases with step size for $h/\delta_0 \leqslant 1$ and this might explain the increase in maximum pressure gradient with decreasing step size. As a first approximation, consider the pressure rise to be a ramp with slope given by equation I-13 and compute the mean pressure gradient for the case where the ramp oscillates over an amplitude $a < \delta_0$. Under these assumptions no change in mean maximum pressure gradient from equation I-13 is noticed. From the shock motion measurements the amplitude of motion is shown to be at most 0.05 inch which is less than δ_0. For unsymmetrical instantaneous pressure rises some slight change in slope would result, but for the situation considered here would be smaller than could probably be measured. This description verifies the data obtained here for the maximum pressure gradient. For Bogdonoff's data it can only be guessed that for some unknown reason the shock motion amplitude in his experiments was different than that given here, but since no measurements are available, this cannot be checked.

In summary, the mean wall pressure distributions reported here have led to the following conclusions:

1. The scaling laws presented by Zukoski[16] for the geometry of the separated region are valid down to $h/\delta_0 \approx 0.5$;

2. for $h/\delta_0 \leqslant 0.5$, the pressure plateau disappears and the wall pressure increases monotonically as the step face is approached;

3. the normalized plateau pressure (or peak pressure for $h/\delta_0 \leqslant 0.5$) is shown to be a function of Mach number and h/δ_0 where the dependence in Mach number is given by Zukoski[16] and the dependence on h/δ_0 determined here; and

4. the maximum pressure gradient at the start of the interaction was found to be relatively independent of h/δ_0.

I. 5. 2 The Approach to a Similar Flow

One of the main reasons for obtaining the velocity profiles and fluctuation profiles in the separated region (aside from the fact that, to the author's knowledge, the latter has not been previously measured) was to either confirm or deny the suspicion from Schlieren photographs that the separated shear layer was, in some sense, approaching a similar flow. That is, whether the flow properties of the shear layer begin to scale linearly with distance along the surface. One might expect that for very small initial boundary layer thicknesses, or $h/\delta_0 \rightarrow \infty$, that the flow properties downstream of the separation point might be similar since there is no characteristic length scale for the flow (recall that the flow is independent of Reynolds number and that the step height just determines the separation point relative to the step face location). In other words, the velocity profiles instead of being a function of both x and y could be represented as a function of $y/L(x-x_0)$ where L(x) is some measure of the layer width. This is commonly done for solutions to laminar boundary layers, turbulent jets, mixing layers, etc.

On the other hand, a finite boundary layer would require some transition distance in order to relax to a similar type of behavior and it seems plausible that this distance would, in some sense, scale with a measure of the initial boundary layer (possibly layer thickness or momentum thickness among many other choices).

If the above argument is logically consistent, then three questions naturally arise. First, does a finite separating boundary layer become in fact similar? And, if it does become similar, what is the length of the transition distance and what is the proper similarity variable represented above by $L(x-x_0)$.

As a first crude answer to two of the questions posed above, consider the plateau pressure ratio as a function of h/δ_0 as presented in Figure I-5 where it is shown that for $h/\delta_0 \geq 2$, the plateau pressure is a constant for a given approaching Mach number. Assuming that the plateau pressure is in some manner related to the dynamic pressure along the dividing streamline ($\frac{1}{2} \rho^* u^{*2}$), then the above implies that the dividing streamline velocity becomes constant for $h/\delta_0 \geq 2$. Similarity solutions for, say, a mixing layer[24] also exhibit this behavior in that the dividing streamline velocity is a constant. From this correlation and the linear growth rates observed in Schlieren photographs it appears then that similarity is achieved. Moreover, using the experimental fact that the separation bubble is about 4.2 step heights in length[16] along with the above value of $h/\delta_0 \approx 2$ gives a value of about 8.5 boundary layer thicknesses as the approximate transition length to a similar flow. This result is independent of Mach number when the transition distance is measured in boundary layer thicknesses (the use of the initial displacement thickness, δ^*, or momentum thickness, θ, to measure the transition length would not exhibit this behavior, since both δ^*/δ and θ/δ are functions of Mach number). The above calculation, of course, relies on two rather weak assumptions and as such only serves as an indication of the approach to similarity and the

transition distance. More definitive information was hoped for from the velocity profile measurements.

Unfortunately, due to the limitation on maximum step size for this tunnel, the velocity profile data obtained here was not as fruitful as was desired. The 0.24 inch step, for which detailed velocity measurements were taken, only permitted profiles up to 5.6 δ_0 downstream of the start of interaction. These profiles, as shown in Figure I-10, do however indicate that the shear layer is perhaps becoming similar although what one might call excellent correlation is not displayed in the profiles. This is probably due to the fact that the local shear layer thickness, δ, is used as the similarity variable rather than some other choice which might take into account the initial boundary layer. More will be said about this later in this section.

The dividing streamline velocity as depicted in Figure I-10 does appear to be approaching a constant value of around 0.7 u_e in a transition distance somewhat around 6 δ_0 which is in good agreement with the plateau pressure scaling result. This value for the dividing streamline velocity is quite close to the value Korst[24] determines theoretically for a compressible turbulent mixing layer at constant pressure ($u^* = 0.65$). It is not clear whether the difference between these is due to measurement error or to the fact that the mixing layer solution is not an adequate model for the reversed flow region. Theoretical solutions for turbulent separated flow have not yet been obtained to compare the effect of the wall and finite reversed flow velocity.

Prior to conducting these experiments, it was felt by the author that the details of a separated shear layer would be qualitatively

like those of, say, an injected boundary layer. This was founded on the close correspondence between the integral properties calculated for each of these flows (this result was established by the author in some preliminary unpublished solutions to the turbulent equivalent of the Falkner-Skan equation). To check this suspicion experimentally, the data for massive injection into a turbulent boundary layer[6] was examined and one remarkable difference was found; the dividing streamline velocity ratio for injected boundary layer is very close to 0.5 - much lower than the value of 0.7 determined for the separated shear layer here. This is probably due to the fact that again in the injected boundary layer there is no reversed flow region. Thus, it appears that these two flows are not alike in details such as the actual velocity distribution. It was noted, however, that 5-10 initial boundary layer thicknesses were required for the injected boundary layer to approach a similar flow behavior which is in good agreement with the distance determined for the separated shear layer.

With regard to this question of the similarity variable, $L(x-x_0)$, it was noticed by the author that the velocity profile data, at least for the outer portion of the shear layer, say $u/u_e \geq 0.3$, collapse remarkably well onto a single curve if plotted against the variable $\frac{y-\delta_D}{\delta-\delta_D}$ where δ_D is the distance from the wall to the dividing streamline. This is pure speculation, however, and the length of the shear layer in this test was not great enough to either prove or disprove this hypothesis. Recent theoretical attempts at solutions utilizing integral moment methods[22] also employ a similarity variable much like that hinted at here. Specifically, this other choice is a modified momentum

thickness where the integrand is as in the usual case, but the lower limit of integration is the zero velocity line rather than the usual choice of the wall. Again, because of the step interference problem with the probes, this quantity cannot be estimated accurately to verify the hypothesis.

The more common similarity variable employed in other investigations such as this is the local momentum thickness $\theta(x)$. It is easily shown that for a separating boundary layer this is an improper choice because a simple control volume analysis, with wall shear stresses neglected, gives the result that the momentum thickness of the separated layer is related to the initial momentum thickness by

$$\theta_2 = \frac{\rho_0 u_0^2}{\rho_e u_e^2} \left\{ \theta_0 + \delta_0^* \left(1 - \frac{u_e}{u_0}\right) \right\} \qquad \text{(I-15)}$$

where θ is the momentum thickness, δ^* is the displacement thickness, $(\ )_0$ refers to the edge or initial conditions ahead of the interaction, and $(\ )_e$ refers to the edge conditions behind the separation shock wave (u_e is velocity parallel to wall). This equation was first derived by Paynter[21] and also independently by the author in the simpler form shown. Thus if the edge velocity is a constant (as verified experimentally), then θ_2 would be a constant (note, θ_2 will actually decrease with x since $\frac{d\theta_2}{dx} \approx C_f/2$ and in the reverse flow region the wall friction coefficient, C_f, is negative). Quite obviously, the separated layer is growing more or less linearly with x and thus, the similarity variable should be linear in x. This incidentally points out another difference between this flow and the injected boundary layer where $\frac{d\theta}{dx} = \frac{\rho_w v_w}{\rho_e u_e}$ = constant.

Up to this point, the test for similarity has been made from the observations of two gross features, namely the plateau pressure and the mean velocity profiles. Conversely, the question of similarity could just as well be tested by considering the fine scale behavior as exhibited by the variation in the level of turbulent energy across the layer. This is more or less equivalent to the mean square hot-wire output which was presented in Section I. 4. 3.

Since the length of the transition to similarity is somewhere around eight boundary layer thicknesses and the hot-wire traces are only taken in the range $3.66 \leq \frac{x_0 - x}{\delta_0} \leq 5.6$, true similarity should not be shown, but the approach to similarity might be indicated as with the velocity profile data. As is evident from the profiles of fluctuation intensity shown in Figure I-12, the separated shear is again shown undergoing a redevelopment as it proceeds downstream from the start of interaction and it appears that possibly the outer portion of the layer ($y/\delta \geqslant 0.7$) becomes independent of x faster than the inner portion. Again, the normalization parameter, δ, is not the best choice for indicating similarity as discussed previously in this section.

The fluctuation intensity along the dividing streamline is also displayed in Figure I-12 and it appears as though this may also be approaching a constant value of around 62% of the maximum fluctuation intensity. This does not mean that the turbulent energy of the flow along the dividing streamline is 62% of the maximum level because the sensitivity of the hot-wire to fluctuations varies across the layer. However, for a given wire current the sensitivity is a function only of

the local Mach number* which is becoming a constant along the dividing streamline. Again, it is apparent that it takes more than $5.6\delta_o$ for the fluctuation intensity to become constant which is in agreement with the velocity profile estimate.

As mentioned earlier, there is the suspicion that the shear layer thickness δ used to normalize the distance from the wall is not the proper choice due to residual effects of the finite undisturbed boundary layer. Since two independent measurements were made the parameter y/δ can then be eliminated by cross-plotting the data from Figures I-10 and I-12. The resultant graph is shown in Figure I-13 where the fluctuation intensity is plotted as function of velocity ratio and distance from start of interaction. Plotted in this manner, the approach to similarity is more noticeable than in previous forms even though the various curves are not markedly different. For instance, for the high speed portion of the layer, say $u/u_e \geq 0.5$, the development of the layer as it progresses downstream is easily seen and the two most downstream stations are almost identical in these coordinates. This is a definite indication of similarity occurring in a transition distance of closer to 5.5 boundary layers and further exhibits the weakness of the assumed similarity parameter δ. Unfortunately, this method does not indicate a better choice and the determination of a better similarity parameter must await future work.

The qualitative hot-wire spectral data displayed in Figure I-14, although it does indicate a definite difference with regard to attached

---

* The Reynolds number $Re_T = \frac{\rho u d}{\mu_T}$ for a constant pressure flow is only a function of the Mach number.

and separated flows, is inconclusive as far as showing an approach to similarity other than that all separated spectra are very much alike in appearance.

In summary, the following points regarding the question of a similar flow have been indicated from the data discussed this far.

1. The separated shear layer does appear to be approaching a similar type of flow especially in the high speed region of the shear layer ($u/u_e \gtrsim 0.5$).
2. The transition distance from the start of interaction to approximately a similar flow is around 8-10 initial boundary layer thicknesses.
3. From the dividing streamline velocity measurement it appears that the high speed region of the shear layer might be adequately represented by a semi-infinite half jet model. The velocity profile measurements were not comprehensive enough to verify this point, however.
4. The compressible mixing on the low speed side of the shear layer appears to be inherently different from that of injected boundary layers.

With regard to the small scale of the experiments and the conclusions drawn from them regarding a similar behavior, a certain degree of criticism is justifiable. In spite of this, the indications presented here point the way to future studies regarding the similarity of turbulent supersonic separated flows in general.

I. 5. 3 A Model for the Unsteady Separation Behavior

The relatively low frequency unsteadiness associated with the separation process, detected here by the shock wave motion and by Kistler[13] from wall pressure measurements, becomes important when one considers the unsteady aerodynamic forces that can be exerted on a surface as a result of this. Measurements conducted near the separation point show that the R. M. S. pressure coefficient fluctuation can be quite high (upwards of 4%[14]). However, two other important pieces of information regarding these fluctuations have not been explained previously to the author's satisfaction, namely the characteristic frequency of the motion and the extent of the region over which these fluctuations are correlated. The latter is necessary in order to make estimates of the unsteady forces exerted on the surface of an aerodynamic structure, and the former is important in order to evaluate the response of this structure to these unsteady forces, i. e., the frequency response.

Quite naturally, it would be an enormous task to test experimentally all geometrical shapes over a wide range of Mach number and Reynolds number to determine these characteristics. A much more efficient procedure is to find out what causes the unsteady behavior and from this and some experimental data formulate a model with which one could predict the magnitude and frequencies of the unsteady forces.

The fluctuating wall pressure in front of a forward facing step has, over the past five years, received some attention and a typical example of the R. M. S. pressure distribution is shown in Figure I-28

(from Speaker and Ailman[15]). This R.M.S. wall pressure distribution can be separated into two distinct regions; the first is the rather sharp peak about 4.1 step heights from the step face* and is due to the motion of the separation point about its mean position; the second is the roughly constant fluctuating pressure level under the separated shear layer which previously has been attributed to the turbulence activity in the separated layer.[13] The separated portion has been most extensively treated by Speaker and Ailman[15] who conducted spectral and R.M.S. pressure measurements in this region at a free stream Mach number of 3.5 and correlated their data with the work of Coe[14] and Kistler.[13] The separation point motion was first observed by Kistler[13] and was measured in this thesis via the separation shock motion in sufficient detail so that a model for the low frequency unsteadiness could be formulated.

One of the more important results of this investigation was the observation that the unsteady behavior of separation was most likely due to acoustic oscillations within the separated flow region. This was first noticed when it was found that the frequency of motion of the shock wave (which is caused by motion of the separation point) varied inversely with the step size. This is shown in Figure I-26 where the reduced frequency of the motion, or the Strouhal number $\equiv \frac{fL}{a_T}$, is seen to be nearly independent of the step height-to-boundary layer thickness ratio. As mentioned in Section I.4.5 the reduced frequency

---

* The length of the separated region for the experiments of Speaker and Ailman is some 50% longer than the scaling law given here and by Zukoski.[16] The nominal value of 4.1 step heights given above occurs at 6.5 step heights in front of the step for this data only.

has a value of 0.256 and, within experimental error, is quite close to a value of 0.25 and is interpreted as a standing 1/4 cycle acoustic wave present in the subsonic cavity. By analogy, this is equivalent to the fundamental mode of vibration of, say, an open ended organ pipe with the open end corresponding to the separation point.

Note also that this variation in shock frequency with stepheight eliminates the probability of a resonant acoustic wave existing in the cavity that propagates transverse to the mean flow direction, i.e. reflecting off of the sidewalls of the wind tunnel.

An acoustic mode of oscillation was first considered by Kistler[13] but rejected because he did not detect a strong low-frequency energy concentration within the separated region. The experiments by Speaker and Ailman[15] do show several strong energy concentrations and with the evidence cited herein, it was necessary to verify the measurements conducted here before formulating a model.

The spectral measurements conducted in the inviscid flow region behind the separation shock wave as shown in Figure I-18 confirmed the shock oscillation frequency measurement. The appearance of a weak signal near the reduced frequency value of $f/f_0 = 3$ was additional evidence that the acoustic wave model is valid since the next mode of oscillation for this model is at three times the fundamental mode.

To show that the shock motion was indeed coupled to the motion of the separation point, the spectra of the wall pressure fluctuations immediately downstream of the separation point[15] were also plotted on Figure I-18. The correspondence between these is remarkable in

light of the fact that the two experiments were conducted at different Mach numbers and different h/δ. This, and the second peak in the spectra at $f/f_0 = 3$, is further indication of an acoustic mode of oscillation.

At this point, the author must apologize for the use of the crude organ pipe analogy to model the standing wave pattern within the separated region. Admittedly, one cannot expect too much from the comparison of a one-dimensional model to the very complicated acoustic vibration of even a simple triangular shaped area which, even with the simplest of boundary conditions, has not yet been theoretically solved to the author's knowledge. The comparison seems even more remote when the problems of reflection and refraction of acoustic waves by the turbulent shear layer are considered. The fact that the one-dimensional model can explain some of the gross features of the oscillation such as the resonant frequencies does justify its use if only for conceptual purposes. It is believed that the complications mentioned above, along with the turbulent noise, are the reason why the peaks in the spectra shown in Figure I-18 are rather broad and of low magnitude compared to sharp, high peaks for tuned oscillator spectra.

The acoustic model hypothesized above also explains qualitatively the shape of the majority of the R. M. S. pressure distribution shown in Figure I-28. The first initial peak near the separation point ($x/h = 6.5$) is due to the oscillation of the steep pressure gradient region and its general shape can be estimated from assuming $p(x/h, t) \approx \overline{p}(x/h) + A[d\overline{p}/d(x/h)].\cos \omega t$ where A is the amplitude of the

the motion and ω is its frequency. Computing the R. M. S. pressure level from this gives

$$\mathcal{C}_p(x) \propto \frac{A}{M_0^2} \frac{d\bar{p}}{dx} \qquad \text{(I-16)}$$

in the vicinity of the separation point. For the separated region, the pressure fluctuations are caused by noise radiated from the shear layer and transmitted through the subsonic region and superposed upon the low amplitude standing 1/4 cycle acoustic wave for which the pressure envelope is a 1/4 cycle sine wave increasing from the level at separation to a maximum at the step face.

Near the step face, $x/h < 2$, this model as described so far, fails to account for the steeper rise in pressure fluctuation level as indicated in Figure I-28. In considering this, the wall pressure spectra in this region shows a distinct peak at $f/f_0 \approx 12$ (see Figure I-28). This peak is not related to a longitudinal standing wave because it corresponds roughly to the 11th or 13th harmonic and one would not expect this harmonic to receive a disproportionate amount of energy when little or no energy is apparent in the 5th, 7th, or 9th harmonics. It was then realized that another standing wave oscillation parallel to the step face could also be excited for which the characteristic length would be the step height as opposed to cavity length. Computing the Strouhal number, $\frac{fh}{a_T}$, for this peak frequency gives a value very close to 0.50 which corresponds to a 1/2 cycle standing wave. This, again by analogy, is equivalent to the fundamental mode of vibration of a closed orgon pipe and seems intuitively correct since one would expect the shear layer to act somewhat like a reflector to acoustic waves in

the vertical direction.

This distinct peak due to a vertical standing wave is also apparent in the spectra taken in region 3 ($2 < x/h < 4.5$) although at a slightly higher frequency due to the decreased height of the cavity. Depending on the phase shift between these two separate modes of oscillation (parallel and perpendicular to the wall) and their relative frequencies, the pressure waves from each of these can be either additive or subtractive. This might account for the slight dip in R.M.S. pressure near $x/h \approx 2$ and the gradual rise in R.M.S. pressure as the step face is neared.

Concerning the representative spectra of wall pressure fluctuations given in Figure I-28, the shift in the fundamental longitudinal mode frequency in regions 1 and 3 to a value of some 60% of the predicted value (which is verified in regions 2 and 4) is inexplicable at the present time.

Since the unsteady behavior associated with separation and the subsonic cavity has been shown to be the result of acoustic oscillations, the question arises as to what is the driving mechanism that supplies the energy that is lost due to viscous forces and the possible transmission of energy through the shear layer with resultant radiation into the supersonic flow.[32] This source must be a broad band distribution of energy since various frequencies are excited depending on oscillation mode and step size. The only source of broad band energy available is the turbulent energy in the approaching boundary layer and separated shear layer, but it is not clear whether this energy enters the cavity at the separation point, the reattachment point, or over the

length of the separated region. It is speculated that the reattachment point is important with regard to this point in view of the relatively high amount of energy contained in the standing acoustic wave parallel to the step face which is quite localized in extent and does not cause any observable motion of the separation point.

Having asserted the acoustic wave model from data taken for forward facing steps, the question of the existence and prediction of this phenomenon for other geometries such as separation caused by ramps or shock waves, or more generally any flow field that contains a subsonic cavity adjacent to a supersonic flow, naturally arises.

With regard to separation caused by ramps, to the author's knowledge the only fluctuation data involving a large separated region is that by Coe[14] who measured $\tilde{p}$ for turbulent boundary layer separation in front of a 45° ramp. From his preliminary data it is evident that the R.M.S. pressure distribution is very much like that for a forward facing step and because of this, the same acoustic oscillation described before is believed present.

For both shock induced separation and rearward facing step separation the data of Speaker and Ailman[15] is used since it contains some spectral measurements. For the shock separation, the spectra show two distinct peaks one of which is close to $\frac{fL}{a_T} = 0.5$ using a very crude estimate for the length of cavity, L. This is intuitively correct from the model standpoint inasmuch as both separation and reattachment can move to some extent. For the rearward facing step data, the spectra show distinct peaks near $\frac{fh}{a_T} = 0.5$ and 1.0 which correspond to vertical standing waves at the step face, and a diffuse peak near $\frac{fL}{a_T} \approx 0.25$

which corresponds to a longitudinal standing wave. The acoustic modes for each of these cases is not as well defined as for the forward facing step case due to the high energy loss through the downstream reattachment point.

It might be worthwhile at this point to mention that an oscillation caused by a modulation of the mass stored in the separated cavity and variations in the mass influx rate at the reattachment point was considered by the author at one time. Using a very simple model for this mechanism, it was seen that small perturbations were stable and that the motion was strongly overdamped which would rule out the oscillating behavior observed. A mechanism of this type was considered by Trilling[34] with regard to laminar boundary layer separation due to an impinging shock wave.

It is also interesting to note that the acoustic phenomenon described here is analogous to the flow over rectangular cut-outs in aerodynamic surfaces[19] except for the fact that coherent acoustic waves have never been detected visually in the inviscid flow region or in the separated cavity. This last point was another reason why acoustic oscillations were previously discounted.[13] The measurements conducted here with regard to the shape of the shock surface show that the shock motion is not correlated over the span of the tunnel which implies that any acoustic waves radiated through the separated shear layer are also not correlated across the span of the tunnel. This is why these acoustic waves cannot be detected by conventional visual means.

I.6 Conclusions

(1) The static wall pressure distributions in front of a forward facing step in supersonic turbulent flow were obtained and the effect of step height to boundary layer thickness ratio determined insofar as the plateau pressure and maximum pressure gradient are concerned.

(2) The approach to a self-similar flow has been established from velocity profile data and use of the hot-wire anemometer. The relaxation distance to a self-similar flow is estimated to be in the range of 5.5 to 9 initial boundary layer thicknesses and is apparently independent of Mach number.

(3) Measurements of the fluctuating quantities within the separated shear layer near the self-similar region were obtained and are shown to be about a factor of two greater than a flat-plate boundary layer at the same edge Mach number.

(4) The low frequency unsteadiness associated with the finite length separated region was studied by observations of the separation shock motion and an acoustic model is proposed that predicts the resonant frequencies and distribution of fluctuating wall pressures to some degree. This model is used to interpret the wall pressure spectral measurements conducted at a different Mach number and Reynolds number.

(5) The use of relatively short hot-wires ($\ell/d \sim 100$) has been shown feasible in light of a theoretical discussion that accounts for effects of end losses.

In light of the results of the experiments reported here the following related experimental investigations are suggested;

1) a more thorough investigation of the question of a similar flow for the separated shear layer. This requires a step size much greater than the local boundary layer, say, $h/\delta_0 \approx 10$;
2) an investigation of the flow field in the separated region concentrating on both the mean velocity distribution and the fluctuating velocity distribution. The means by which this should be accomplished is unclear, but the use of the hot-wire anemometer as a mean flow instrument could be exploited with some effort;
3) a thorough investigation of the effects of both Mach number and step height on the unsteady behavior for forward facing steps and other geometries such as ramps and backward facing steps.

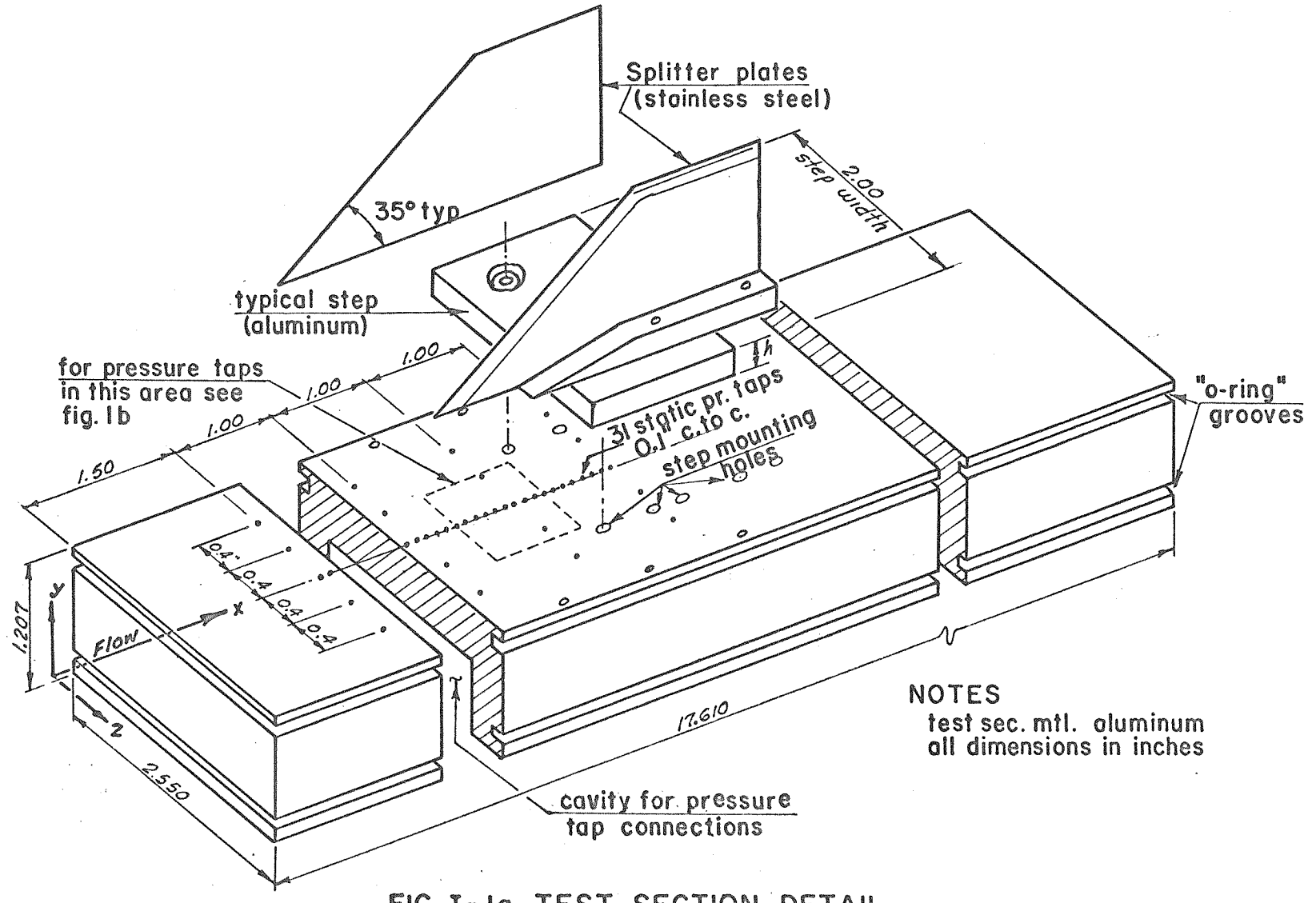

FIG. I-1a TEST SECTION DETAIL

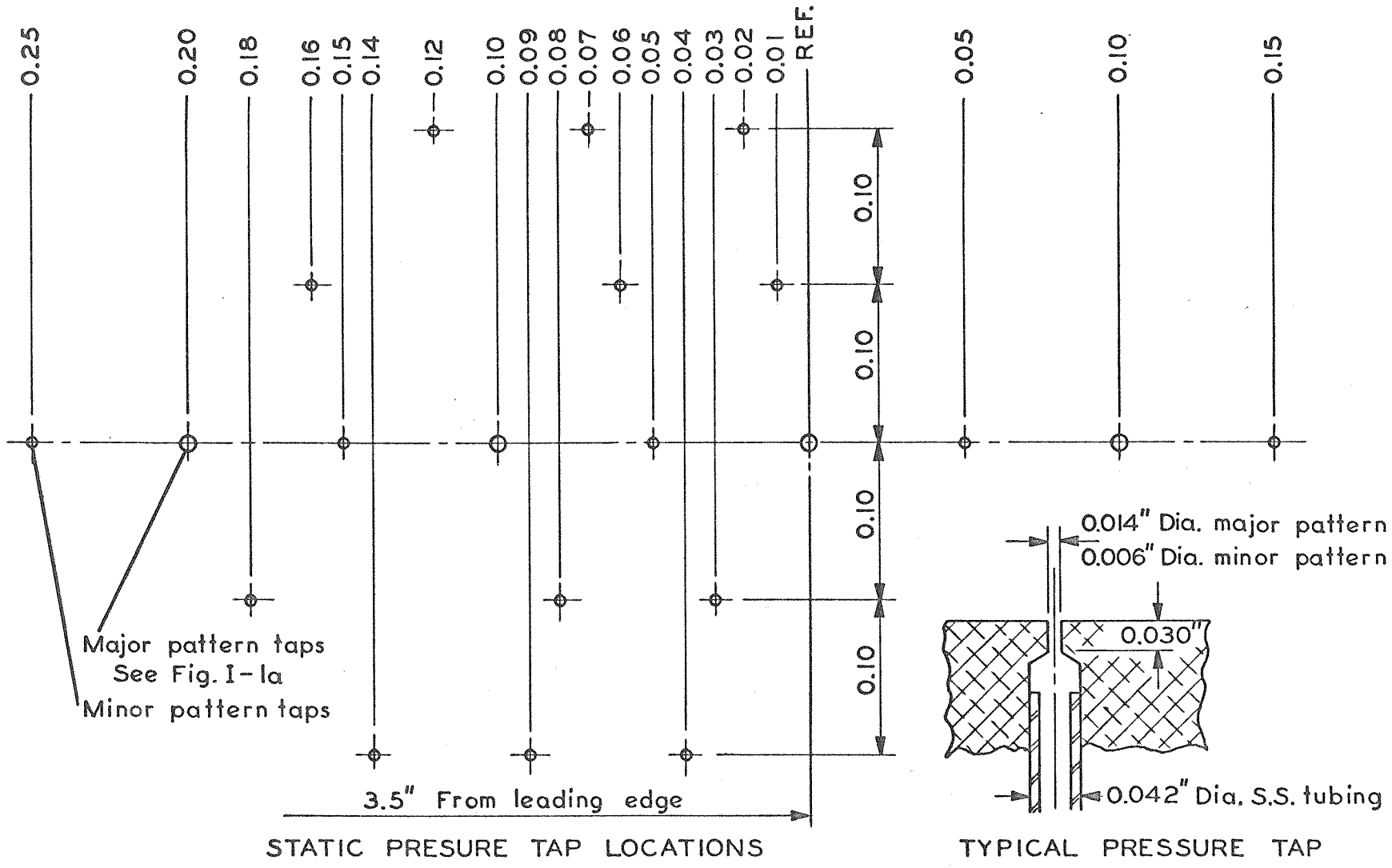

FIG. I-1b TEST SECTION DETAILS

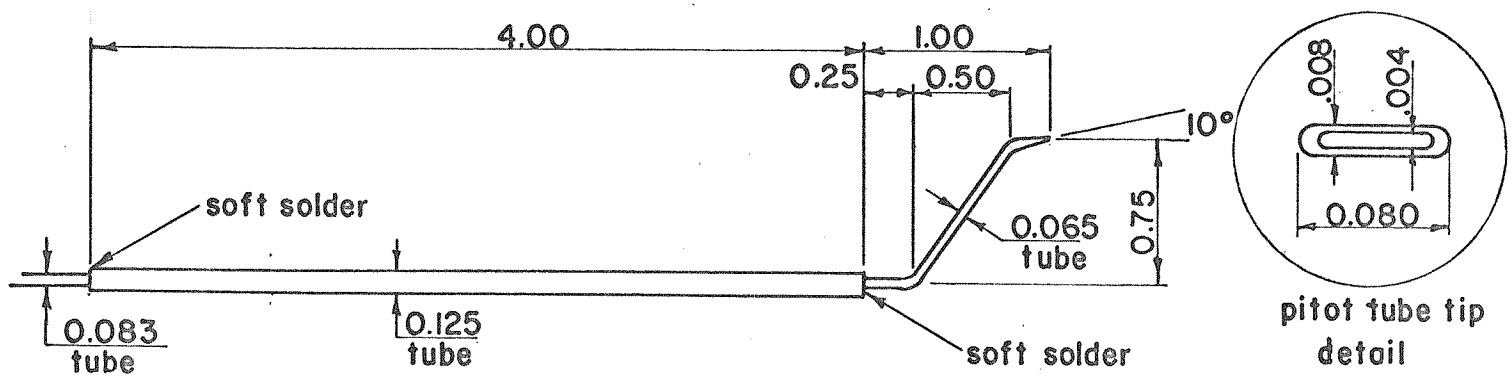

PITOT TUBE DETAIL

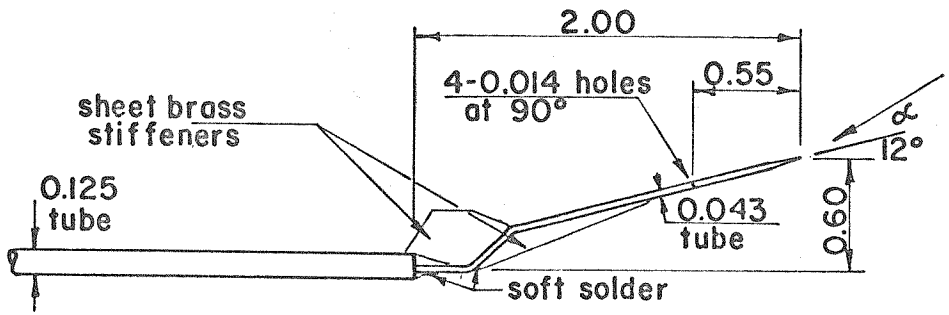

STATIC PRESSURE PROBE DETAIL

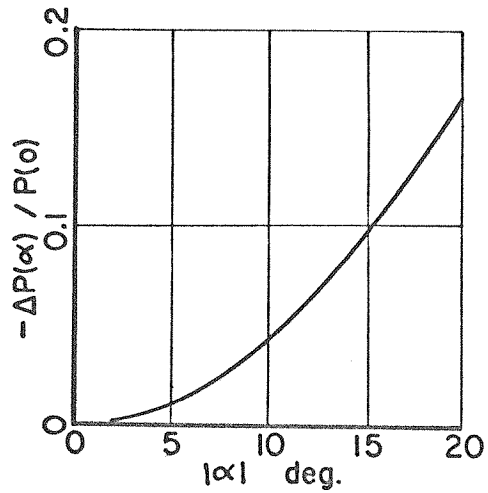

angle-of attack characteristics
of static pressure probe

FIG. I-2 PROBE DETAILS

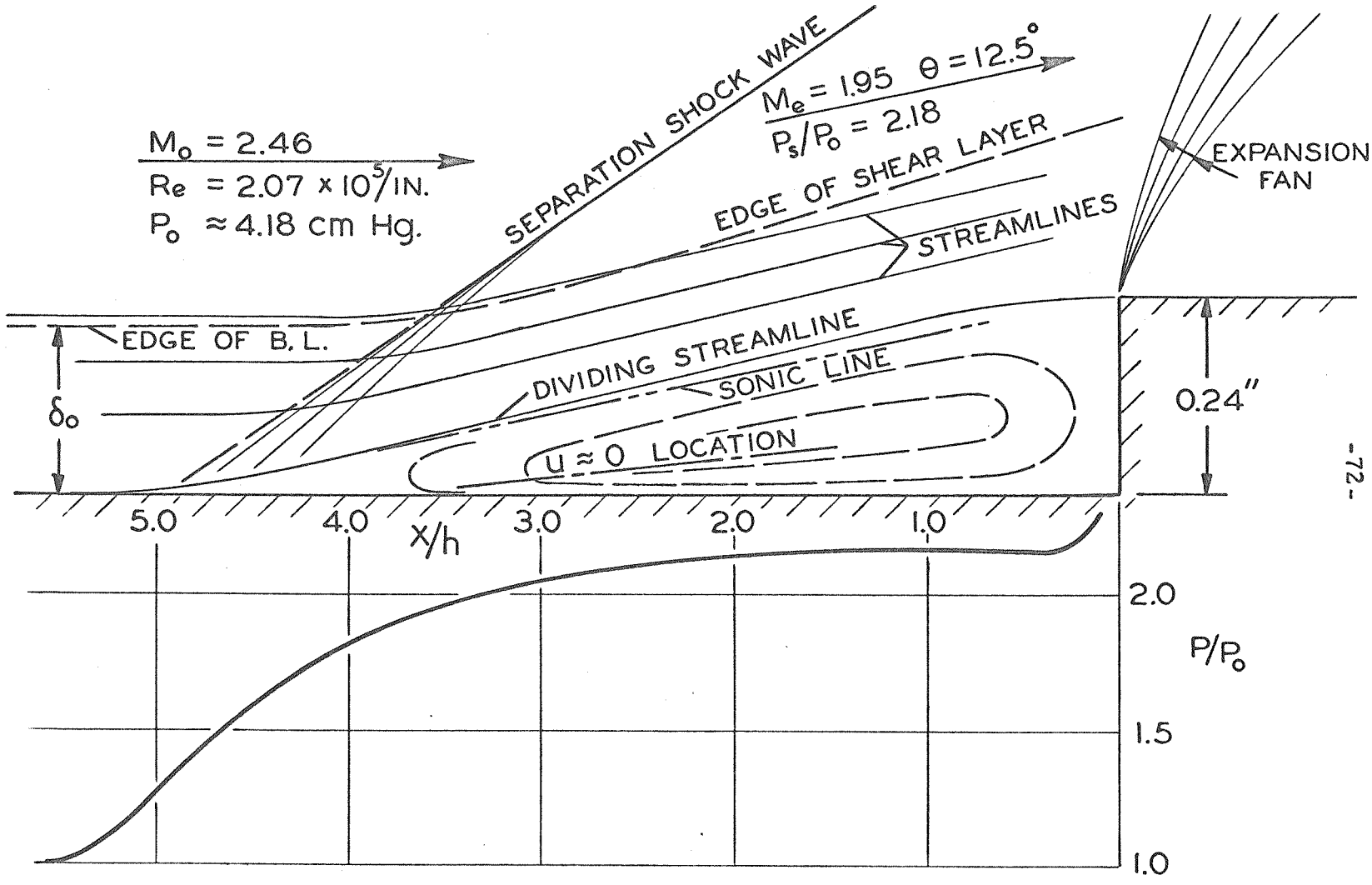

FIG. I-3 SCHEMATIC OF FLOW FIELD AND TYPICAL WALL PRESSURE DISTRIBUTION

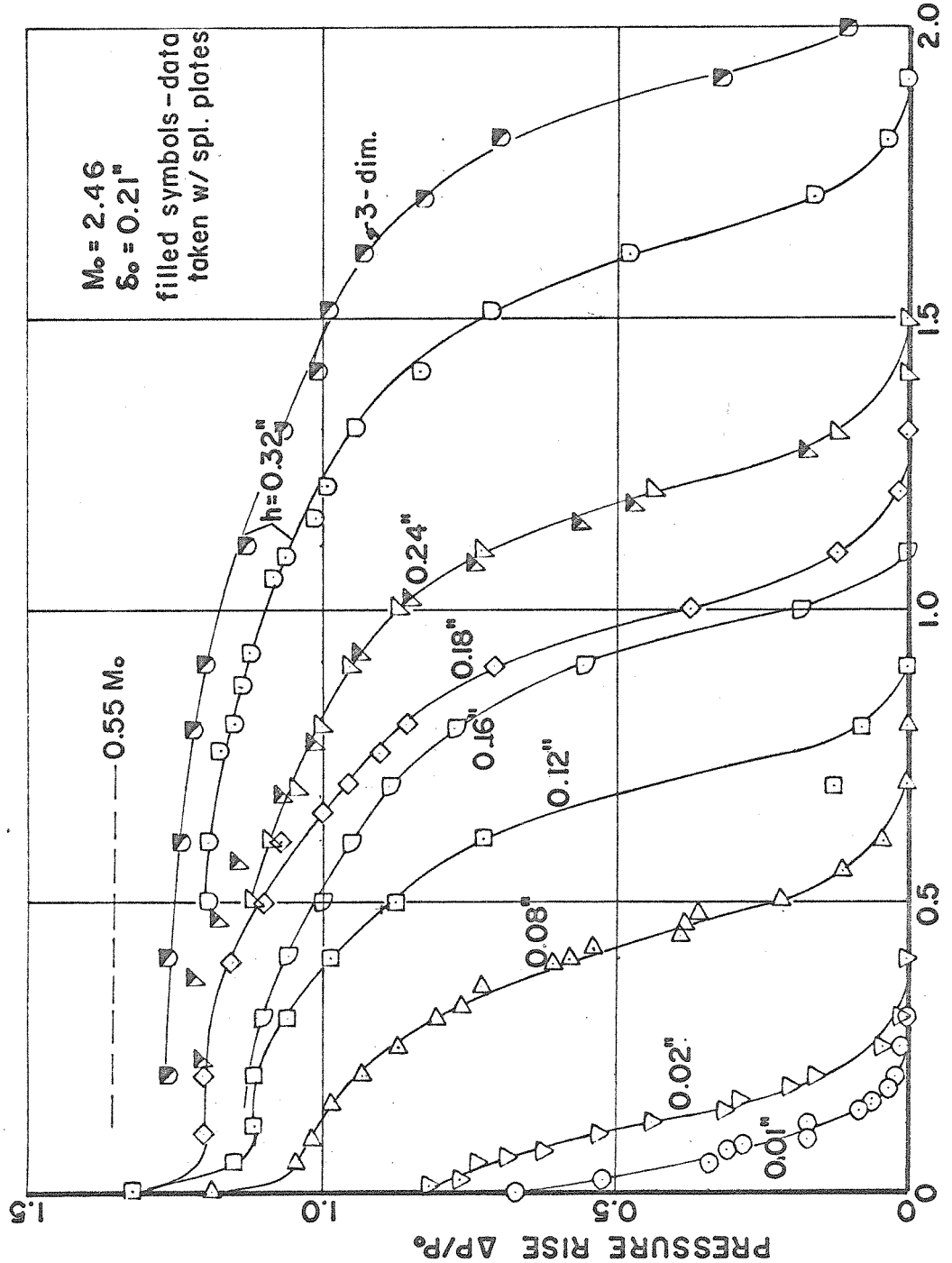

FIG. I-4 PRESSURE RISE IN FRONT OF NORMAL STEPS

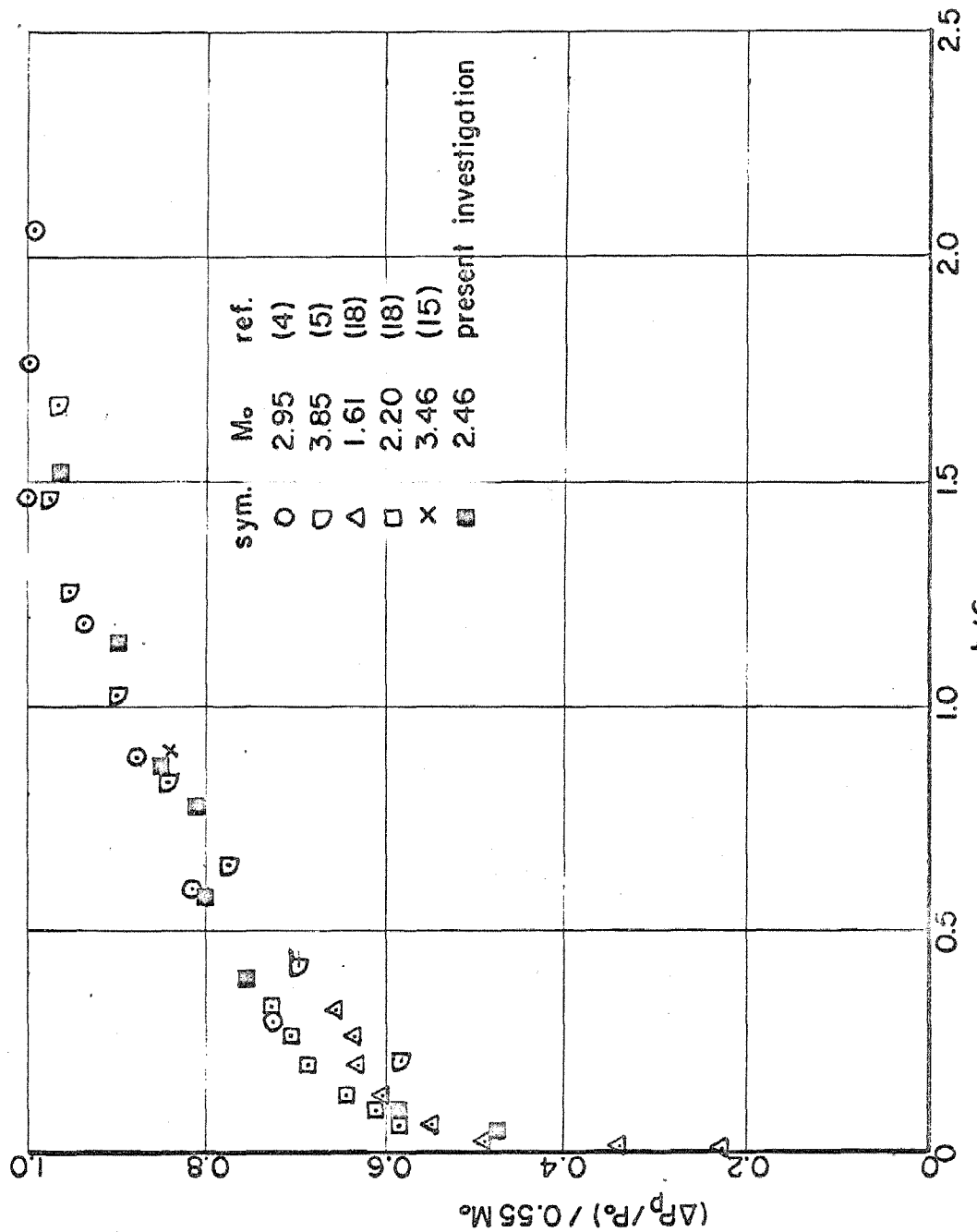

FIG. I-5 NORMALIZED PLATEAU PRESSURE AS FUNCTION OF STEP HEIGHT

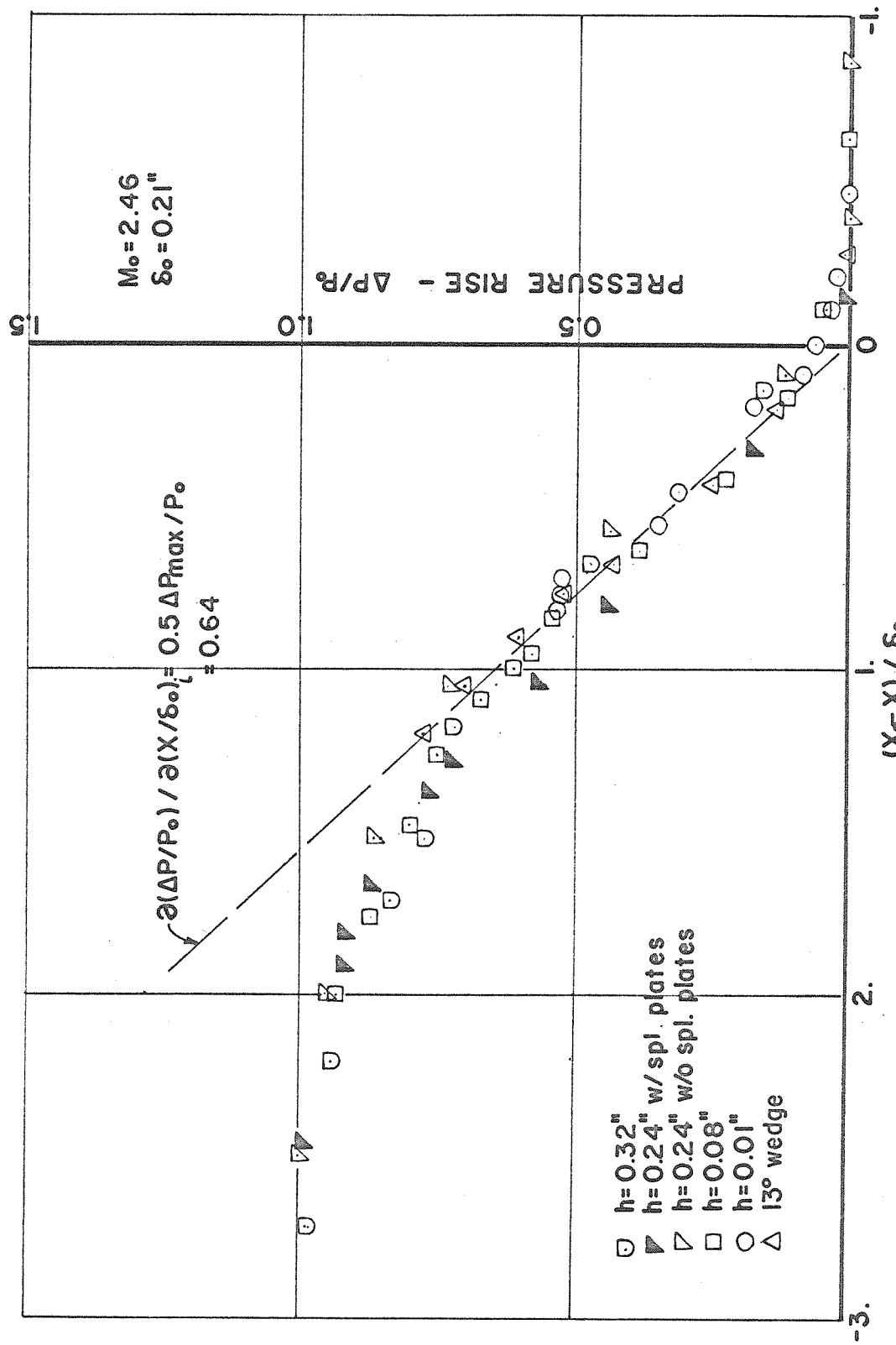

FIG. I-6 INITIAL PRESSURE RISE DISTRIBUTION

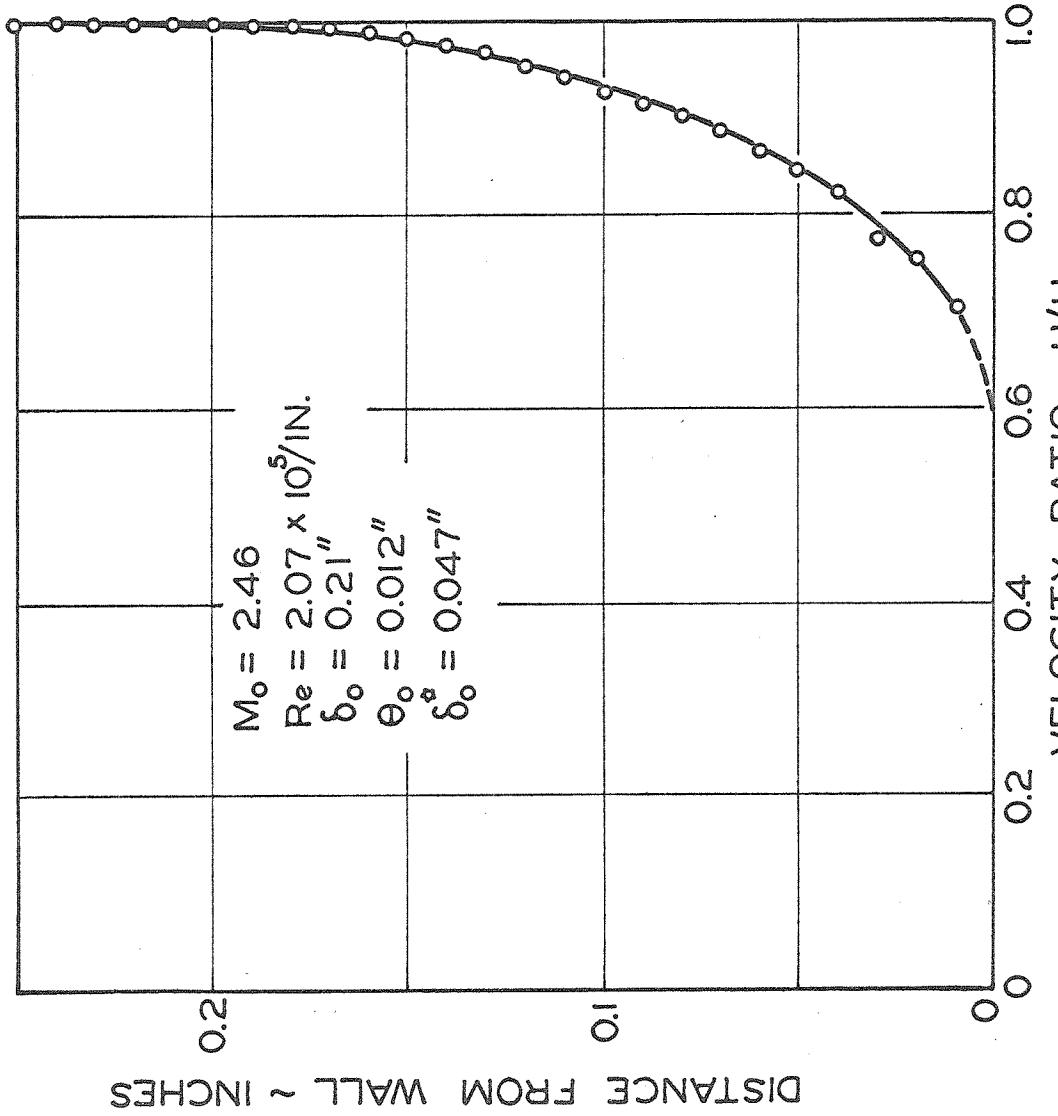

FIG. I-7 VELOCITY PROFILE - APPROACHING BOUNDARY LAYER

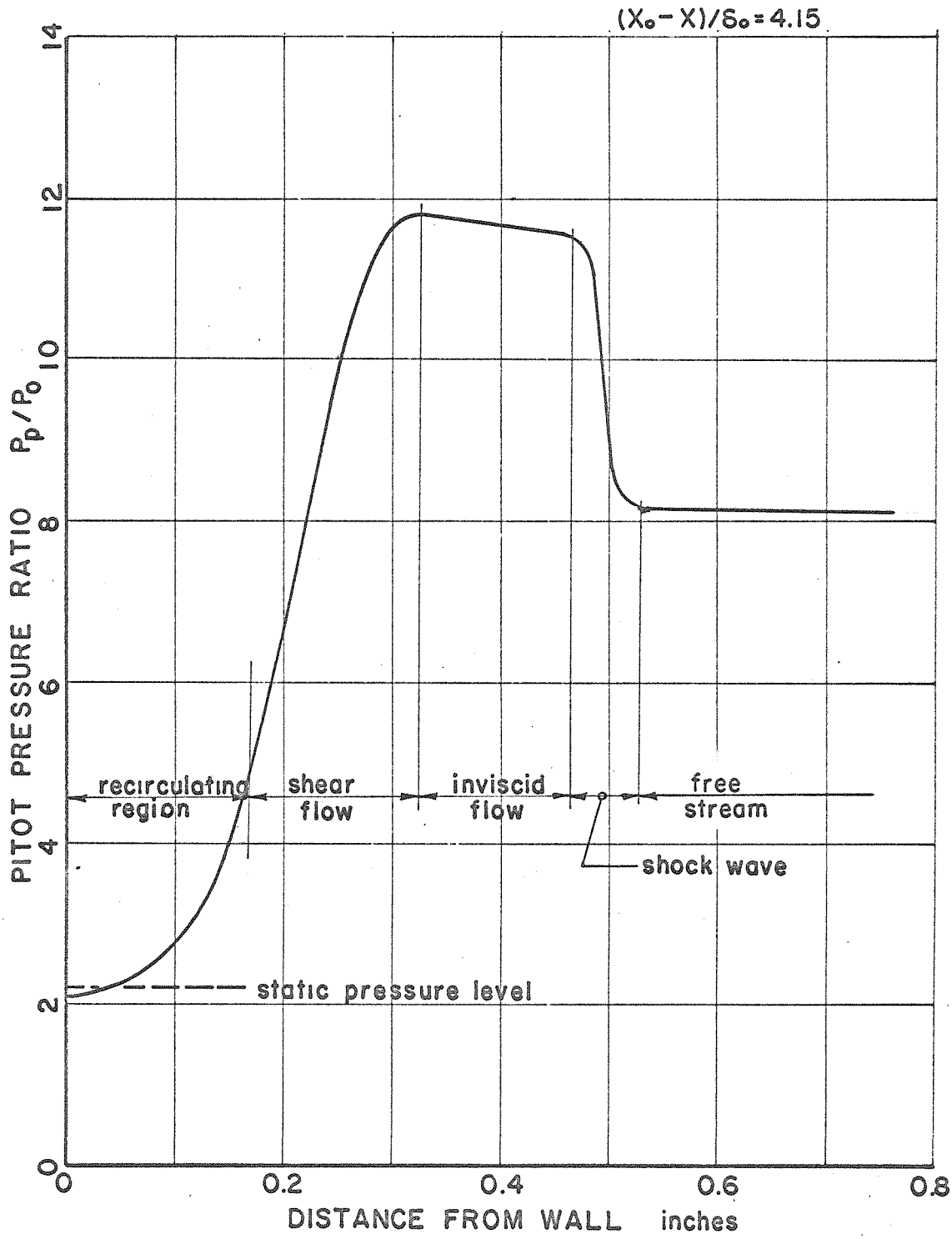

FIG. I-8 TYPICAL PITOT TUBE TRAVERSE

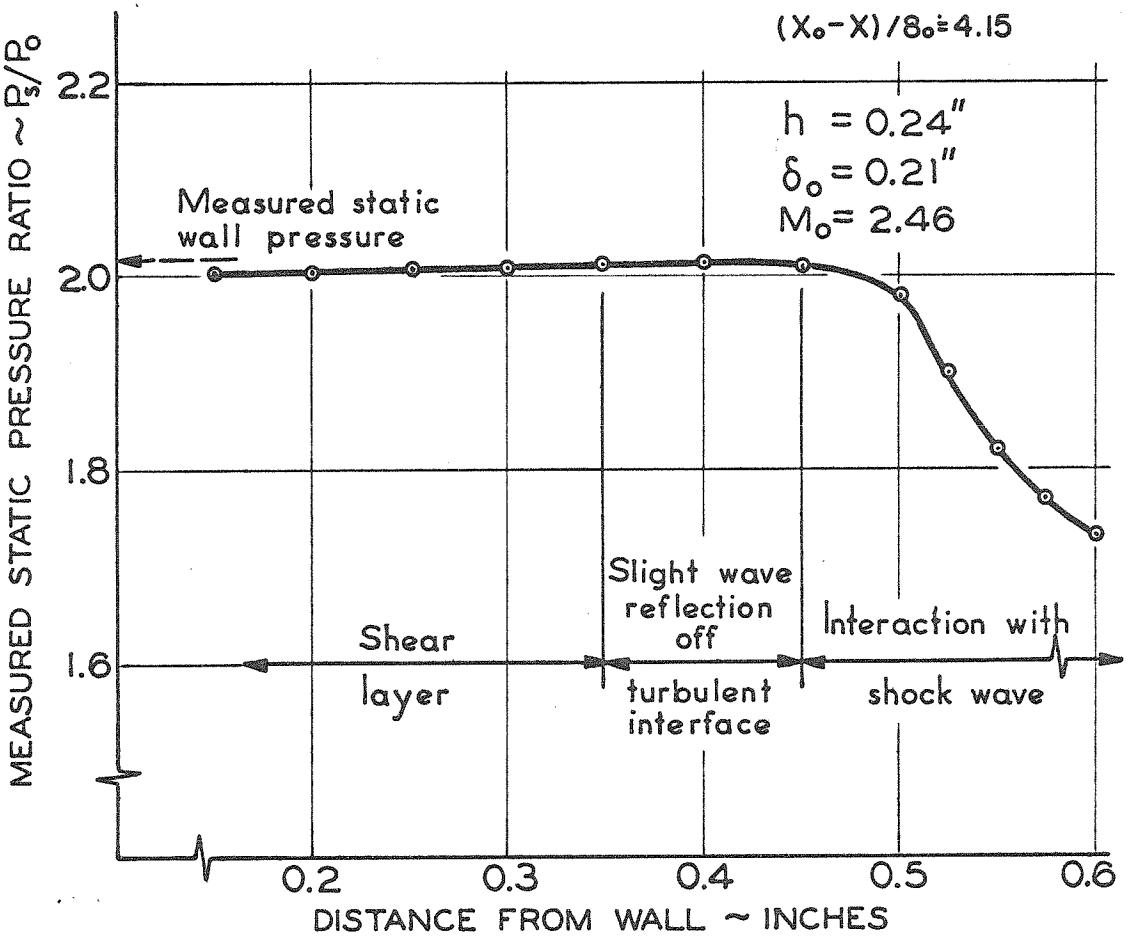

FIG. I-9 TYPICAL STATIC PRESSURE TRAVERSE

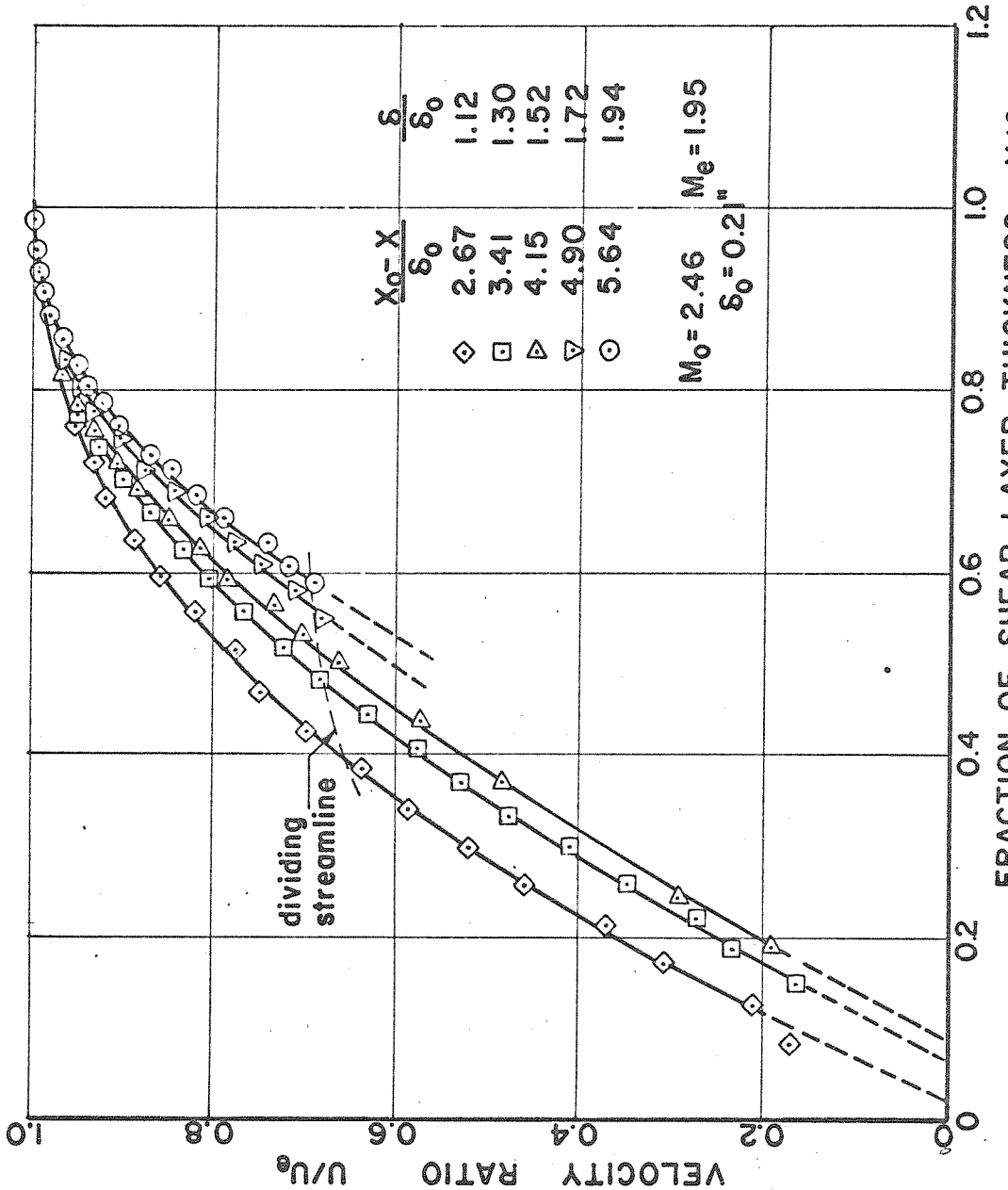

FIG. I-10 VELOCITY PROFILES - SEPERATED FLOW

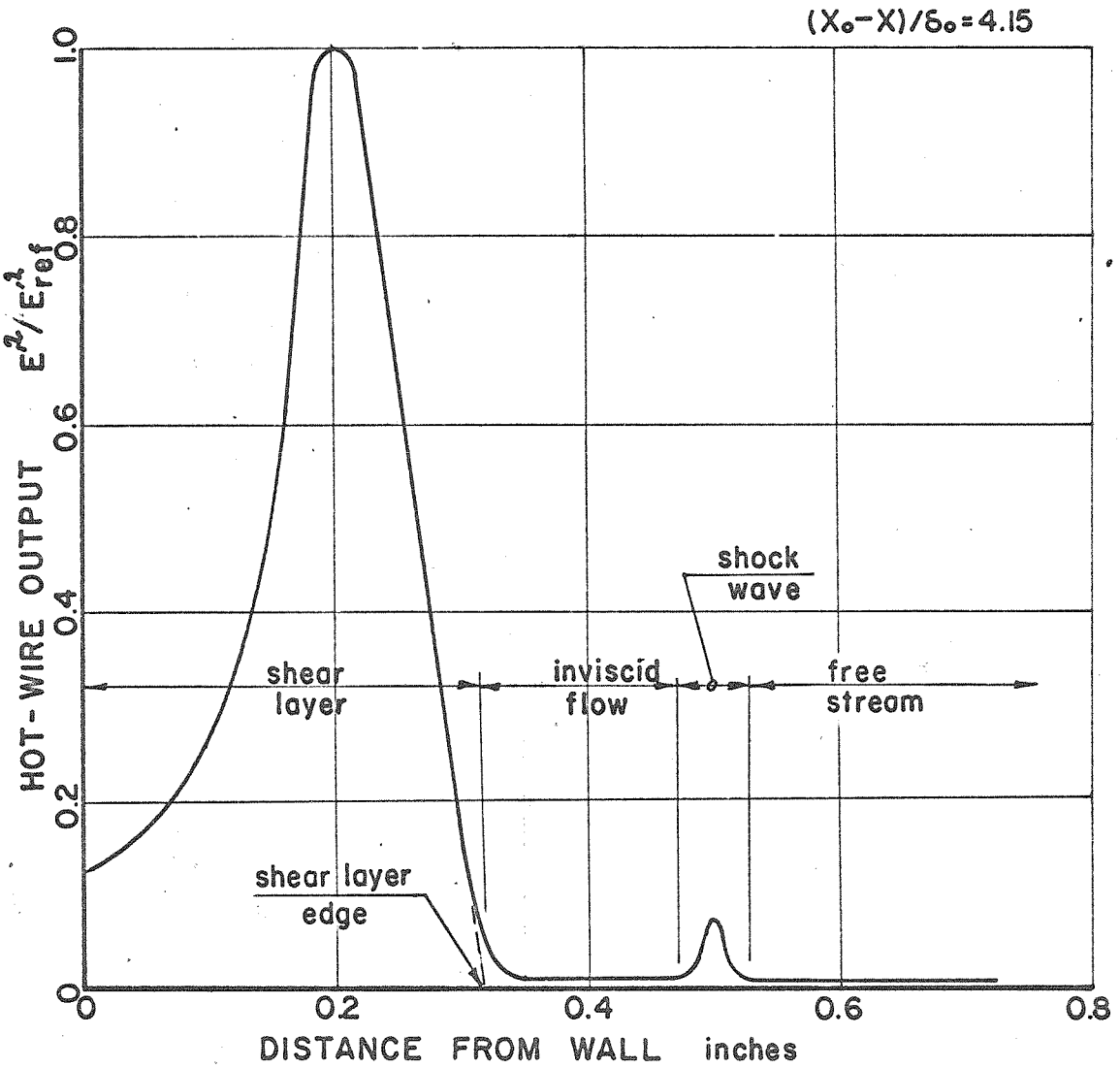

FIG. I-11 TYPICAL HOT-WIRE OUTPUT TRAVERSE

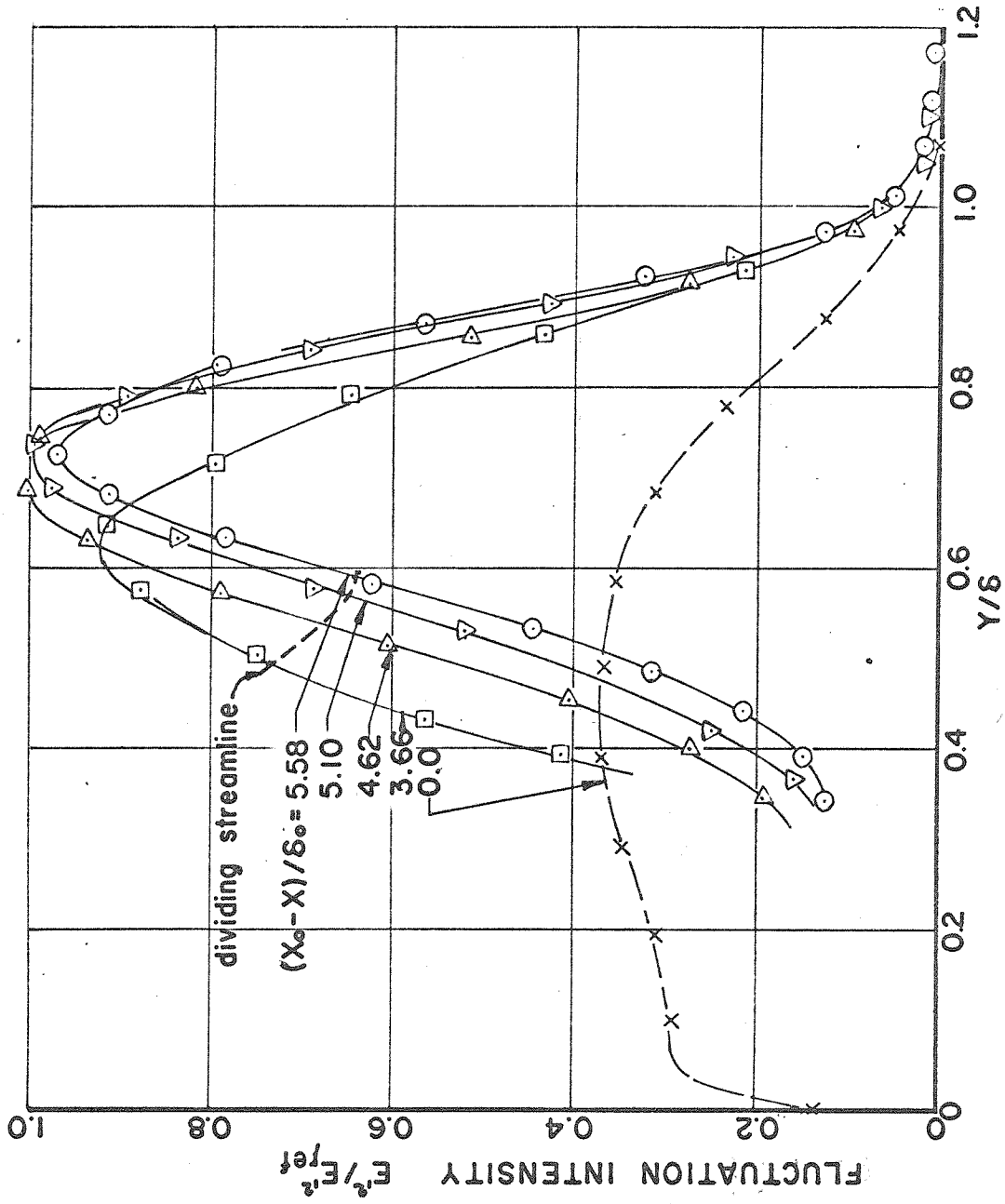

FIG. I-12 SHEAR LAYER HOT-WIRE OUTPUT PROFILES

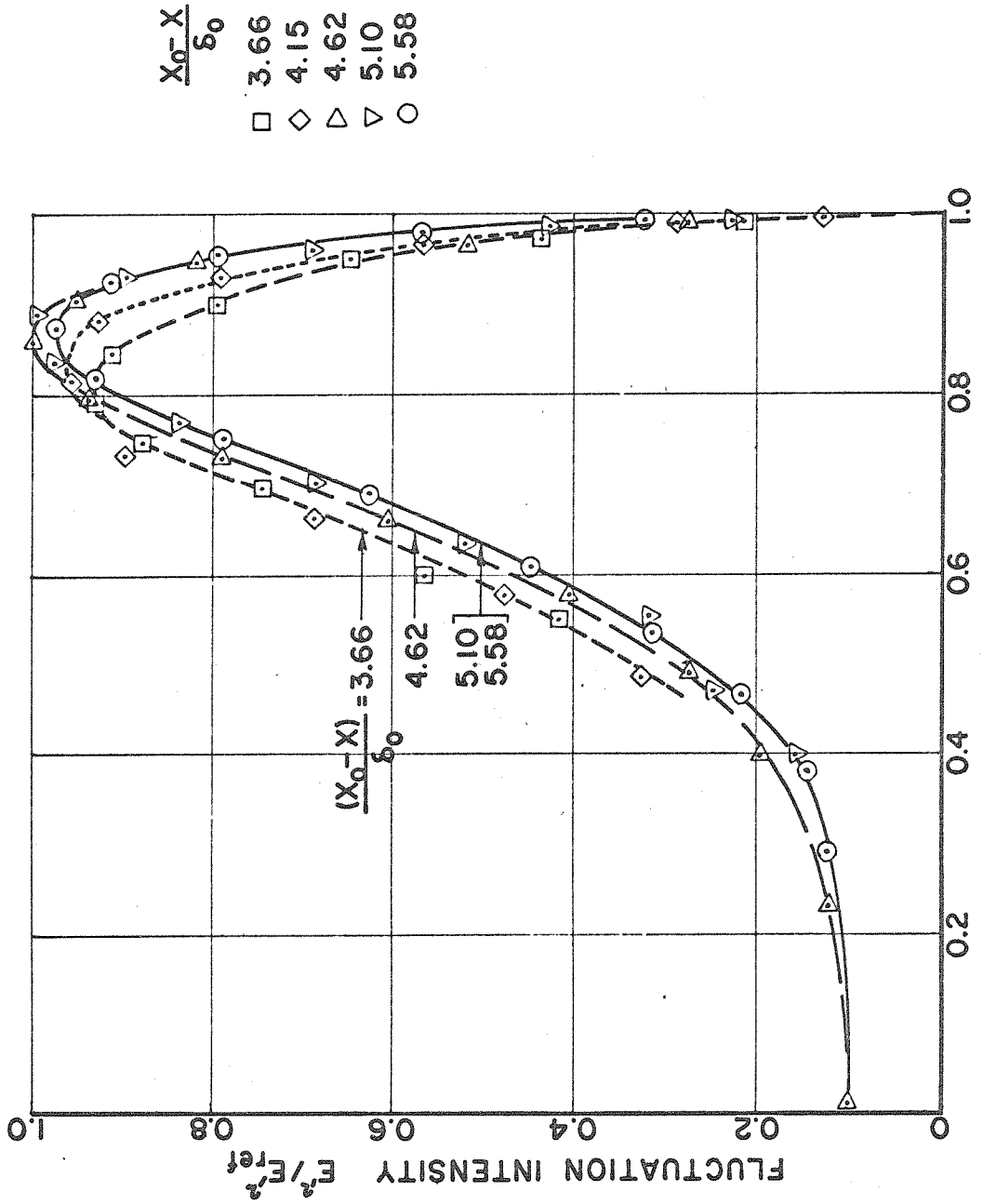

FIG. I-13 APPROACH TO SIMILARITY OF SEPARATED FLOW

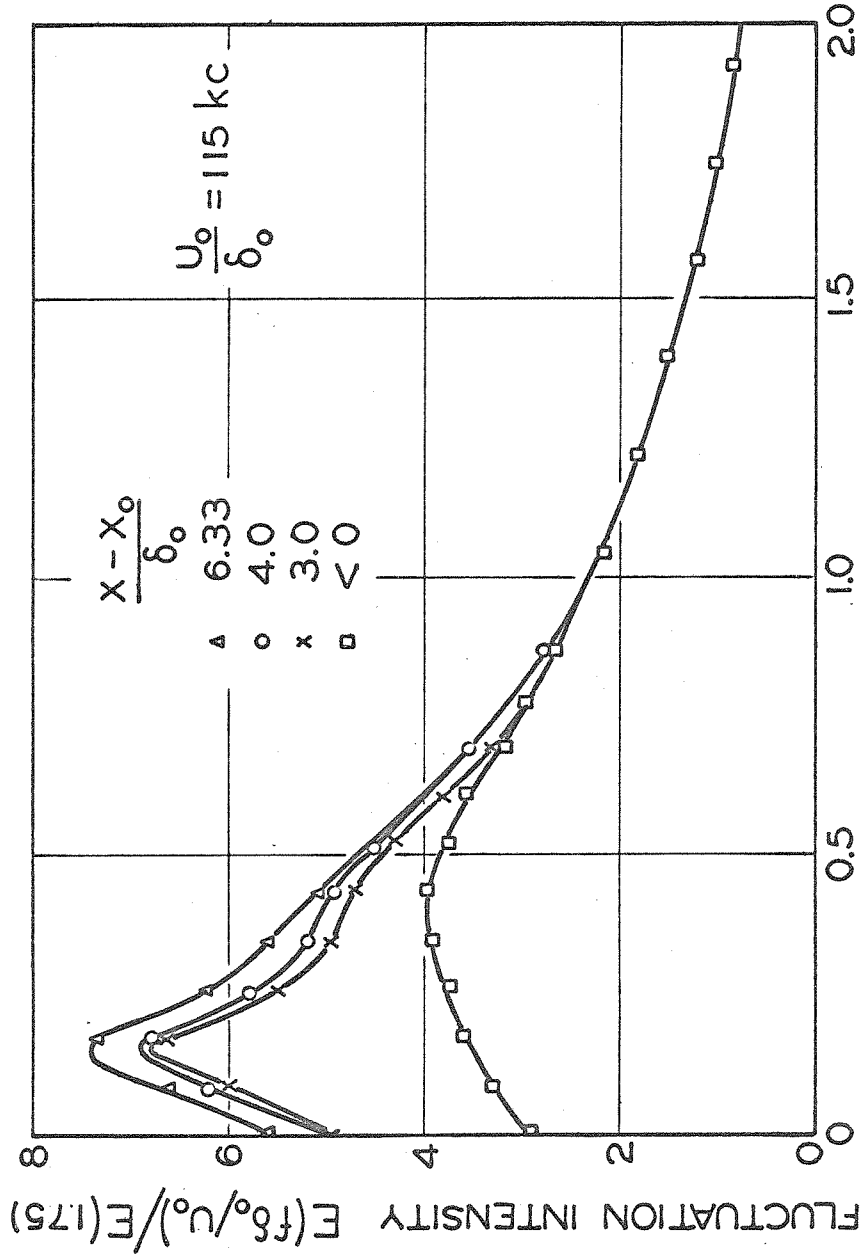

FIG. I-14 TURBULENT SPECTRA AT MAXIMUM SIGNAL LOCATION

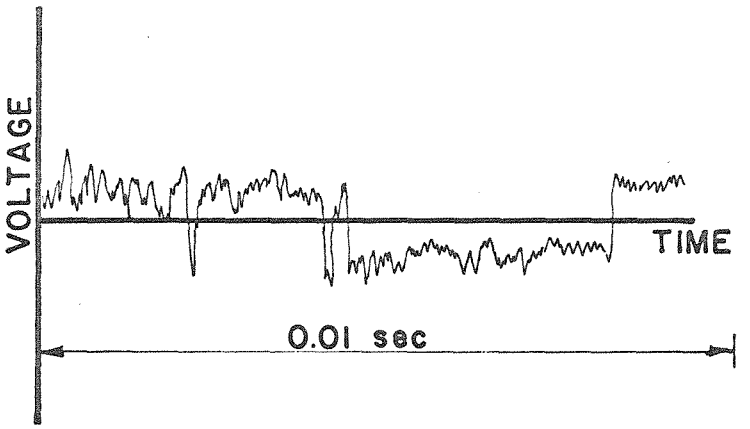

TYPICAL OSCILLOGRAM OF AMPLIFIED HOT-WIRE OUTPUT WHEN IN SHOCK WAVE LIMITS

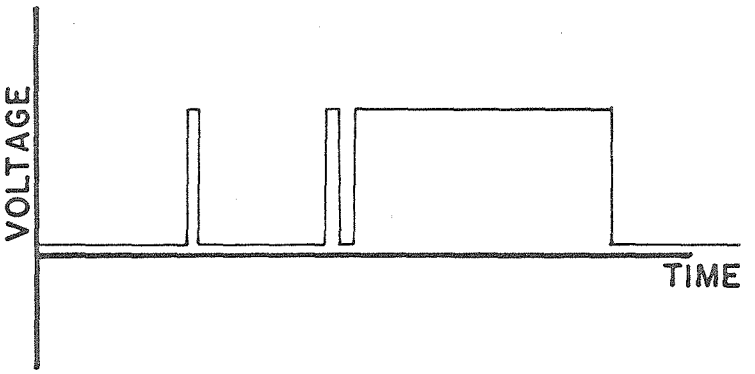

OSCILLOGRAM OF INTERMITTANCY METER OUTPUT FOR ABOVE SIGNAL AS INPUT

FIG. I-15 TYPICAL HOT-WIRE OUTPUT AT MEAN SHOCK LOCATION

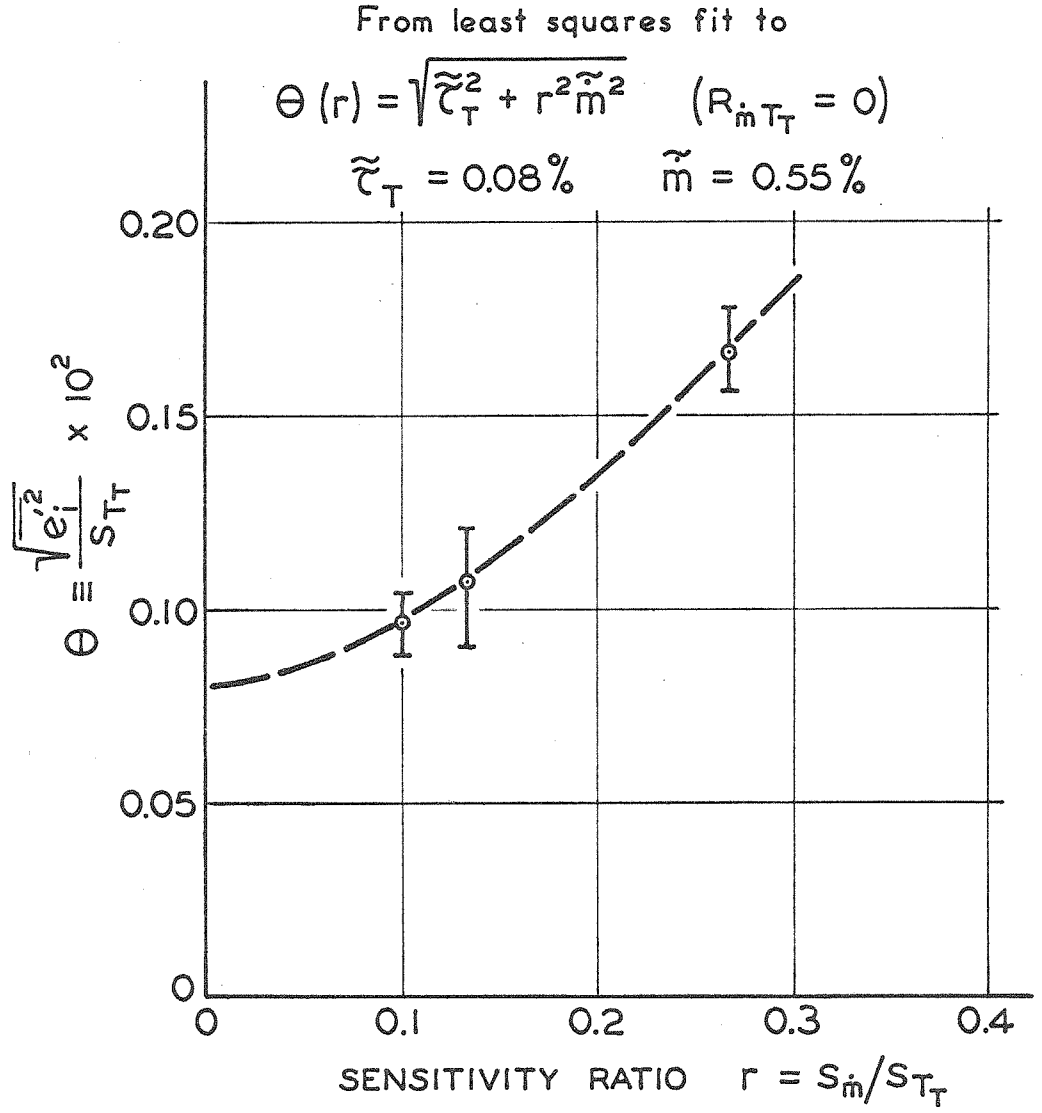

FIG. I-16 FLUCTUATION DIAGRAM - FREE STREAM

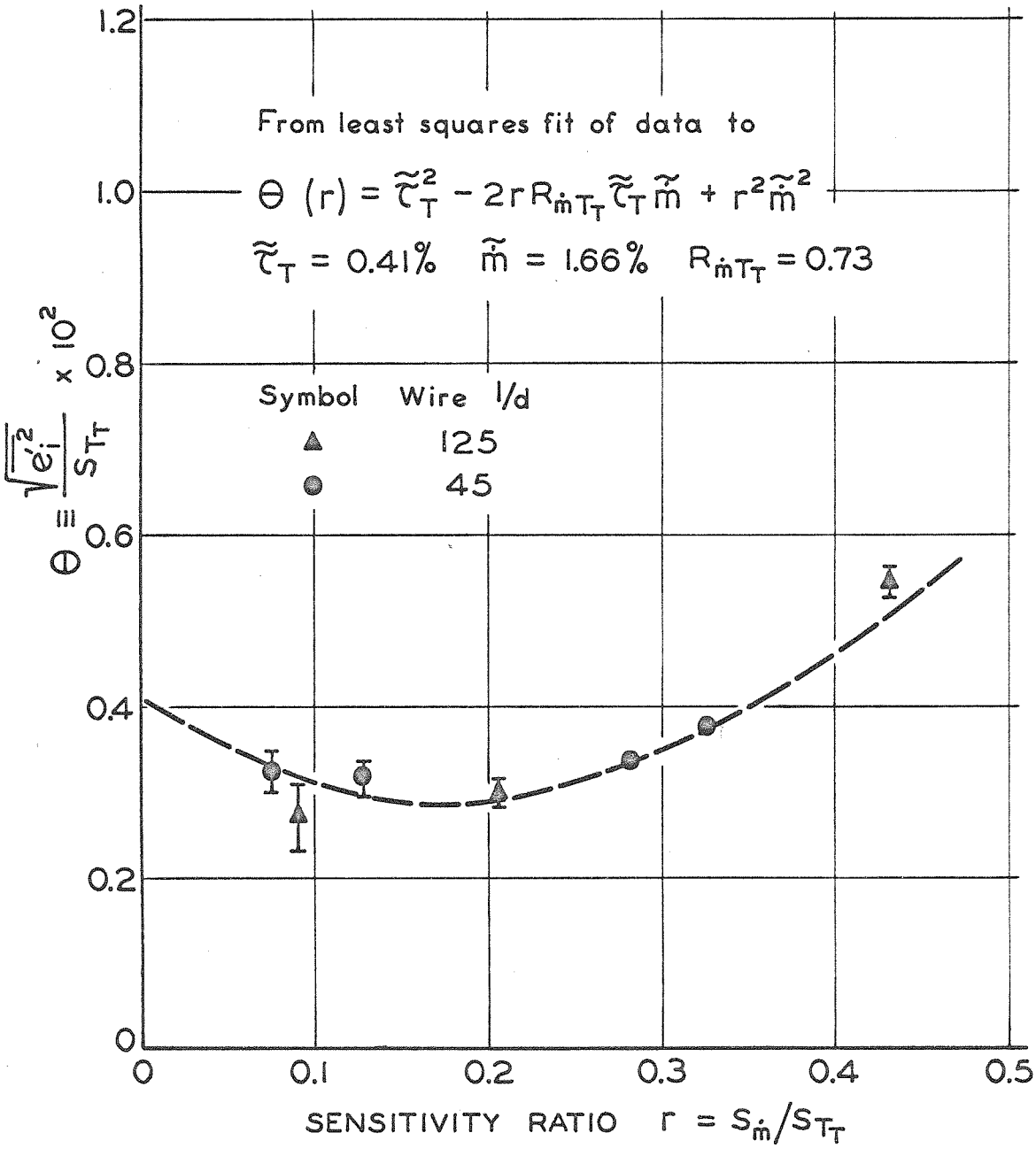

FIG. I-17 FLUCTUATION DIAGRAM - BEHIND SEPARATION SHOCK WAVE

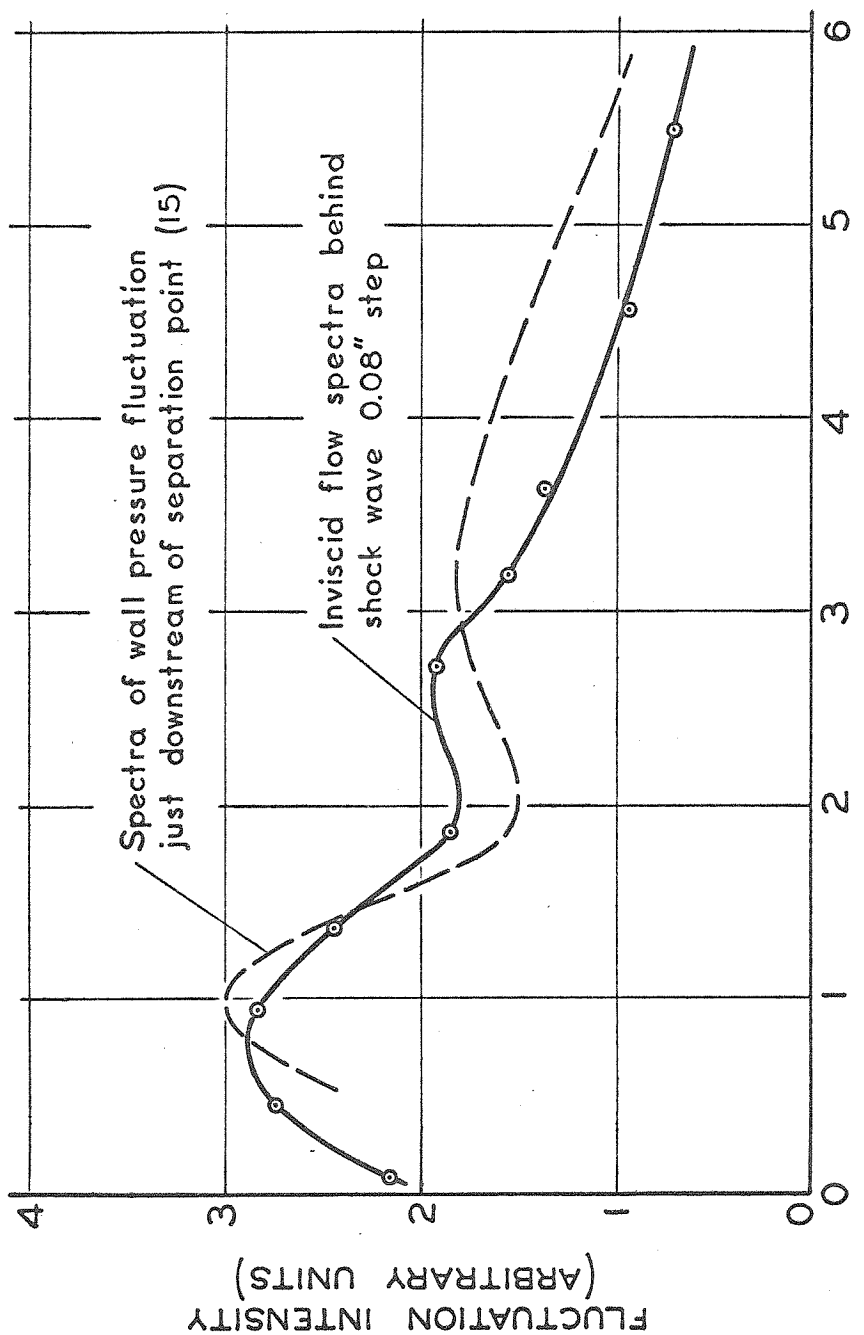

FIG. I-18 FLUCTUATION SPECTRA BEHIND SEPARATION SHOCK WAVE

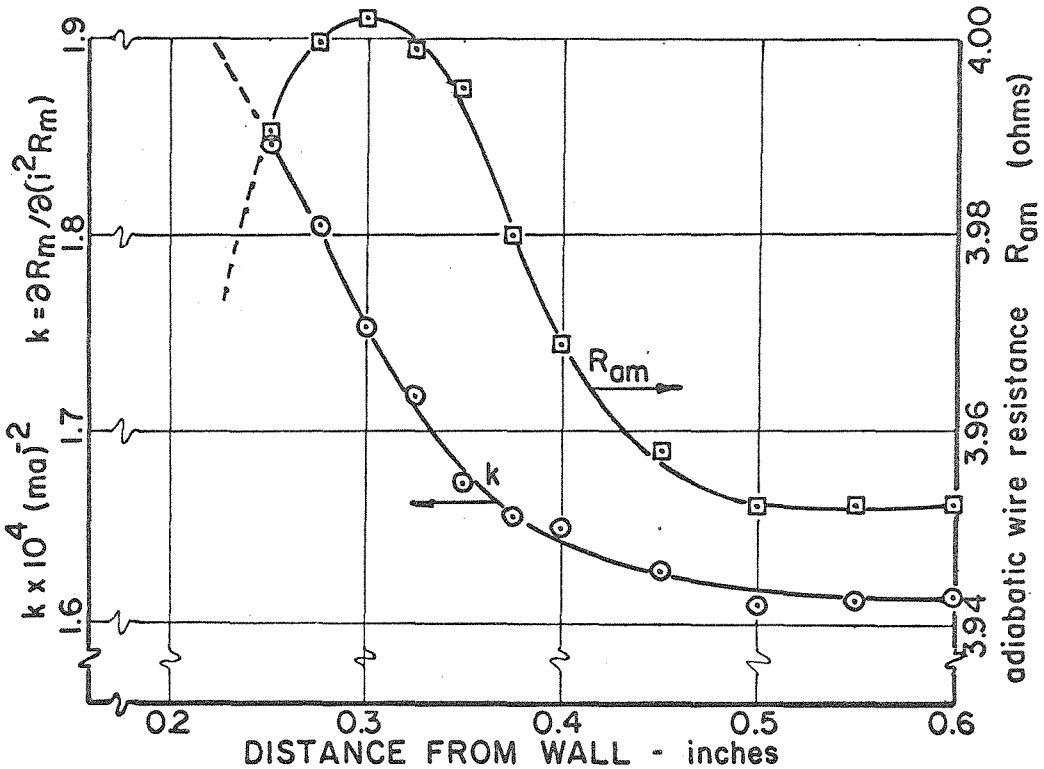

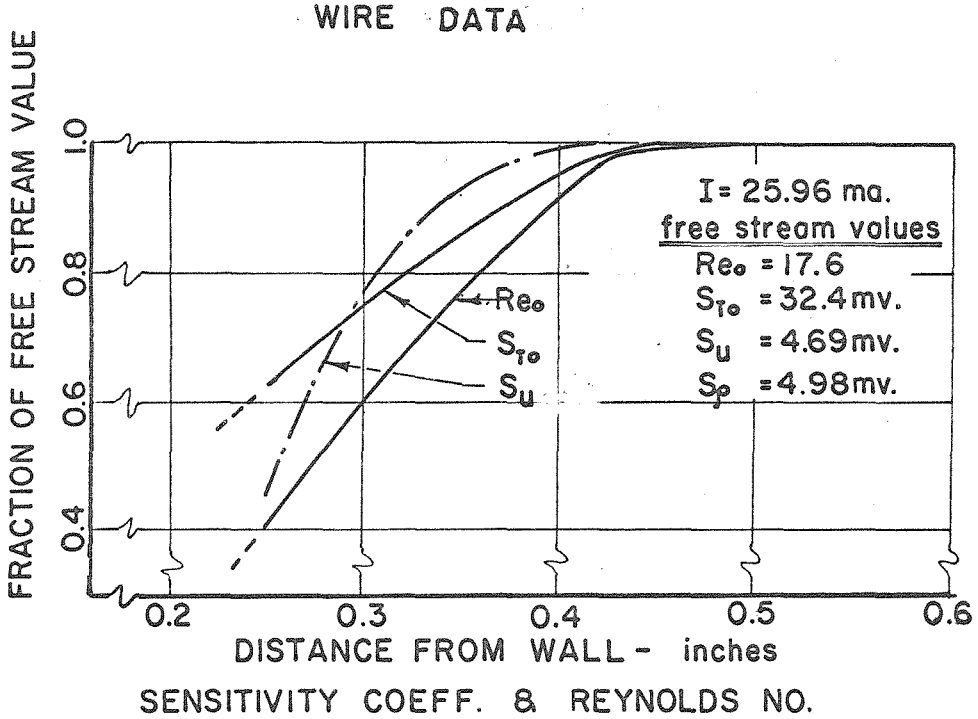

FIG. I-19 WIRE PROPERTIES ACROSS SHEAR LAYER

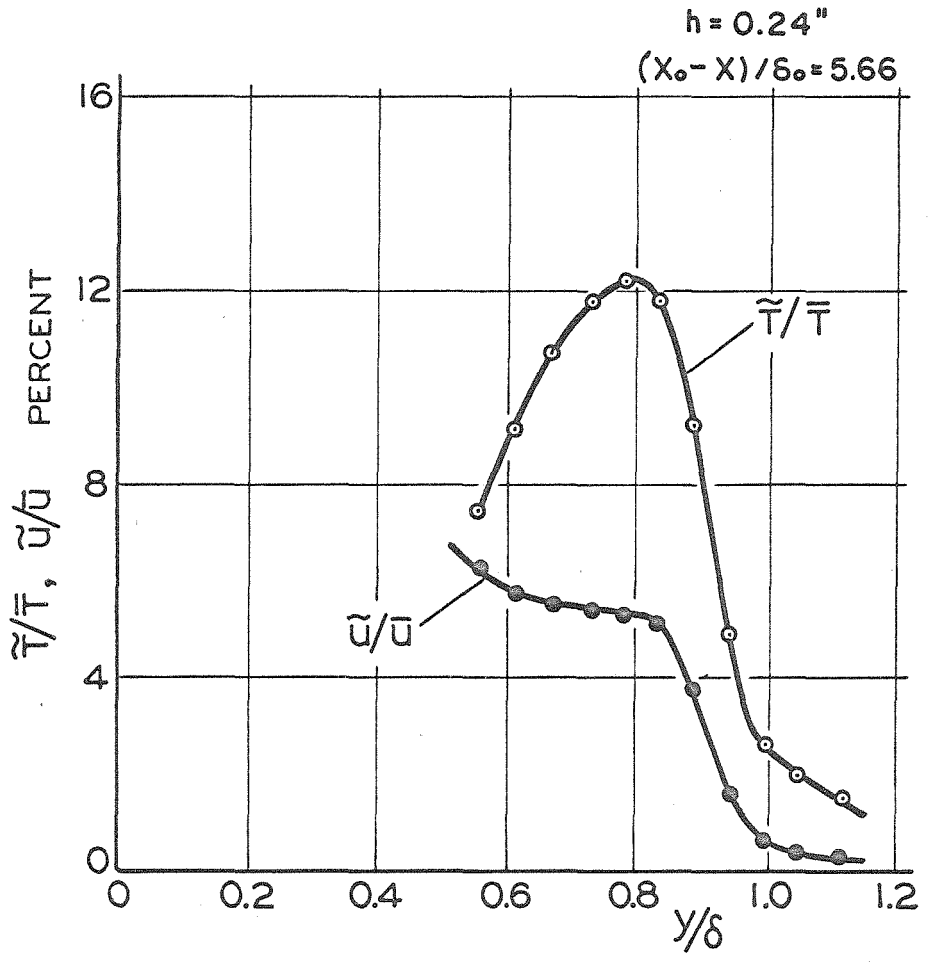

FIG. I-20 FLUCTUATION MEASUREMENTS IN SEPARATED SHEAR LAYER

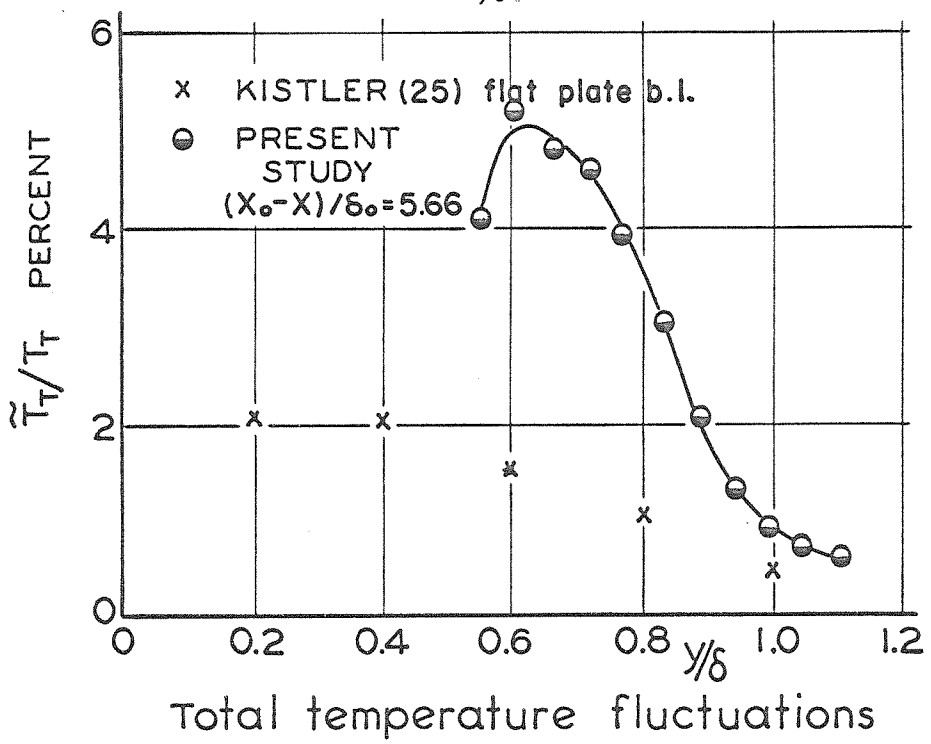

Total temperature fluctuations

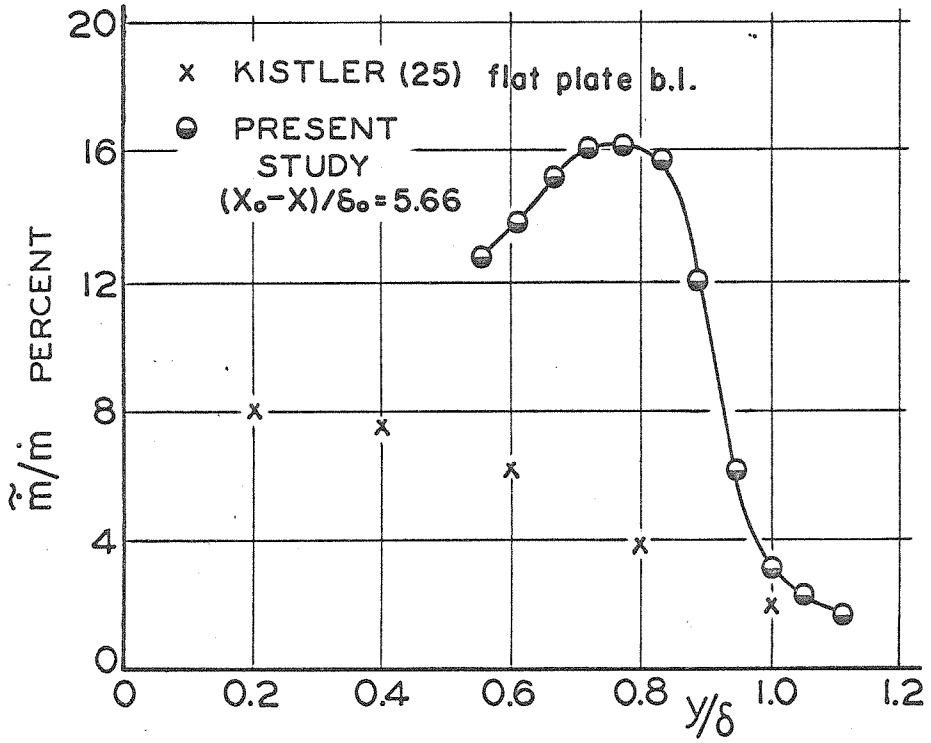

Mass flow fluctuations

FIG. I-21 FLUCTUATION MEASUREMENTS IN SEPARATED SHEAR LAYER

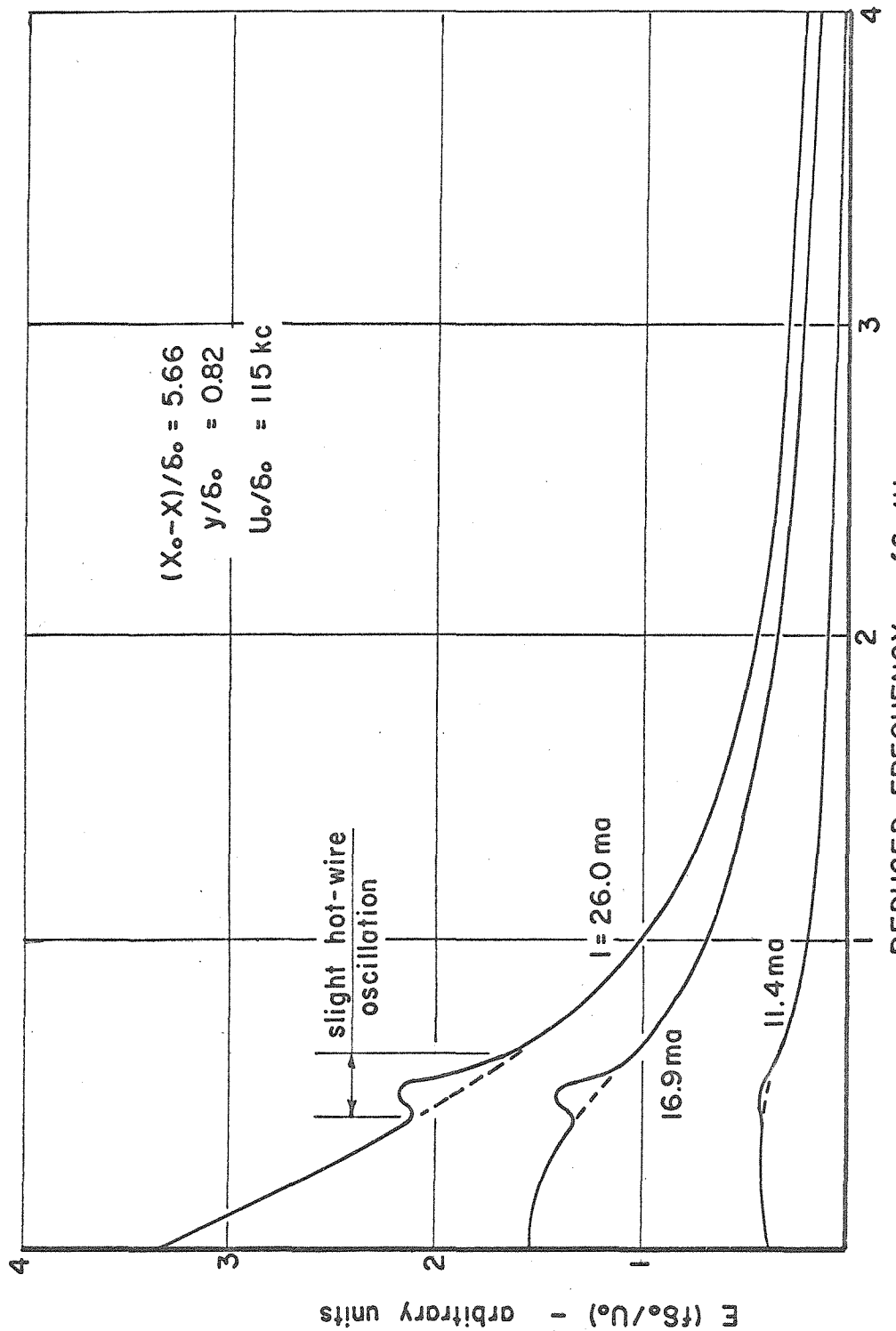

FIG. I-22 TURBULENT SPECTRA AS FUNCTION OF WIRE CURRENT

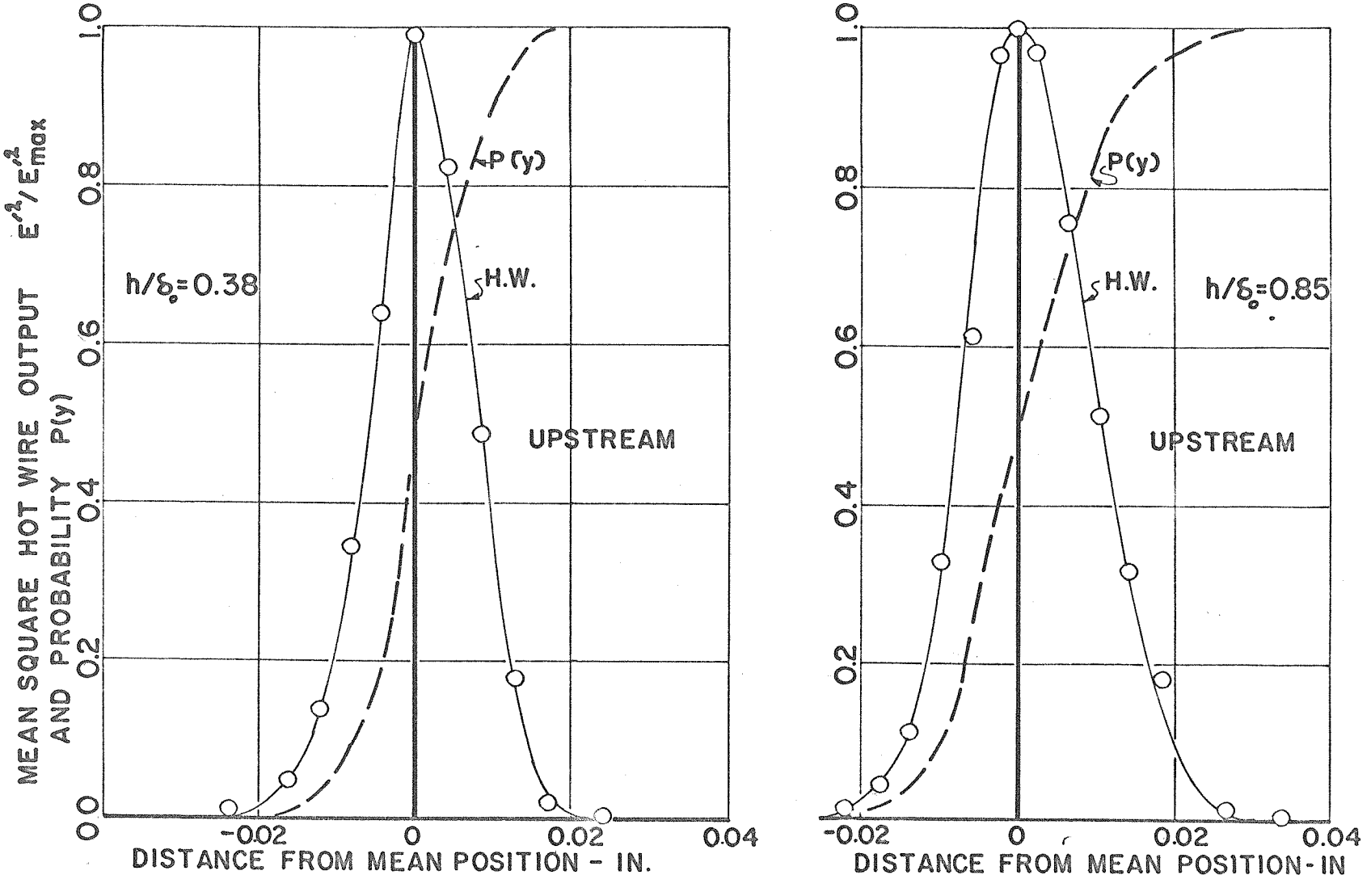

FIG. I-23 MEASUREMENT OF SHOCK MOTION

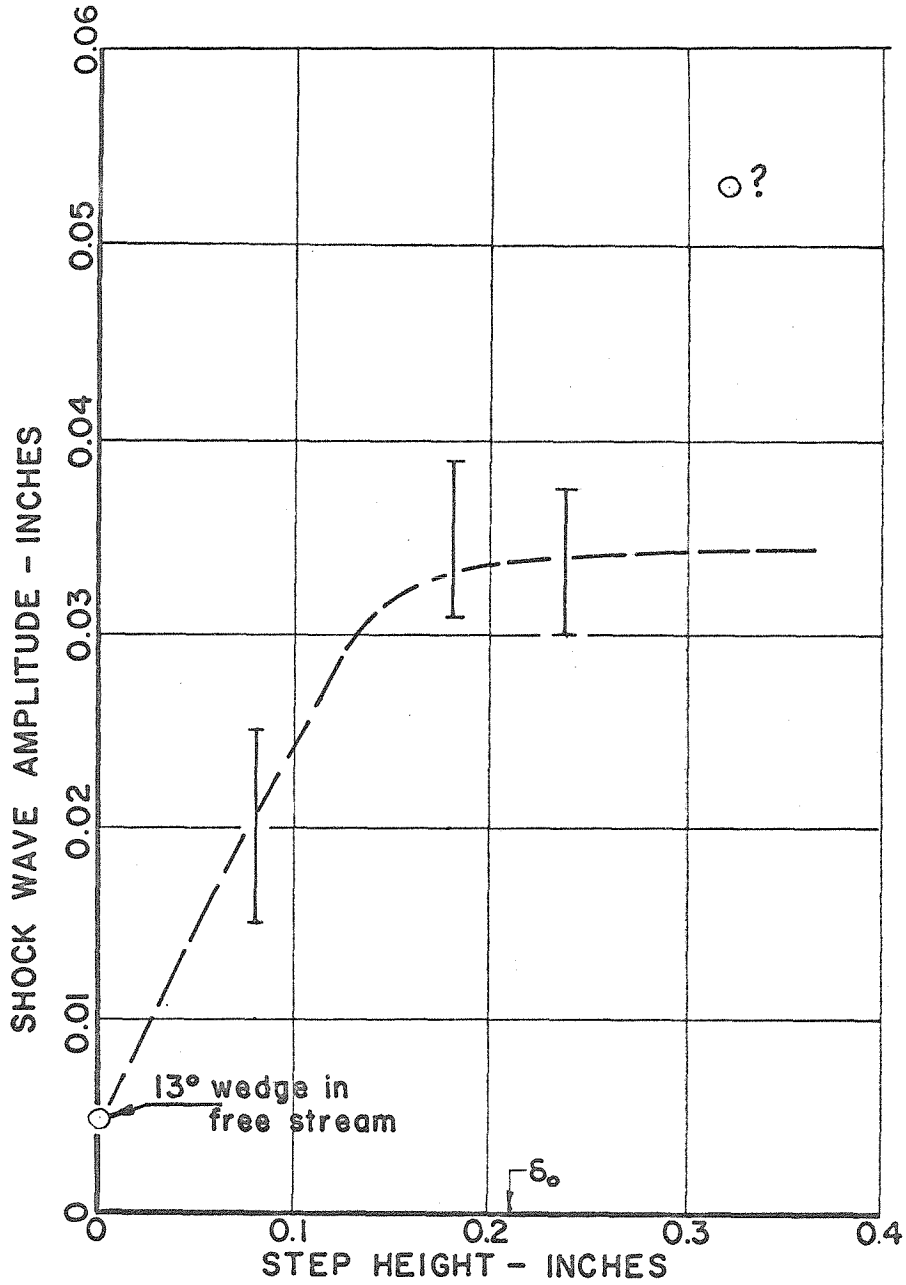

FIG. I-24 SHOCK MOTION AMPLITUDE AS FUNCTION OF STEP SIZE

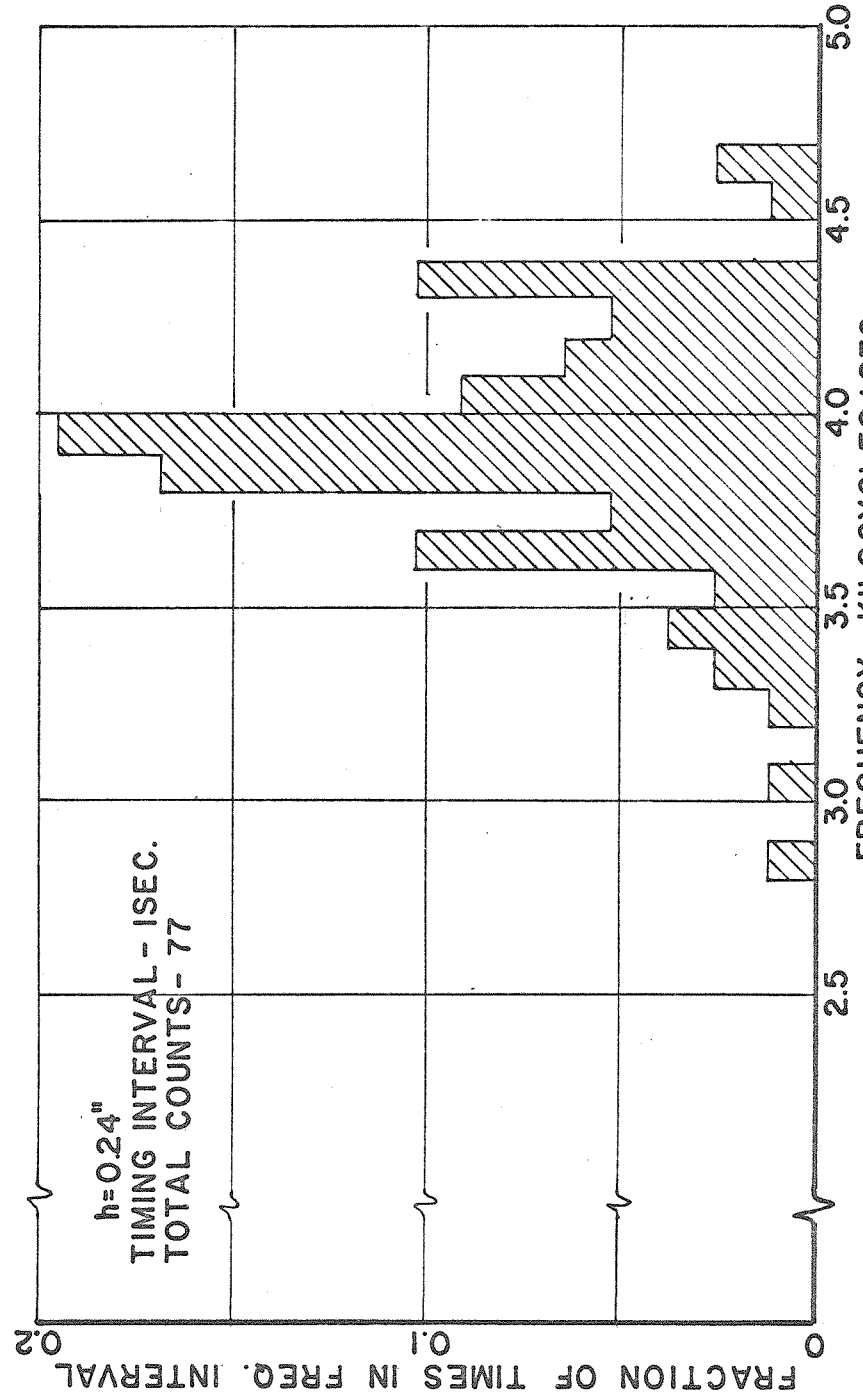

FIG. I-25 FREQUENCY HISTOGRAM OF SHOCK MOTION

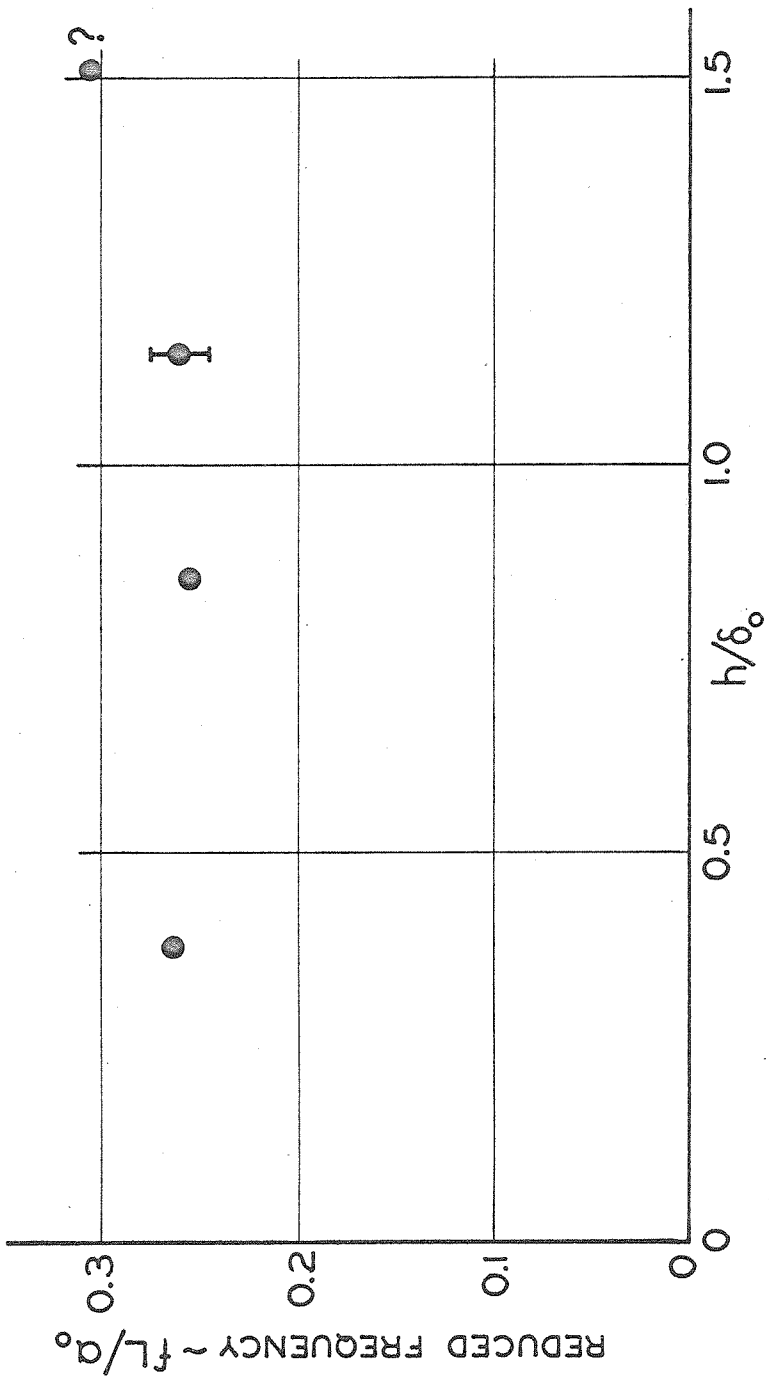

FIG. I-26 SHOCK MOTION FREQUENCY AS FUNCTION OF STEP SIZE

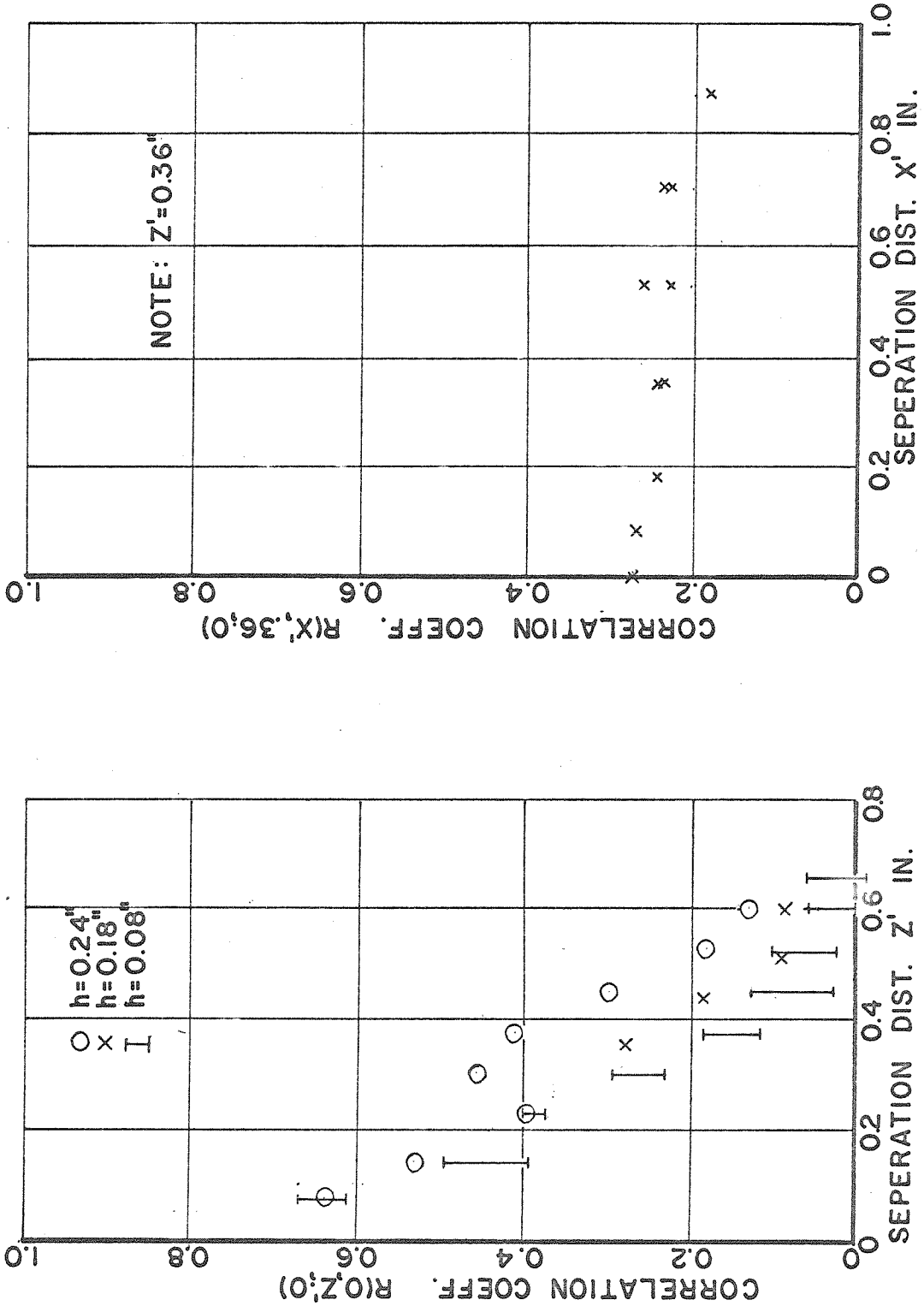

FIG. I-27 SHOCK MOTION CORRELATION MEASUREMENTS

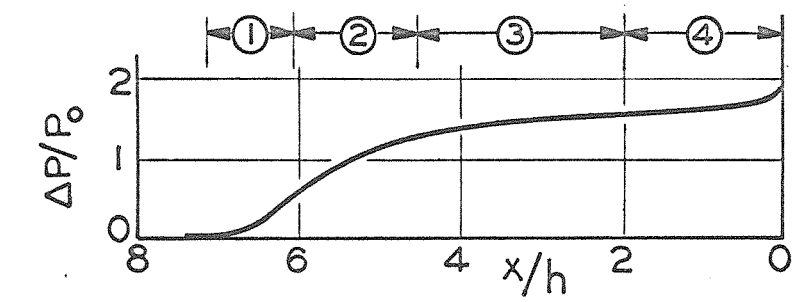

Mean wall pressure

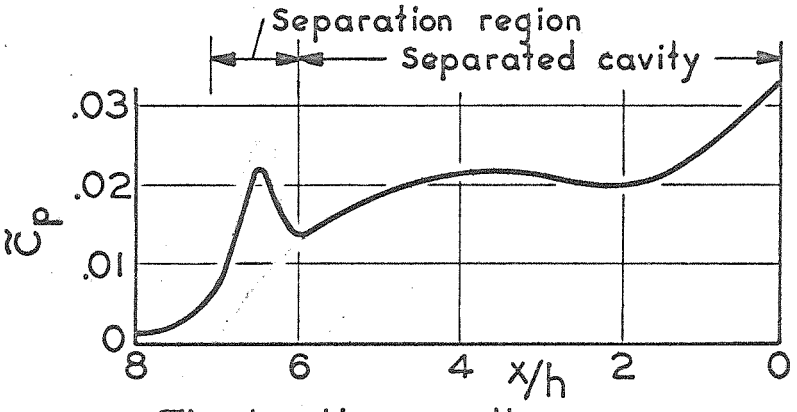

Fluctuating wall pressure

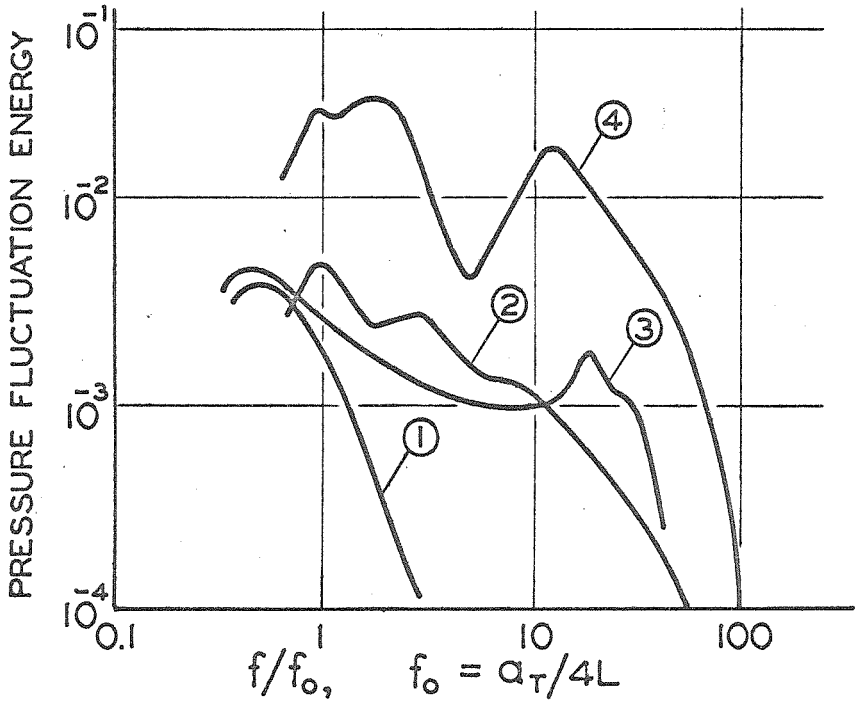

Spectra of wall pressure fluctuations

FIG. I-28 FLUCTUATING WALL PRESSURE DISTRIBUTION AND TYPICAL SPECTRA (taken from ref. 15)

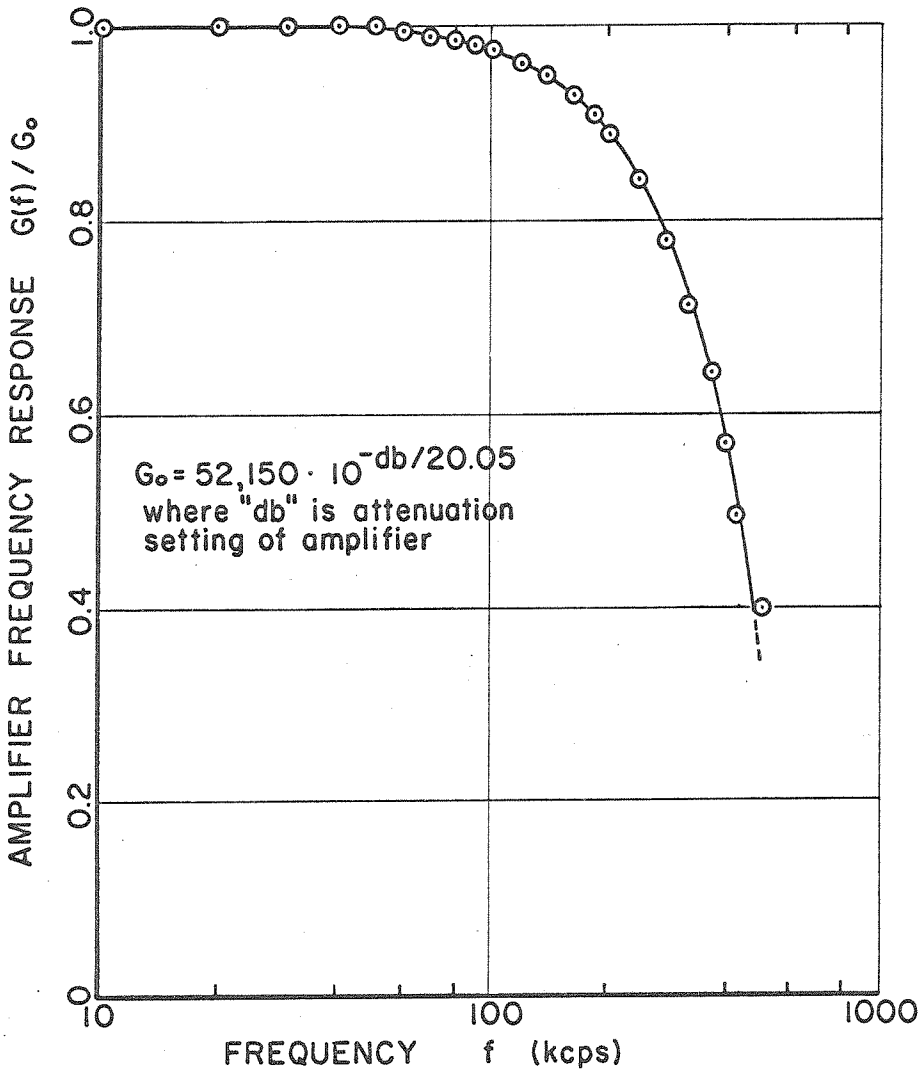

FIG. I-29 HOT-WIRE AMPLIFIER CHARACTERISTICS

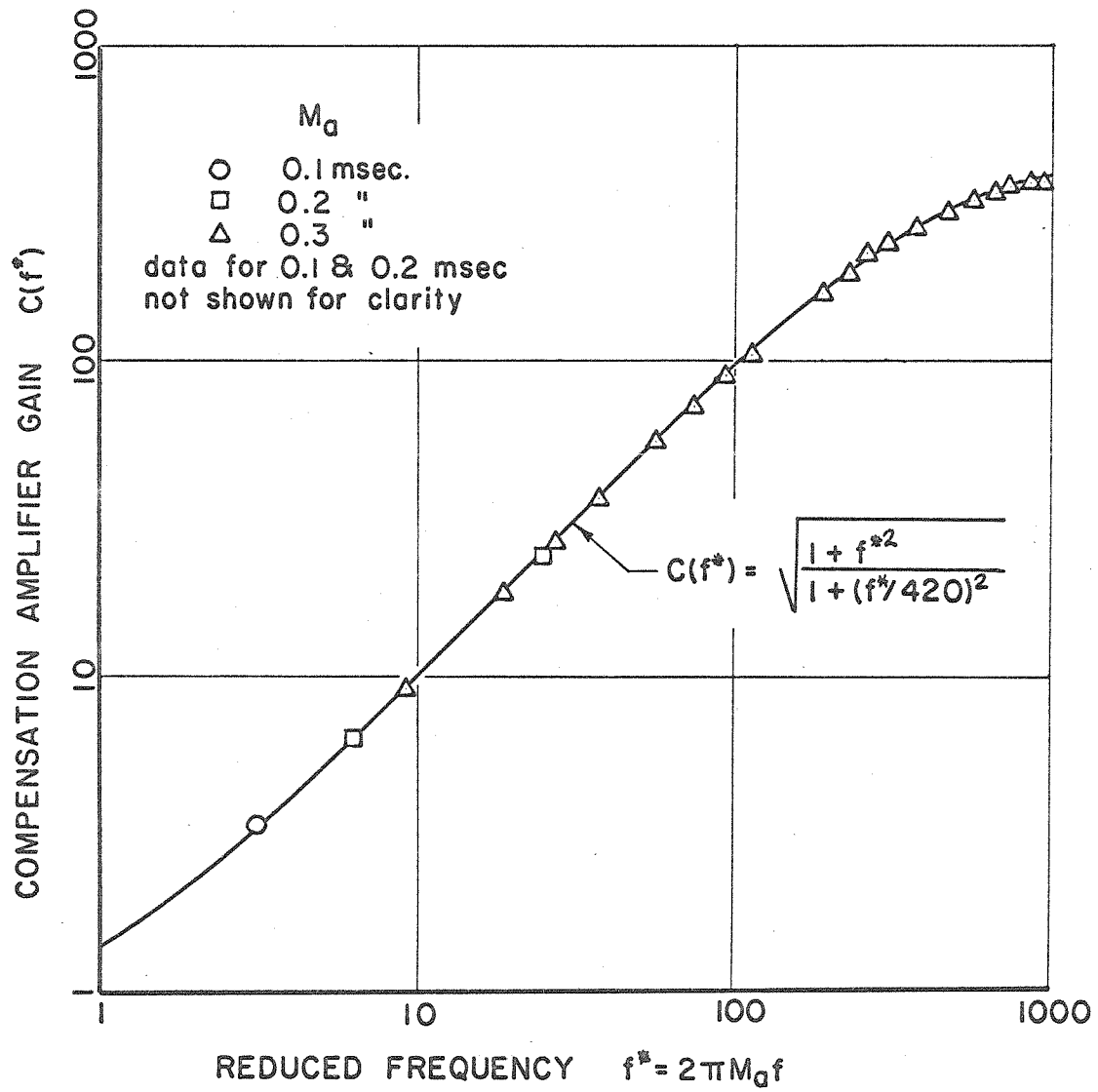

FIG. I - 30 COMPENSATION AMPLIFIER CALIBRATION

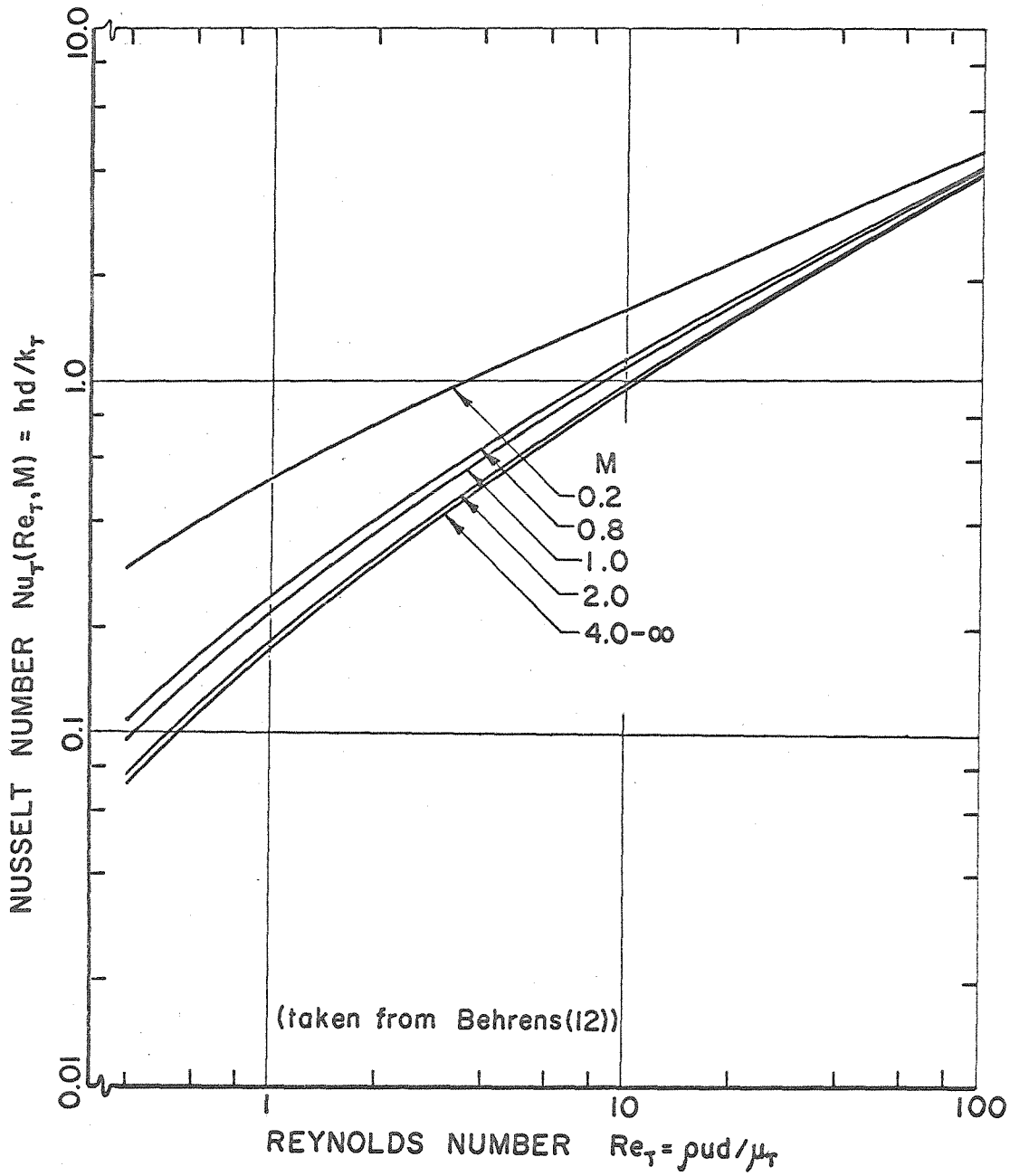

FIG. I-31 INFINITE CYLINDER NUSSELT NUMBER

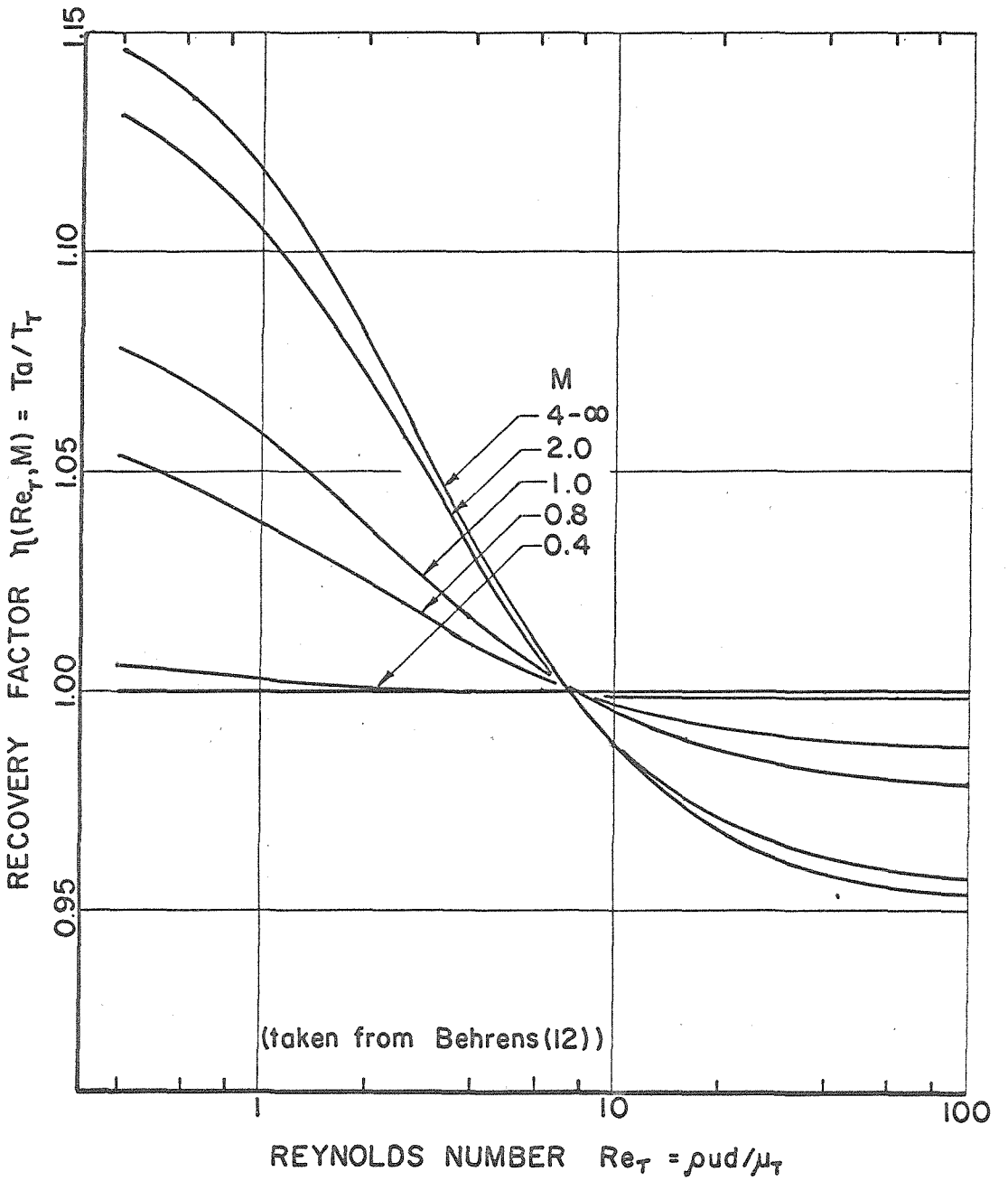

FIG. I-32 INFINITE CYLINDER RECOVERY FACTOR

APPENDIX I-A

Derivation of Finite Hot-Wire Response Equation and Sensitivity Coefficients

This appendix is essentially an abridged version of a derivation first completed by Behrens.[12] It is included in this thesis mainly for completeness and to display the necessary parameters that must be measured in order to reduce the actual data into its final form. The paper by Behrens is as yet unpublished but should be forthcoming soon and should be consulted for many of the details omitted.

I-A. 1 Derivation of Finite Hot-Wire Equations

Consider a wire of length ℓ and diameter d immersed in a compressible fluid moving at velocity u(t) normal to the axis of the wire. The stagnation temperature of the fluid is at $T_T(t)$, and the viscosity and thermal conductivity at the stagnation condition are denoted by μ_T and k_T respectively. The wire is attached to massive supports at $x = \pm \ell/2$ and a current i(t) is passing through the wire. Assuming also that the convective heat transfer to the fluid from the wire is given by

$$\dot{q} = hA(T_w - \overline{\eta}\,\overline{T}_T) \qquad \text{(IA. 1)}$$

where h is the heat transfer coefficient and $\overline{\eta}$ is the recovery factor of an infinitely long cylinder normal to the mean flow, the differential equation for the local wire temperature, $T_w(x, t)$, is derived from the energy equation which results in

$$\rho_w c_w \left(\frac{\pi d^2}{4}\right) \frac{\partial T_w}{\partial t} + \pi d\, h(T_w - \overline{\eta}\,\overline{T}_T) = i^2 r_w + k_w \frac{\partial^2 T_w}{\partial x^2} \qquad \text{(IA. 2)}$$

together with the boundary conditions

$$T_w(\pm \ell/2, t) = T_s$$

$$\text{and} \quad \frac{\partial T_w}{\partial x}(0, t) = 0 \quad . \tag{IA. 3}$$

The second of the boundary conditions arises from the assumption that the wire length is small compared to the scale of inhomogeneities in the fluid and is thus a symmetry condition.

Define a Nusselt number, $Nu_T \equiv \frac{h\,d}{k_T}$, and non-dimensionalize the wire temperature, x coordinate, and time according to the following format;

$$\tau \equiv \frac{T_w - \overline{\eta}\,\overline{T}_T}{\overline{\eta}\,\overline{T}_T} \quad ;$$

$$x^* \equiv 2x/\ell \; ; \quad \text{and} \tag{IA. 4}$$

$$t^* \equiv \left(\frac{4\,\overline{k}_T}{\rho_w c_w d^2}\right) t = t/K \quad .$$

It is also known that the wire resistance per unit length, r_w, varies approximately linearly with temperature[12] so that

$$r_w = r_r\,[1 + \alpha_r(T_w - T_r)] \tag{IA. 5}$$

where r_r and T_r are constant reference quantities. With the above, equations IA. 2 and IA. 3 become;

$$\frac{\partial \tau}{\partial t^*} + \left[\frac{Nu_T\,k_T}{\overline{k}_T} - \frac{i^2\,\overline{\alpha}_r\,r_r}{\pi\,\overline{k}_T}\right]\tau - \frac{k_w}{\overline{k}_T(\ell/d)^2}\,\frac{\partial^2 \tau}{\partial x^{*2}} =$$

$$\frac{Nu_T\,k_T}{\overline{k}_T}\,\frac{(\eta\,T_T - \overline{\eta}\,\overline{T}_T)}{\overline{\eta}\,\overline{T}_T} + \frac{i^2 r_r}{\overline{\eta}\,\overline{T}_T}\,[1 + \alpha_r(\overline{\eta}\,\overline{T}_T - T_r)] \tag{IA. 6}$$

with boundary conditions

$$\tau(\pm 1,\ t^*) = \bar{\tau}_s$$
$$\frac{\partial \tau}{\partial x^*}(0, t^*) = 0 \quad , \tag{IA. 7}$$

where the barred ($\bar{}$) quantities are constants. To aid in the solution to equation IA. 6, all quantities will be assumed to fluctuate about a mean value and that the fluctuation is small compared to the mean value along with being sinusoidal in time, e. g.

$$\begin{aligned}
\tau(x^*, t^*) &= \bar{\tau}(x^*) + \tau'(x^*)\, e^{i\bar{\omega}t^*} \\
Nu_T(x^*,t^*) &= \overline{Nu}_T \left[1 + Nu_0'(x^*) e^{i\omega t^*}\right] \\
\eta(x^*, t^*) &= \bar{\eta}\left[1 + \eta'(x^*)\, e^{i\omega t^*}\right] \\
\bar{T}_T(t^*) &= T_T \left[1 + \tau_T'\, e^{i\omega t^*}\right] \\
k_T(t^*) &= \bar{k}_0 \left[1 + n\, \tau_T'\, e^{i\omega t^*}\right] \\
\mu_T(t^*) &= \bar{\mu}_0 \left[1 + m\, \tau_T'\, e^{i\omega t^*}\right] \\
i(t^*) &= \bar{i}\left[1 + i'\, e^{i\omega t^*}\right]
\end{aligned} \tag{IA. 8}$$

where
$$n \equiv \frac{d\ell n\, \bar{k}_T}{d\ell n \bar{T}_T} \approx 0.885 \text{ for air @ } 300^\circ K$$
$$m = \frac{d\ell n\, \bar{\mu}_T}{d\ell n \bar{T}_T} \approx 0.765 \text{ for air @ } 300^\circ K \ .$$

Substituting equations IA. 8 into IA. 6 and separating the resulting equation by order of magnitude gives first the equation for the mean temperature distribution

$$\frac{\bar{k}_w}{\bar{k}_T(\ell/d)^2}\frac{d^2\bar{\tau}}{dx^{*2}} - (\bar{Nu}_T - \frac{\bar{i}^2 r_r \alpha_r}{\pi \bar{k}_T})\bar{\tau} - \frac{\bar{i}^2 r_r}{\bar{\eta}\bar{T}_T \pi \bar{k}_T}\left[1+\alpha_r(\bar{\eta}\bar{T}_T - T_r)\right] = 0 \qquad \text{(IA. 9)}$$

with boundary conditions

$$\bar{\tau}(\pm 1) = \tau_s$$

$$\frac{d\bar{\tau}}{dx^*}(0) = 0 \quad ;$$

and secondly the unsteady wire temperature distribution

$$\left[\bar{Nu}_T - \frac{\bar{i}^2 r_r \alpha_r}{\pi \bar{k}_T} + i\bar{\omega}\right]\tau' - \frac{k_w}{\bar{k}_T(\ell/d)^2}\frac{d^2\tau'}{dx^{*2}}$$

$$= -\left[\bar{Nu}_T(Nu'_T + k'_T) - \frac{2\bar{i}^2 r_r \alpha_r}{\pi \bar{k}_T} i'\right]\tau' + 2\frac{\bar{i}^2 r_r}{\pi \bar{k}_T \bar{\eta}\bar{T}_T}\left[1+\alpha_r(\bar{\eta}\bar{T}_T - T_r)\right]$$

$$+ \bar{Nu}_T(\tau'_T + \eta') \qquad \text{(IA. 10)}$$

with boundary conditions

$$\tau'(\pm 1) = 0$$

$$\frac{d\tau'}{dx^*}(0) = 0 \quad .$$

I-A. 2 Steady State Solution and Mean Measurable Quantities

With regard to the mean temperature equation (IA. 9) the solution is easily found. However, in practice the quantity that is directly measured is the total wire resistance which is given by,

$$\bar{R}_m \equiv \int_{-\ell/2}^{\ell/2} r_w(x)dx \quad . \qquad \text{(IA. 11)}$$

Using equations IA. 5 and IA. 8, equation IA. 11 is equivalent to

$$\overline{R}_m = R_r[1+\alpha_r(\overline{\eta}\,\overline{T}_T - T_r)] + \frac{\alpha_r R_r \overline{\eta}\,\overline{T}_T}{2}\int_{-1}^{1}\overline{\tau}(x^*)dx^*. \qquad \text{(IA. 12)}$$

The mean wire temperature given by the integral in equation IA. 12 is computed by Behrens[12] to be

$$\overline{\tau}_m \equiv \frac{1}{2}\int_{-1}^{1}\overline{\tau}(x^*)dx^* = \frac{c}{b} + (\tau_s - \frac{c}{b})\frac{\tanh\sqrt{\alpha}}{\sqrt{\alpha}} \qquad \text{(IA. 13)}$$

where;

$$a \equiv k_w / \overline{k}_T(\ell/d)^2$$

$$b = \overline{Nu}_T - \frac{\overline{i}^2 r_r \alpha_r}{\pi \overline{k}_T}$$

$$c \equiv \frac{\overline{i}^2 r_r}{\pi \overline{k}_T \overline{\eta}\,\overline{T}_T}[1 + \alpha_r(\overline{\eta}\,\overline{T}_T - T_r)]$$

$$\alpha = b/a$$

It will be shown that the quantity $\overline{\tau}_m$ is necessary for evaluation of the sensitivity coefficients derived from the unsteady equation. In theory, $\overline{\tau}_m$ could be computed directly from equation IA. 13, however, this is quite difficult in practice because of a lack of confidence in the evaluation of the wire support temperature factor, τ_s, and the wire unit reference resistance for a very small length of wire. Furthermore, the quantity that is directly measured is the total wire resistance and it would be advantageous to evaluate $\overline{\tau}_m$ using known accurate quantities. The hint for accomplishing this was provided from an experimental observation; as mentioned in the text of this thesis, the measured total wire resistance, $\overline{R}_m$, is a linear function of the Joule heating in the wire, $\overline{i}^2\overline{R}_m$, i. e.

$$\overline{R}_m = \overline{R}_{am} + k(\overline{i}^2\,\overline{R}_m) \qquad \text{(IA. 14)}$$

where $\overline{R}_{am}$ is the adiabatic wire resistance and k is the slope of the $\overline{R}_m$ vs. $i^2 \overline{R}_m$ line. This equation is easily solved for the fractional change in wire resistance as,

$$\frac{\Delta R_m}{R_{am}} \equiv \frac{\overline{R}_m - \overline{R}_{am}}{R_{am}} = \frac{k i^2}{1 - k i^2} \qquad \text{(IA. 15)}$$

Now from equation IA. 12 it can be shown that

$$\overline{\tau}_m = \overline{\tau}_{am} + \left(\frac{\Delta R_m}{\overline{R}_{am}}\right) \frac{\overline{R}_{am}/R_r}{\alpha_r \overline{\eta}\, \overline{T}_T} \qquad \text{(IA. 16)}$$

and that

$$\overline{\tau}_{am} = \frac{1}{\alpha_r \overline{\eta}\, \overline{T}_T} \left\{ \frac{\overline{R}_{am}}{R_r} - 1 + \alpha_r (T_r - \overline{\eta}\, \overline{T}_T \right\} \quad . \qquad \text{(IA. 17)}$$

All quantities on the right-hand-sides of equations IA. 15, IA. 16, and IA. 17 are either known (α_r & T_r), measured (k, $\overline{R}_{am}$, R_r, $\overline{T}_T$), or can be calculated ($\overline{\eta}$ - see later). Thus, $\overline{\tau}_m$ can be calculated from the most accurate measurable quantities.

In the event that the quantities τ_s, r_r, etc. can be accurately measured, then from measurement of $\overline{R}_{am}$ and $\overline{R}_m$ the local Nusselt number $\overline{Nu}_T$ and local recovery factor $\overline{\eta}$ can be evaluated which can be utilized to determine the local mean flow quantities. For details of this procedure one should consult the forthcoming paper by Behrens.

I. A. 3 Approximate Solution to the Unsteady Response Equation

It is advantageous in considering the fluctuating temperature equation to rewrite it using the definitions given after equation IA. 13, whence equation IA. 10 becomes

$$(b + i\overline{\omega})\tau' - a \frac{d^2 \tau'}{dx^{*2}} = C_1 + C_2 \frac{\cosh \sqrt{\alpha}\, x^*}{\sqrt{\alpha}} \qquad \text{(IA. 10')}$$

where $C_1 \equiv 2(1+\frac{d}{b})\,c\,i' + Nu_T\left[(1-n\frac{c}{b})\tau'_T - \frac{c}{b}Nu'_T + \eta'\right]$

$C_2 \equiv (\tau_s - \frac{c}{b})\left[2d\,i' - \overline{Nu}_T(Nu'_T + n\,\tau'_T)\right]$

$d = \overline{Nu}_T - b$

with $\tau'(\pm 1) = 0$

$\frac{d\tau'}{dx^*}(0) = 0$

This equation can be solved for $\tau'(x^*)$ exactly but because of its complexity its application is difficult. Several approximations can be used to simplify equation IA. 10′ which in turn simplify the expression for τ'. The first of these is the realization that for the wires employed in this experiment, the quantity $\overline{\omega} \equiv K\omega$ has a value of about 1.6f where f is the fluctuation frequency in kilocycles, whereas the value of "a" is less than 0.51 for wire length-to-diameter ratios greater than 50. Furthermore, the quantity "b" is at most equal to local Nusselt number $\overline{Nu}_T$ which has a value in the neighborhood of 1.4. Thus, for frequencies greater than, say, 3 KC we can neglect both "a" and "b" in comparison to the quantity $\overline{\omega}$. Physically, the neglect of the term a $\frac{d^2\tau'}{dx^{*2}}$ is equivalent to assuming that for high frequencies the wire responds as would an infinite length wire. Using these assumptions the solution to equation IA. 10′ is then approximately

$$i\overline{\omega}\,\tau'(x^*) \approx C_1 + C_2\frac{\cosh\sqrt{\alpha}\,x^*}{\sqrt{\alpha}} \qquad \text{(IA. 18)}$$

Integrating this over the length of the wire to get the measured wire temperature fluctuation in the same spirit as with the mean wire

temperature and using the values of C_1 and C_2 and the value of $\frac{\tanh \sqrt{\alpha}}{\sqrt{\alpha}}$ from equation IA. 13 gives;

$$i\bar{\omega}\,\tau'_m \approx \overline{Nu}_T\,[(1-n\,\bar{\tau}_m)\,\tau'_T - \bar{\tau}_m\,Nu'_T + \eta'] \qquad \text{(IA. 19)}$$

where i' has been taken identically equal to zero in C_1 and C_2.

Up to this point, the response of a real wire has been considered whereas the sensitivity coefficients or voltage generated by the fluctuation of specified quantity (for example, ρ, u, or T_T) are computed for an ideal or massless wire. This is done because of the "thermal lag" or attenuation of high frequency signals due to the wire mass.

Digressing a moment to consider the responses of a real wire and an ideal wire both of infinite length, it can be shown from a formulation similar to that given above that the ratio of the respective wire temperature fluctuations is

$$\frac{\tau'_\infty}{\tau'_{i,\infty}} = \frac{1}{1+i\,\bar{\omega}/b} \quad . \qquad \text{(IA. 20)}$$

This is the well known relation[28] that displays the attenuation of high frequency signals due to the mass of the real wire and also defines the infinite wire time constant

$$\bar{M}_{t,\infty} = 1/b \quad . \qquad \text{(IA. 21)}$$

Returning to the hot-wire of finite length, assume that the attenuation due to the real wire can be expressed in the same form as equation IA. 20, i. e.

$$\frac{\tau'_m}{\tau'_{i,m}} = \frac{1}{1+i\bar{M}_t\bar{\omega}} \quad . \qquad \text{(IA. 21)}$$

It is shown by Behrens, using the approximation that $\bar{M}_t\,\bar{\omega} >> 1$, that the actual hot-wire time constant is given by

$$M_t \approx M_{t,\infty}\left(1 - \frac{\tanh\sqrt{\alpha}}{\sqrt{\alpha}}\right) F\left(\frac{C_2}{C_1}, \alpha\right) \quad . \qquad \text{(IA. 22)}$$

The particular form of the function $F(C_2/C_1, \alpha)$ shown in equation IA. 22 is unimportant for the purposes here except to display the fact that it depends explicitly on the relative amplitudes of the fluctuating quantities through the term C_2/C_1. An apparent discrepancy has been revealed now because in order to calculate the sensitivity coefficients the fluctuating quantities are required, whereas the fluctuating quantities cannot be computed without knowledge of the actual wire time constant. This would imply a lengthy iterative method of data reduction. For the moment, however, this will be disregarded and the derivation will proceed as though $\bar{M}_t$ could be evaluated in some unprescribed manner.

If the frequency of oscillation is high enough so that both $\bar{M}_t\,\bar{\omega} >> 1$ and $\bar{M}_t\,\bar{\omega} >> b$ in equations IA. 19 and IA. 21 respectively, then these two equations can be combined to give the response of an ideal (massless) wire of finite length

$$\tau'_{i,m} = \frac{4\,M_t\,\bar{N}u_T\,\bar{k}_T}{\rho_w\,c_w\,d^2}\left[(1-n\bar{\tau}_m)\,\tau'_T - \bar{\tau}_m\,Nu'_T + \eta'\right] \qquad \text{(IA. 21)}$$

where the value of $\bar{M}_t$ has been replaced by the identity of $M_t = K\bar{M}_t$. The voltage fluctuations of the ideal wire are the desired result of this derivation and these are related to $\tau'_{i,m}$ through Ohm's law

$$e_i = \bar{i} R_{w,i} \quad . \tag{IA. 22}$$

Utilizing the fact that $R_{w,i} = R_r[1+\alpha_r(T_{i,m}-T_r)]$, it is easily shown that the voltage and temperature variations are related by

$$e_i' = \bar{i} \alpha_r R_r \bar{\eta} \bar{T}_T \tau_{i,m}' \tag{IA. 23}$$

Combining this with equation IA. 21 gives finally as the response of the ideal (massless) wire

$$e_i' = M_t \frac{4\bar{i}\alpha_r R_r \bar{\eta} \bar{T}_T \overline{Nu}_T \bar{k}_T}{\rho_w c_w d^2} [(1-n\bar{\tau}_m)\tau_T' - \bar{\tau}_m Nu_T + \eta'] \tag{IA. 24}$$

To calculate the desired sensitivity coefficients it remains to relate the quantities τ_T', Nu_T', and η' to the desired set of fluctuating quantities. This will be done shortly, but first it is obvious from equation IA. 24 that all sensitivity coefficients will be proportional to the, as yet unknown, quantity M_t. To resolve the apparent discrepancy associated with this, utilize the relation between the output of the hot-wire amplifier, $E'(f)$, and the ideal wire voltage which is derived in Appendix I-B of this thesis under essentially the same restrictions as were used in the derivation of equation IA. 24, thus

$$e_i' \propto \left(\frac{M_t}{M_A}\right) E' \tag{IA. 25}$$

where M_A is the time constant of the compensating amplifier. Comparing equations IA. 24 with IA. 25 it is seen that each is multiplied by the quantity M_t. Hence equating the right-hand sides, the unknown quantity, M_t, cancels out of the equation which makes its determination unnecessary! Thus, if we define a revised ideal voltage

$e_i^{*\prime} = e_i' \left(\frac{M_A}{M_T}\right)$, equations IA. 24 and IA. 25 combine to yield finally

$$e_i^{*\prime} = C[(1-n\bar{\tau}_m)\tau_T' - \bar{\tau}_m \, Nu_T' + \eta'] \qquad \text{(IA. 26)}$$

where $$C \equiv \frac{4\bar{i}\, R_r \alpha_r \bar{\eta}\, \bar{T}_T \overline{Nu}_T \bar{k}_T M_A}{\rho_w c_w d^2}$$

IA. 4 Transformation of Hot-Wire Response to Display Physical Fluctuations

It is desired now to modify equation IA. 26 into a form which displays the physical fluctuating quantities, say, u', ρ', and τ_T' as opposed to Nu_T' and η'. To do this it is first necessary to mention that Behrens[12] has shown that both the Nusselt number, $\overline{Nu}_T$, and the recovery factor, $\bar{\eta}$, are functions only of the Mach number and the Reynolds number, $Re_T \equiv \frac{\rho u d}{\mu_T}$, and that the implicit relations given for these have been computed numerically and are shown in Figures I-31 and I-32. Using the above functional dependence, the quantities Nu_T' and η' are then given by

$$\begin{aligned} Nu_T' &= \frac{\partial \ell n\, Nu_T}{\partial \ell n\, Re_T} Re_T' + \frac{\partial \ell n\, Nu_T}{\partial \ell n\, M} M' \\ \eta' &= \frac{\partial \ell n\, \eta}{\partial \ell n\, Re_T} Re_T' + \frac{\partial \ell n\, \eta}{\partial \ell n\, M} M' \end{aligned} \qquad \text{(IA. 27)}$$

where

$$\begin{aligned} Re_T' &\equiv \frac{\Delta Re_T}{Re_T} = \rho' + u' - m\,\tau_T' \\ M' &\equiv \frac{\Delta M}{M} = a_1(u' - \tfrac{1}{2}\tau_T') \qquad \text{(IA. 28)} \\ a_1 &\equiv 1 + \frac{\gamma-1}{2} M^2 \end{aligned}$$

Combining equations IA. 26 through IA. 28 and taking the coefficients of the quantities $-u'$, $-\rho'$, and τ_T' as defining the sensitivity coefficients so that

$$e_i^{*\prime} = -S_u u' - S_\rho \rho' + S_{T_T} \tau_T' \qquad \text{(IA. 29)}$$

gives after some algebra

$$S_u = C \frac{\partial}{\partial(\ell n\, Re_T)} \left[\overline{\tau}_m(\ell n\, Nu_T) - \ell n\, \eta\right]$$

$$S_\rho = C\left(\frac{\partial}{\partial(\ell n\, Re_T)} + a_1 \frac{\partial}{\partial(\ell n\, M)}\right)\left[\overline{\tau}_m(\ell n\, Nu_T) - \ell n\, \eta\right] \qquad \text{(IA. 30)}$$

$$S_{T_T} = C\left\{(1 - n\overline{\tau}_m) + \left(m \frac{\partial}{\partial(\ell n Re_T)} + \frac{a_1}{2} \frac{\partial}{\partial(\ell n\, M)}\right)\left[\overline{\tau}_m(\ell n Nu_T) - \ell n \eta\right]\right\}$$

and again

$$C = \frac{4\,\overline{i}\, R_r\, \alpha_r\, \overline{\eta}\, \overline{T}_T\, \overline{Nu}_T\, k_T\, M_A}{\rho_w\, c_w\, d^2}$$

All the quantities in the above equations are known or measured and the four terms like $\frac{\partial \ell n Nu_T}{\partial \ell n Re_T}$ are evaluated numerically from the implicit relations $Nu_T(Re_T, M)$ and $\eta(Re_T, M)$. Physically, the sensitivity coefficients are equivalent to the R. M. S. voltage output of an ideal wire due to a 100% R. M. S. fluctuation in the subscripted quantity. Note also that these coefficients are constants for a given mean flow situation and operating point and as such are independent of the frequency of the disturbance. Thus, these can also be used to spectrally separate the modes of fluctuation if the spectra of the output voltage is measured.

APPENDIX I-B

Relation Between Ideal (Massless) Hot-Wire Output and Amplifier Output

In Appendix I-A the response of an ideal hot-wire (that is with zero mass but identical resistance and thermal conductivity) to the various modes of fluctuation was derived. Naturally, this output cannot be measured since such an ideal wire does not exist. The only measurable quantity is the actual output which is usually of very small magnitude (in these experiments the R. M. S. wire voltage was something less than 100 μa.) and also is not representative of the flow field fluctuations because of the thermal lag phenomena caused by the finite wire mass. It is assumed in Appendix I-A that the relation between the actual output and the ideal output is given by

$$e'_{wire}(f) = \frac{e'_i(f)}{1 + i(2\pi f M_t)} \qquad (IB.1)$$

which is easily derivable from equations IA. 21 and IA. 22, and M_t is the hot-wire time constant and is derived in Appendix I-A. Note that not only is the real signal attenuated but also there is a phase shift in the real signal that approaches 90° for high frequencies.

The function of the hot-wire amplifier is to not only amplify the actual wire voltage but also to compensate for the above described attenuation (the means by which this is accomplished is given in (28)). The actual wire time constant, M_t, is approximated by the standard method of a square wave current injection.[28] For long wires where end effects are negligible this is usually very close to M_t, but some difference can be expected for the short wires ($\ell/d \sim O(50)$) employed

in these tests; moreover, this measurement was very subjective and in regions of high turbulence was not repeatable to within 20% or so. To account for this, let the time constant setting of the compensating amplifier be denoted by M_A.

From the calibration of both the amplifier and the compensating amplifier the relation between the output of the amplifying system, $E'(f)$ and the actual wire output is then

$$E'(f) = G_0\, A(f)\, C(f)\, e'_{wire}\,(f) \qquad \text{(IB. 2)}$$

where G_0 is the "zero frequency" gain of the amplifier, $A(f)$ is the amplifier attenuation (see Figure I-29) and $C(f)$ is the response of the compensating amplifier (see Figure I-30). The function $C(f)$ is shown from the calibration to be adequately represented by

$$C(f) = \left\{ \frac{1 + (2\pi f M_A)^2}{1 + (2\pi f M_A/\kappa)^2} \right\}^{\frac{1}{2}} \qquad \text{(IB. 3)}$$

where κ is the "ceiling-to-floor ratio" and has a value of about 420 for the particular set used. Ignoring the phase shift represented in equation IB. 1 and combining equations IB. 1 through IB. 3 gives

$$e'_i(f) = \frac{E'(f)}{G_0\, A(f)} \left[\frac{1+(2\pi f M_t)^2}{1+(2\pi f M_A)^2} \right]^{\frac{1}{2}} \sqrt{1 + (2\pi f M_A/\kappa)^2} \qquad \text{(IB. 4)}$$

The typical value of M_A was around 0. 1 msec and assuming that this is of the same order as M_t, then for frequencies greater than, say, 3 KC, $1 \ll (2\pi f M_A)^2, (2\pi f M_t)^2$ and equation IB-4 becomes

$$e'_i(f) = \left(\frac{M_t}{M_A}\right) \frac{E'(f)}{G_0\, A(f)} \sqrt{1 + (2\pi f M_A/\kappa)^2} \qquad \text{(IB. 5)}$$

which is the desired relation.

In most situations, it is usual to compute the total mean square fluctuation rather than the spectral distribution which is a very time consuming measurement. Indeed, the mean square voltage $\overline{E'^2}$ could be computed from the spectral distribution but it is much easier to measure $\overline{E'^2}$ directly. The question then naturally arises as to the error involved in representing the quantity $\overline{e_i'^2}$ by the approximation

$$\overline{e_i'^2} \approx \overline{e_{i*}'^2} \equiv \left(\frac{M_t}{M_A}\right)^2 \frac{1}{G_0^2} \int_0^\infty \overline{E'^2}(f)\,df \qquad \text{(IB. 6)}$$

rather than the expression

$$\overline{e_i'^2} = \left(\frac{M_t}{M_A}\right)^2 \frac{1}{G_0^2} \int_0^\infty \frac{\overline{E'^2}(f)}{A^2(f)} \left[1+(2\pi f M_A/\kappa)^2\right] df \quad . \qquad \text{(IB. 7)}$$

Obviously, the error involved depends upon the actual distribution of $\overline{E'^2}(f)$ but it shouldn't be too bad since $\overline{E'^2}(f)$ falls off rather rapidly for $f > U_e/\delta \approx 116$ KC and the corrective factor $\frac{\left[1+(2\pi f M_A/\kappa)^2\right]}{A^2(f)}$ is unity up to around this value. To evaluate the error, however, the ratio $\overline{e_i'^2} / \overline{e_{i*}'^2}$ was computed for each of the spectra shown in Figure I-22. The maximum value of this ratio was 1.12 and occurred in the highest current level.

PART II. A MODEL FOR INCOMPRESSIBLE FLOW IN A CHANNEL

List of Tables - Part II

List of Figures - Part II

List of Symbols - Part II

a, b, c	logarithms of velocity ratios defined in equation II-9
C_p	pressure coefficient = $(p-p_0)/\frac{1}{2}\rho q_0^2$
f	complex potential $f = \varphi + i\psi$
$f_i(C_p;\alpha)$	integral functions for i = 1, 2, 3, 4 defined in Section II-4
$g_n(k)$	function defined in equation II-20
h	step height
H	channel height
h'	wake width (including step height)
j, k, ℓ	velocity ratios defined in equation II-8
p	static pressure
q	magnitude of fluid velocity, $q \equiv \sqrt{u^2+v^2}$, or $\exp(-\pi^2/2c)$
r	distance to step face reattachment point
s	distance to upstream separation point
$S_n(j, \ell)$	function defined in equation II-20
$T_n(a, b, c)$	function defined in equation II-26
u, v	velocity components in x and y directions respectively
w	hodograph plane variable $w = u-iv = q\exp(-i\theta)$
x, y	orthogonal coordinate system defined in Figure II-3
z	physical plane variable $z = x+iy$
$Z(\zeta;\alpha)$	function defined in equation II-16
α	dummy variable
δ	boundary layer thickness
ζ	$\log\frac{q}{q_s} - i\theta \equiv \xi - i\theta$
θ	fluid flow angle in physical plane

λ blockage ratio, $\equiv h/H$

ρ fluid density (constant)

φ velocity potential

ψ stream function

Γ -stepface angle parameter - see Fig. II-12

subscripts

c conditions on cavity or separated region on top of step

0 upstream infinity conditions

s upstream separated region conditions

2 downstream infinity conditions

superscripts

$*$ dimensional quantity

II. 1 Introduction

The problem considered in this part of this thesis, that of the two-dimensional incompressible flow of a turbulent boundary layer over a normal step mounted in a channel, was first conceived during a series of experiments conducted on this subject by Dr. E. E. Zukoski, Lt. Robert Stevenson, and the author. The results of this experiment and preliminary results of the solution presented here are reported in the thesis by Stevenson[36] and a sketch of the flow field and wall pressure distribution for a typical situation is shown in Figure II-1.

The difference between the supersonic flow over a normal step considered in Part I of this thesis and the incompressible analogue presented here is exemplified mainly by the finite upstream influence of the supersonic flows whereas for subsonic flows the region of upstream influence is infinite. Moreover, the appearance of the separation shock wave in the supersonic flow situation gives rise to a relation between the flow angle and static pressure does not exist for the subsonic case. It is also known experimentally that the scale of the supersonic interaction region is affected mostly by the geometry. For subsonic flows it was thought that the characteristic length scale of the upstream influence was the boundary layer thickness.[41, 43]

Another of the difficulties associated with incompressible turbulent boundary layer separation is that the location of the actual separation point is markedly affected by the local pressure distribution as pointed out by Stratford[37] and Townsend.[38] Of course this pressure distribution is not known a priori since it depends to some extent on the interaction between the boundary layer and the inviscid

flow in addition to the step itself, the blockage of the channel by the step, and the turbulent wake observed on top of the step.

One of the major impressions resulting from the experiments by Stevenson[36] was that the wall pressure distribution ahead of the separated region appeared to be influenced only by geometric parameters rather than a strong interaction between the boundary layer and the inviscid flow. Also it appeared that the viscous forces within the boundary layer contributed only significantly to the pressure within the separated region ahead of the step and that this region possibly could be accounted for by a suitable inviscid model. Thus, if the wake region could also be approximated by an inviscid model, the whole flow field could then be computed analytically. This solution could then be utilized to assess the effects of finite channel height on the pressure distribution ahead of the step location which hitherto has usually been neglected.

The purpose then of this portion of this thesis is to construct and solve an approximate inviscid model that can be used to predict the upstream wall pressure field and accounts for the influence of the separated region ahead of the step, the wake region on top of the step, and the finite blockage ratio of the channel. Obviously, all the viscous effects cannot be accounted for by this model and it is expected that in certain regions of the flow (e.g., near the separation point) the solution will fail to give accurate information. The solutions presented here are to be compared to experiment to verify the adequacy of the flow model.

Before developing the model described above it is first advantageous to consider previous theoretical solutions for this particular flow field. The major difficulty in formulating the flow field is, as stated, in modeling the separation region and the wake region. The first attempt at this was completed by Lighthill[39] who utilized free streamline theory, i.e., constant pressure and hence constant velocity along the dividing streamline to account for both the separated region and the wake region. His model consisted of a normal flat plate in an infinite flow field with a forward protruding plate along which separation occurred. To get a unique solution the velocity ratio between the separated region and the leading edge of the protruding plate was assumed as known. Moreover, the dividing streamline which forms the separated region and downstream cavity did not reattach on the step face as is observed experimentally.

Barrows[40] extended Townsend's method to include wedge shaped obstacles mounted in a finite channel. Again, he utilizes the same assumption as Lighthill to get a unique solution and was similarly interested in the determination of the separation point location. The comparison between the measured and predicted wall pressures in front of the separated region leaves much to be desired since the prediction of the separation point is off by a factor of 2.

Taulbee[41] considered an alternate approach to the solution of flow over a normal step. His major assumption is that the vorticity is conserved along streamlines throughout the flow including the boundary layer which ultimately gives a non-linear Poisson equation in an "L"-shaped region which he then solved numerically. The comparison

of experimental data and his theoretical solution is quite good but requires a detailed knowledge and some obscure assumptions concerning the distribution of vorticity in the approaching boundary layer and in the separated region. No attempt was made to account for the influence of the wake, or variable channel height.

Because of the poor experimental agreement of the Lighthill-Barrows theory and the detailed boundary layer assumption and lengthy relaxation solution required by Taulbee, it was felt that perhaps another attempt at modeling the flow was justifiable.

II. 2 Factors Considered in the Construction of the Flow Model

In considering the flow field as sketched in Figure II-1, it is seen that several parameters can be used to characterize the flow. These include the geometry (step height and channel height), the boundary layer thickness or some other measure of the boundary layer, and the fluid properties (such as density and viscosity). These dimensional variables can be collected into several sets of dimensionless variables of which the following represents one possible set;

1. The ratio of step height to channel height (h/H), termed here the blockage ratio;
2. the ratio of step height to boundary layer thickness (h/δ) where δ is the undisturbed boundary layer thickness at the step face location; and
3. the Reynolds number ($\rho \frac{q_0 \delta}{\mu}$).

This dimensionless analysis implies that the pressure field that results from the flow over the step would depend upon not only the non-dimensional position but also on each of the dimensionless groups presented above, i.e.,

$$C_p(z/h) \equiv \frac{p - p_0}{\frac{1}{2}\rho q_0^2} = \text{fcn}\,(z/h; h/H, h/\delta, Re_\delta) \qquad \text{(II-1)}$$

In order to determine this dependence in the parameters several recent experimental investigations[36, 41, 42, 43] were studied to determine which of these groups had the most marked effect on the flow field and which could be correlated with some other more computationally useful parameters.

With regard to the Reynolds number effect, it has been observed[42] that the form drag of bluff bodies immersed in turbulent boundary layers is sensibly independent of Reynolds number provided the Reynolds number is greater than several thousand and h/δ is greater than about 0.7. Similarly, the Reynolds number effect on the wall pressure distribution upstream of the step is very small[36] provided the previous restrictions are observed. Thus, for the model considered here, the dependence of the flow field on Reynolds number will be neglected.

It has also been found experimentally[43] that the variation in total pressure $(p + \frac{1}{2} \rho q^2)$ along a streamline upstream of the step is sensibly the same as the variation in an undisturbed boundary layer except very close to the wall. This verifies the assumption employed in the separation analysis presented by Stratford[37] and can be used hereto account for the interaction between the boundary layer and the inviscid flow except for the region close to the wall which itself is very thin compared to, say, the initial boundary layer thickness.[43] Since the length scale employed here is the step height which in turn is larger than the boundary layer, this viscous dominated region close to the wall will be neglected upstream of the separation point.

The separated region ahead of the step has been assumed previously[37, 38] to be a region of stagnant fluid and hence at constant pressure. The plausibility of this is supported somewhat by experimental investigations both from data on the wall and along the step face.[36, 42, 43] In view of this, it appears feasible to use the free-streamline approximation for the separated region in the same manner

as Lighthill.[39] It remains, however, to relate the velocity along the dividing streamline (or equivalently, the separation pressure coefficient C_{ps}) to the non-dimensional variables h/H, h/δ, Re_{δ}.

Because the pressure within the separated region is the result of a complicated mixing process between the high speed external flow and the low speed recirculating flow, the influence of the blockage ratio h/H on the separated pressure coefficient, C_{ps}, would seem negligible. At best, this might change the length of the mixing region but this appears small as long as the blockage ratio h/H is much less than one.[36] The influence of the Reynolds number has already been shown small if fully turbulent flow is considered and if $h/\delta \geq 0.7$. Thus, the separated region pressure coefficient is assumed to be a function of only the parameter h/δ. To display this dependence in graphical form, the values of C_{ps} (h/δ) from several experiments have been plotted in Figure II-2. The data points show some scatter, especially in the range $0 \leq h/\delta \leq 1$, which may reflect both Reynolds number effects and blockage ratio effects. For $h/\delta > 1$, the data scatter is less pronounced and seem to indicate $C_{ps} \rightarrow 0.5 \pm .05$ as $h/\delta \rightarrow \infty$.

Thus, with the assumption that $C_{ps} = C_{ps}$ (h/δ), the effect of the parameter h/δ on the flow field can be replaced by the more computationally useful parameter C_{ps} in view of the free-streamline approximation to the separated region.

At this point, it might be well to examine some of the consequences of the free-streamline approximation to the separation bubble. The first of these is that the separation point is a bifurcation

in the dividing streamline and thus the separation angle is 0°. In viscous flow, in terms of the actual local properties at the separation point, the separation angle is given by;

$$(\tan\theta)_{sep} = -3\left[\frac{d\tau_w}{dx}\Big/\frac{dp_w}{dx}\right]_{sep.} \qquad \text{(II-2)}$$

where $\frac{d\tau_w}{dx}$ is the wall shear stress gradient at separation and $\frac{dp_w}{dx}$ is the wall pressure gradient. This formula is originally due to Oswatatich and was brought to the author's attention by Roshko.[44] Utilizing the measurements of $\tau_w(x)$ and $p_w(x)$ obtained by Bradshaw and Galea,[43] equation II-2 predicts a separation angle of something less than 4°. Other things being equal, for instance the bulk of the dividing streamline location, the calculated length of the separation region is expected to be slightly longer than the actual length.

The second consequence of the free streamline approximation is that $\frac{dC_p}{dx}$ will be discontinuous at separation and furthermore, will be infinite just upstream of the theoretical separation point. Although the pressure gradient observed experimentally upstream of separation is large there is a sharp drop just prior to the actual separation point (see for example Figure 9 of Ref. 43). It is expected then that the theoretical solution will be in error near the actual separation point, but should give good results elsewhere in the flow.

The behavior of the wake on top of the step is the last factor which is anticipated to have a marked effect on the entire flow field because the approaching upstream flow "sees" an effectively larger step because of the separation bubble on top of the step.

It was thought at one time that the flow field downstream of the separated region on top of the step might be likened to the incompressible flow over a rearward facing step. If this were the case, the relation between the minimum pressure coefficient, C_{pc}, (analogous to the base pressure for backward facing step) and the maximum wake pressure coefficient, C_{p2}, could be estimated from the correlation scheme of Roshko and Lau[48] who deduced (in the present notation)

$$C_{p2} \approx 0.35 + 0.65\, C_{pc} \qquad \text{(II-3)}$$

The experimental data from Stevenson[36] for flow over a normal step was compared to this relation and the comparison was rather poor. In particular, effects due to blockage ratio, h/H, and step height-to-boundary layer thickness ratio, h/δ, were significant. This was unfortunate because, as will be seen, only two parameters, C_{ps} and h/H, would have been necessary to completely determine the solution using the wake model to be presented here. It was decided then to use a wake width parameter h'/h (or equivalently C_{p2} using Bernoulli's theorem) as a third input parameter. To do this, however, requires some means of estimating the wake width from the parameters h/H, h/δ, and Re_{δ}.

The values of the wake width parameter h'/h were taken from Stevenson[36] and are shown in Table II-1 for various values of h/H, h/δ, and Re_{δ}. Disregarding the values for h/H = 0.05, it is apparent that h'/h has an almost constant value of 1.23 (within ± 5%) in spite of the fact that h/δ changes by a factor of 4, h/H changes by a factor of 2,

and Re_δ changes by a factor of 2.4. Admittedly, these changes in h/H and Re_δ are not large but no consistent change in h'/h can be correlated to any of the parameters. The comparatively high value of h'/h at a blockage ratio of 0.05 is an anomaly which is inexplicable in view of the other data. Some justification for the independence of h'/h on the parameters h/δ, and Re_δ is given by Good and Joubert[42] for flow over a bluff plate. For lack of additional information with regard to the wake of the step, the value of h'/h will be taken constant at the value of 1.23.

For the mathematical model of the wake region on top of the step, a form of cavity or free-streamline approach was decided upon due to its relative mathematical simplicity. The first model treated was an infinite constant pressure wake but preliminary calculations using this wake model (and the separation model discussed previously) failed to give good upstream comparison to experiment except when the region on top of the step actually was, in fact, a cavity[36] (this solution can be shown to be a special case of the solution presented here). To improve the situation for the flow as shown in Figure II-1, the "dissipation wake" model was then chosen because it appeared to give at least qualitative agreement to the downstream pressure distribution and because it has been used with some success previously.[46, 47] This wake model gives a constant pressure cavity for some distance behind the step to a "reattachment" point where the pressure recovers asymptotically to a far downstream value much like that depicted in Figure II-1. This far-downstream-value is, of course, that value computed from the wake parameter, h'/h and

h/H by

$$C_{p2}(h/H, h'/h) = 1 - \left(1 - \frac{h'}{h}\frac{h}{H}\right)^{-2} \qquad \text{(II-4)}$$

This step completes the modeling of the flow field and the complete mathematical model is shown in the physical plane sketch (or $z = x + iy$ plane where $i = \sqrt{-1}$) in Figure II-3. In summary, the flow approaches from the far left ($x = -\infty$, or Point I) with velocity q_0 and pressure p_0. The dividing streamline, $\psi = 0$, separates from the wall at $z^* = -s + i0$ (point A) and continues along the line AB with constant velocity, $\frac{q_s}{q_0} = \sqrt{1-C_{ps}}$, $0 < C_{ps} < 1$, and reattaches on the step face at $z^* = 0 + ir$ (point B). The dividing streamline continues along the step face BA where it separates at the step corner $z^* = 0 + ih$ (point C) and where the velocity is in the y^*-direction. It then curves downstream forming the constant pressure cavity with a constant velocity $\frac{q_c}{q_0} = \sqrt{1-C_{pc}}$, $C_{pc} < 0$, until it "reattaches" at $z^* = x_R + ih'$ (point D) and proceeds downstream parallel to the original flow direction along DE where the velocity asymptotically approaches $\frac{q_2}{q_0} = \sqrt{1-C_{p2}}$, $C_{p2} = 1 - \left(1 - \frac{h'}{h}\frac{h}{H}\right)^{-2} < 0$. The upper wall of the channel is straight and the total fluid flux contained in the channel is $q_0 H$.

It must be mentioned at this point that the modeling of the flow described here is essentially the same as in the Townsend-Barrows theories with the exception of the wake region. What distinguishes the physics of the upstream model presented here from that by Barrows is the elimination of the finite protruding flat plate necessary in his solution for uniqueness. This artifice in the manner employed by Barrows essentially implies that the separation pressure coefficient is a function of the blockage ratio alone. As described above, this is

not the situation observed for turbulent boundary layer flows and even appears doubtful for laminar boundary layer flows. The theory presented here allows both the parameters h/H and C_{ps} to be selected independently and thus is more applicable to real flow field situations.

The problem to be solved then is to determine the complex potential $f^*(z^*;h/H, h/\delta, h'/h) = \varphi + i\psi^*$ from which the velocity and pressure fields can be computed. Prior to embarking upon this it is first advantageous to select C_{ps}, C_{pc}, and C_{p2} as input parameters instead of the parameters h/H, h/δ, and h'/h for computational ease since the free-streamline approximations are related to the former set. The values of h/H and h'/h are then computed from the solution and h/δ is determined from C_{ps} using Figure II-2.

It is also useful to non-dimensionalize all velocities by the separation bubble velocity, q_s, and to define

$$j \equiv q_0/q_s, \quad k \equiv q_c/q_s, \quad \text{and} \quad \ell \equiv q_2/q_s \quad . \tag{II-5}$$

Clearly, the values j, k, and ℓ are related to C_{ps}, C_{pc}, and C_{p2} through

$$C_{p2} = 1 - 1/j^2, \quad C_{pc} = 1 - k^2/j^2, \quad \text{and} \quad C_{12} = 1 - \ell^2/j^2 \quad . \tag{II-6}$$

Clearly, the following relation between j, k, and ℓ also holds;

$$k \geq \ell \geq j \geq 1 \tag{II-7}$$

The hodograph plane or $w = \frac{U}{q_s} - i\,\frac{V}{q_s} = \frac{q}{q_s} e^{-i\theta}$ plane is shown in Figure II-4a where the physical flow shown in Figure II-3 maps into the 4th quadrant of the w-plane. The other three quadrants of the

w-plane have been constructed from $f^*(w) = \overline{f^*(\bar{w})}$ (where $\overline{(\ )}$ defines complex conjugate) and reflection about the $\frac{V}{q_s}$ - zxis. If we also non-dimensionalize the complex potential f^* by $q_0 H$ then the values of the non-dimensional stream function $\psi = \frac{\psi^*}{q_0 H}$ are indicated in the figure as are the corresponding points in the z^* and w-planes.

To facilitate in the solution to be described later the w-plane is mapped into the complex ζ-plane by the transformation

$$\zeta = \text{Log}\, w = \text{Log}\left(\frac{q}{q_s}\right) - i\theta \qquad \text{(II-8)}$$

and is shown in Figure II-4b. Again, the values of the stream function ψ are shown as are the corresponding points in the z and ζ planes. For convenience the quantities a, b, and c have been defined by

$$a \equiv \text{Log}\, j, \qquad b \equiv \text{Log}\, \ell, \qquad c \equiv \text{Log}\, k \quad . \qquad \text{(II-9)}$$

One implicit assumption employed in the construction of the hodograph plane is that the flow angle in the physical plane (z-plane) is never less than zero. This fact is only pertinent for the flow on the top of the step and is tantamount to assuming that the wake height is the same as the cavity bubble. This eliminates the use of this model for flows such as over a bluff plate where the effective wake width, h', can be less than the obstacle height, h, but the complications of considering this case make the solution much more difficult. These types of flows, and those over arbitrary shaped bodies, can be handled by a method analogous to that presented by Wu et. al.[47] which, in the general case, leads to non-linear integral equations for the solution.

Barring this one restriction then, the problem at hand is to evaluate the complex potential $f(\zeta;a, b, c)$ which satisfies the boundary conditions on IM $\{f\}$ as shown in Figure II-43 and to derive the transformation back to the physical plane.

II. 3 The Complex Potential $f(\zeta;a, b, c)$ and Transformation to the Physical Plane

One straightforward technique of determining the complex potential $f(\zeta;a, b, c) = \varphi + i\psi$ that satisfies the boundary conditions on ψ as depicted in Figure II-4b is by superposition of an infinite number of sources and sinks of strength $Q = 2$ located at

$$\begin{aligned} &(2nc \pm a,\ m\pi) \quad \text{(sources)} \\ &(2nc \pm b,\ m\pi) \quad \text{(sinks)} \end{aligned} \tag{II-10}$$

where $m, n = \ldots -2, -1, 0, 1, 2 \ldots$

Upon doing this, however, it is clear that the ζ-plane will be covered with a series of rectangles identical to the "unit cell" shown. Thus, one can conclude that the function $f(\zeta;a, b, c)$ is doubly-periodic, i.e., periodic in the real direction with period 2π, and periodic in the imaginary direction with period $i\pi$. Functions which exhibit this behavior, and are single valued, are termed Elliptic Functions (see Whittaker and Watson, ref. 49). The complex potential $f(\zeta;a, b, c)$ is not single valued, however, due to the branch cuts from $\zeta = \pm a + i0$ to $\zeta = \pm b + i0$. If we instead consider the function $G(\zeta) \equiv e^{\pi f(\zeta)}$, then these branch cuts are eliminated and $G(\zeta)$ is both single-valued and doubly periodic and hence is an elliptic function which has zeroes at $\zeta = \pm a + i0$ and poles at $\zeta = \pm b + i0$. It is known[49] that this Elliptic function can be written as the product and quotient of the quasi doubly-periodic Theta functions of the first kind, $\vartheta_1(z,q)$ where z is the argument and $q \equiv e^{i\pi\omega_2/\omega_1}$ (ω_2/ω_1 is the ratio of the imaginary and real periods). Taking $f(0;a, b, c) = 0$, the resultant expression for the complex potential $f(\zeta;a, b, c)$ is then found to be

$$f(\zeta;a,b,c) = \frac{1}{\pi}\log\left\{\frac{\vartheta_1^2(\frac{\pi b}{2c},q)}{\vartheta_1^2(\frac{\pi a}{2c},q)}\cdot\frac{\vartheta_1(\frac{\pi(\zeta-a)}{2c},q)\,\vartheta_1(\frac{\pi(\zeta+a)}{2c},q)}{\vartheta_1(\frac{\pi(\zeta-b)}{2c},q)\,\vartheta_1(\frac{\pi(\zeta+b)}{2c},q)}\right\} \tag{II-11}$$

where $q = \exp(-\pi^2/2c)$

and $\vartheta_1(z,q) = 2\,q^{\frac{1}{4}}\sum_{n=0}^{\infty}(-1)^n\,q^{n(n+1)}\,\mathrm{Sin}(2n+1)\,Z$

It remains now to complete the solution by deriving the transformation to the physical plane (z-plane). To accomplish this, use the fact that

$$\frac{df^*}{dz^*} = u - iv = q\,e^{-i\theta} = q_s\,w(\zeta) \quad . \tag{II-12}$$

Non-dimensionalizing f^* with q_0H and z^* with H and using $j \equiv \frac{q_0}{q_s}$ allows equation II-12 to be written as

$$dz = \frac{j}{w(\zeta)}\,df(\zeta) = j\,e^{-\zeta}\,\frac{df}{d\zeta}\,.\,d\zeta \quad . \tag{II-13}$$

This equation can be integrated along any path in the ζ-plane that does not cross the branch cuts. If point (C) is taken as the start of this path then equation II-13 integrates to

$$\frac{z(\zeta) - i\lambda}{j} = \int_{c-\frac{i\pi}{2}}^{\zeta} e^{-\zeta}\,\frac{df}{d\zeta}\,d\zeta \tag{II-14}$$

where from equation II-11 the derivative $\frac{df}{d\zeta}$ may be evaluated. Carrying out this procedure and inserting it in equation II-14 results in the expression

$$\frac{z(\zeta)-i\lambda(a,b,c)}{j} = Z(\zeta;a) + Z(\zeta;-a) - Z(\zeta;b) - Z(\zeta;-b) \tag{II-15}$$

$$\text{where } Z(\zeta;\alpha) \equiv \frac{1}{2c} \int_{c-\frac{i\pi}{2}}^{\zeta} e^{-\tilde{\zeta}} \frac{\vartheta_1'\left[\frac{\pi}{2c}(\tilde{\zeta}-\alpha),\, q\right]}{\vartheta_1\left[\frac{\pi}{2c}(\tilde{\zeta}-\alpha),\, q\right]}\, d\tilde{\zeta} \qquad \text{(II-16)}$$

Thus, the transformation to the physical or z-plane is complete requiring only quadratures of the type shown in equation II-16. The evaluation of this integral is facilitated by employing the infinite series formulations for $\vartheta_1'(\zeta)/\vartheta_1(\zeta)$ as (49);

$$\frac{\vartheta_1'(\zeta,\, q)}{\vartheta_1(\zeta,\, q)} = \text{Cot}\, \zeta + 4 \sum_{n=1}^{\infty} \frac{q^{2n}\, \text{Sin}\, 2n\, \zeta}{1-q^{2n}} \quad . \qquad \text{(II-17)}$$

Even using this expression, the evaluation of equation II-16 is rather long and not as straightforward as it might seem due principally to convergence problems. Because of the length, only one representative integration will be presented here and is shown in Appendix II-A. The derivation shown in Appendix II-A is actually more general than the solution presented here in that it accounts for a wedge shaped obstacle rather than a normal step. Results are shown for the normal step alone because the availability of the experimental evidence allows the two parameters C_{ps} and h'/h to be evaluated in a realistic manner. The numerical evaluation of the formulae derived in Appendix II-A is straightforward.

The locations of the various points in the flow field (e.g., the separation point) along with the wall pressure distributions upstream of separation and in the downstream portion of the wake have been computed and are presented in Section II-4.

The velocity at any point within the flow can be determined by using the relations $z(\zeta)$ (equation II-15) and $\zeta = \log(q/q_s) - i\,\theta$. This

is not presented here except along the upstream wall and in the wake where the pressure coefficient, C_p, has been evaluated from q/U_s.

It is worthwhile at this point to mention that at one time it was thought more advantageous to integrate equation II-14 by parts first which results in an alternate expression for the transformation to the z-plane

$$\frac{z - i\lambda}{j} = e^{-\zeta} f(\zeta) - \frac{i}{k} f(c - \frac{i\pi}{2}) + \int_{c-\frac{i\pi}{2}}^{\zeta} e^{-\tilde{\zeta}} f(\tilde{\zeta}) d\tilde{\zeta} \quad . \tag{II-18}$$

The evaluation of this expression requires numerical integration which is expensive because of the iterative method to determine $C_{pc}(C_{ps_1}, C_{p2}, h/H)$. With the present formulation, however, solutions are obtained in infinite series form which can be rapidly evaluated on a high-speed computer at a considerably less expense. In addition the closed form solution permitted a verification of the mathematics by comparison to an independent solution of a special case of the present formulation.

II. 4 Results

II. 4. 1 Downstream Cavity Shape and the Evaluation of h/H

Carrying out the quadrature indicated in equation II-16 along the path C → D or $\zeta = C - i(\frac{\pi}{2} - \eta)$, $0 \leq \eta \leq \frac{\pi}{2}$, gives the parametric equations for the constant pressure cavity on top of the step (this solution is shown in some detail in Appendix II-A). The result of this integration is

$$\frac{x_c(\eta)}{H} = \frac{4j}{\pi k} \sum_{n=1}^{\infty} (-1)^n g_n(k)\, S_n(j, \ell) \left[\sin\eta \cos 2n\eta - \frac{1}{2n} \cos\eta \sin 2n\eta\right]$$

$$\frac{y_c(\eta)}{H} = 1 - \frac{j}{\ell} + \frac{4j}{\pi k} \sum_{n=1}^{\infty} (1-)^n g_n(k)\, S_n(j, \ell) \left[\cos\eta \cos 2n\eta + \frac{1}{2n} \sin\eta \sin 2n\eta\right]$$

$$\text{for } 0 \leq \eta \leq \pi/2 \qquad \text{(II-19)}$$

where; $g_n(k) \equiv \dfrac{k^{2n}}{k^{4n} - 1}$

$$S_n(j, \ell) \equiv \frac{2n}{4n^2 - 1} \frac{(\ell^{2n} - j^{2n})(\ell^{2n} j^{2n} - 1)}{(\ell j)^{2n}} \qquad \text{(II-20)}$$

and the fact that the wake width, h', is given by $h'/H = 1 - j/\ell$ has been used.

Evaluating equation II-19 at $\eta = 0$ and $\eta = \pi/2$ respectively gives that

$$\lambda \equiv h/H(j, \ell; k) = 1 - j/\ell + \frac{4j}{\pi k} \sum_{n=1}^{\infty} (-1)^n g_n(k)\, S_n(j, \ell)$$

$$x_c/h = \frac{4j}{\lambda\, \pi\, k} \sum_{n=1}^{\infty} g_n(k)\, S_n(j, \ell) \qquad \text{(II-21)}$$

The series representation for h/H is absolutely convergent for all values of $\ell/k \leq 1$ (or $C_{p2} \leq C_{pc}$). The representation for x_c/h is absolutely convergent only if $\ell/k < 1$ and is divergent for $\ell/k = 1$. Both of these are reasonable in the light of physical reasoning since, as

$C_{p2} \rightarrow C_{pc}$, one would expect the wake model to approach the "open wake" formulation where the "reattachment point" moves to downstream infinity.

As a check on this solution consider the case where there is no separated region in front of the step, i.e., $q_s \rightarrow 0$ and let $j, k, \ell \rightarrow \infty$ in such a manner that $j/k = \frac{q_0}{q_c} \equiv U$, $\ell/k = \frac{q_2}{q_c} \equiv V$. The product $g_n(k)\, S_n(j, \ell)$ then can be shown to be

$$g_n(k)\, S_n(j, \ell) \rightarrow (V^{2n} - U^{2n})\, \frac{2n}{4n^2-1} \quad . \tag{II-22}$$

Utilizing the identity

$$1 + \sum_{n=1}^{\infty} (-1)^n x^{2n} \frac{4n}{4n^2-1} = (\frac{1}{x} - x)\tan^{-1}x \tag{II-23}$$

in the expression for h/H(equation II-21) it can be shown that

$$\lambda \equiv \frac{h}{H} \rightarrow \frac{V-U}{V} - \frac{2U}{\pi}\left\{(V - \frac{1}{V})\tan^{-1}V - (U - \frac{1}{U})\tan^{-1}U\right\}$$

$$\text{as } q_s \rightarrow 0 \tag{II-24}$$

This checks an independent derivation by Wu.[47]

II. 4. 2 Reattachment and Separation Locations

Integrating equation II-16 from point "C" to point "B" (i.e., $\zeta = c - i\pi/2$ to $\zeta = 0 - i\pi/2$) gives as the reattachment point location

$$\frac{r}{h} = 1 - \frac{8j}{\lambda c k} \sum_{n=1}^{\infty} (k+(-1)^{n-1})T_n(a, b, c) \tag{II-25}$$

where

$$T_n(a, b, c) \equiv \frac{q^n}{1-q^{2n}} \frac{(\frac{n\pi}{c})}{(\frac{n\pi}{c})^2+1} \text{ Sin } \frac{n\pi}{c}(\frac{a+b}{2}) \text{ Sin } \frac{n\pi}{c}(\frac{b-a}{2}) \tag{II-26}$$

and $q = \exp\{-\pi^2/2c\}$

This expression is absolutely convergent for all $c > 0$ which is satisfied if $C_{ps} > 0$ and $C_{pc} < 0$.

Now integrating equation II-16 from B towards A or along the line $\zeta = 0 - i(\frac{\pi}{2} - \eta)$, $0 < \eta < \pi/2$, gives the parametric equations for the separation region:

$$\frac{x_s(\eta)}{h} = \frac{2j}{\lambda\pi}\left\{f_1(\eta, b) - f_2(\eta, b) - 2\sum_{n=1}^{\infty}(-1)^n \frac{g_n(k)S_n(j, \ell)}{k^{2n}} \times \right.$$

$$\left. \left[\frac{1}{2n}\cos\eta \sin 2n\eta - \sin\eta \cos 2n\eta\right]\right\}$$

$$\frac{y_s(\eta)}{h} = \frac{r}{h} + \frac{2j}{\lambda\pi}\left\{f_2(\eta, b) - f_2(\eta, a) - 2\sum_{n=1}^{\infty}(-1)^n \frac{g_n(k)S_n(j, \ell)}{k^{2n}} \cdot \right.$$

$$\left. \left[1 - \cos\eta \cos 2n\eta - \frac{1}{2n}\sin\eta \sin 2n\eta\right]\right\} \qquad \text{(II-27)}$$

$$(0 \le \eta \le \pi/2)$$

where

$$f_1(\eta, \alpha) = \tfrac{1}{2}\log\left\{\frac{\cosh\alpha + \sin\eta}{\cosh\alpha - \sin\eta}\right\}\cosh\alpha$$

$$f_2(\eta, \alpha) = -\tan^{-1}\left\{\sinh\alpha \frac{1 - \cos\eta}{\sinh^2\alpha + \cos\eta}\right\}\sinh\alpha \qquad \text{(II-28)}$$

and $g_n(k)$ and $S_n(j, \ell)$ are as shown in equation II-20.

Setting $\eta = \pi/2$ gives as the separation point location

$$\frac{S}{h} = -\frac{j}{\lambda\pi}\left\{\frac{\ell^2+1}{\ell}\log\left[\frac{\ell+1}{\ell-1}\right] - \frac{j^2+1}{j}\log\left[\frac{j+1}{j-1}\right] + 4\sum_{n=1}^{\infty}\frac{g_n(k)S_n(j, \ell)}{k^{2n}}\right\} \qquad \text{(II-29)}$$

which is absolutely convergent for all $\ell < k^2$.

II. 4. 3. Wall Pressure Distribution Upstream of Separation

Integrating equation II-16 along the path A-I gives the wall pressure coefficient distribution upstream of the separated region as

$$\frac{x(C_p)+S}{h} = \frac{1}{2c\lambda}\left[f_3(C_p;b)-f_3(C_p;a)\right] + \frac{8j}{c\lambda}\sum_{n=1}^{\infty} q^n\, T_n(a,b,c)\cdot \left\{1-e^{-\xi}\left[\cos\frac{n\pi\xi}{c}+\left(\frac{c}{n\pi}\right)\sin\frac{n\pi\xi}{c}\right]\right\} \qquad \text{(II-30)}$$

where $q = \exp\{-\pi^2/2c\}$

$$\xi(C_p) = a + \tfrac{1}{2}\log(1-C_p) \qquad 0 \le C_p \le C_{ps}$$

$$f_3(C_p;\alpha) = \csc^2\frac{\pi\alpha}{2c}\int_{C_{ps}}^{C_p} \frac{\operatorname{Ctn}\frac{\pi\xi(\tilde{C}_p)}{2c}}{\operatorname{Ctn}^2\frac{\pi\alpha}{2c}-\operatorname{Ctn}^2\frac{\pi\xi(\tilde{C}_p)}{2c}}\,\frac{d\tilde{C}_p}{(1-\tilde{C}_p)^{\frac{3}{2}}} \qquad \text{(II-31)}$$

The infinite series in equation II-30 can be shown to be absolutely convergent for all $c > 0$ (or if $C_{pc} < 0$ and $C_{ps} > 0$). The function $f_3(C_p;b)$ is convergent for $0 \le C_p \le C_{ps}$, the function $f_3(C_p;a)$ is logarithemically singular as $C_p \to 0$. Thus since $x \sim -\log(C_p)$ as $C_p \to 0$, the pressure coefficient decays exponentially as $x \to -\infty$. A closed form representation for the integral appearing in $f_3(C_p;\alpha)$ could not be found and was evaluated numerically.

II. 4. 4 Wake Pressure Recovery

Integrating equation II-16 along D → E gives as the pressure distribution on top of the step as

$$\frac{x(C_p)-x_R}{h} = \frac{1}{2c\lambda}\left[f_4(C_p;b) - f_4(C_p;a)\right] + \frac{8j}{\lambda ck}\sum_{n=1}^{\infty}(-q)^n\, T_n(a,b,c)\left\{1-e^{\xi}\left[\cos\frac{n\pi\xi}{c} - \left(\frac{c}{n\pi}\right)\sin\frac{n\pi\xi}{c}\right]\right\} \qquad \text{(II. 32)}$$

where

$$\xi(C_p) = (c-a) - \tfrac{1}{2}\log(1-C_p) \qquad C_{pc} \le C_p \le C_{p2}$$

$$f_4(C_p;\alpha) = \csc^2\frac{\pi\alpha}{2c}\int_{C_{pc}}^{C_p} \frac{\tan\pi\xi(\tilde{C}_p)/2c}{\operatorname{Ctn}^2\frac{\pi\alpha}{2c}-\tan^2\frac{\pi\xi(\tilde{C}_p)}{2c}}\,\frac{d\tilde{C}_p}{(1-\tilde{C}_p)^{\frac{3}{2}}} \qquad \text{(II. 33)}$$

The remarks after the formulation of the pressure distribution in front of separation are applicable here except both $f_4(C_p;b)$ and $f_4(C_p;a)$ are convergent as $C_p \rightarrow C_{p2}$.

II. 4. 5 Extension to Other Flow Models

The equations II-19 through II-33 inclusive, have been derived using the flow model described in Section II. 3. The theory presented is not limited to this model alone, however, by considering various limiting cases of the parameters a, b, and c (or j, k, ℓ);

1. Flow models without the forward separated region are obtained by letting $q_s \rightarrow 0$ with $q_0/q_c \equiv U$ and $q_2/q_c \equiv V$ as indicated in Section II. 4. 1;
2. Flow models with infinite constant pressure cavities downstream are obtained by setting $q_2 = q_c$ (or equivalently $k = \ell$ or $c = b$);
3. Infinite flow fields (no channel wall) are obtained by setting $q_2 = q_0$ (or equivalently, $j = \ell$ or $a = b$);
4. Flow fields without separation on top of the step are obtained by letting $C_{p2} = 1 - (1-h/H)^{-2}$ and $C_{pc} \rightarrow -\infty$ (or $j = (1-h/H)\ell$ and $k \rightarrow \infty$).

The solutions obtained from the limiting cases indicated above are in some cases solvable by alternate methods and as such can be used to check the results presented here as was done in Section II. 4. 1. The solutions so obtained are not presented here explicitly because they are presented elsewhere or are quite complicated.

II. 5 Evaluation of Results and Comparison with Experiment

The infinite series solutions for the geometry and wall pressure distributions presented in the previous section were evaluated numerically on an I. B. M. 360/75 digital computer. This utilized a straightforward computer program written by the author for this purpose. Since it was desired to use known or estimated values of C_{ps}, C_{p2}, and h/H as input parameters, the relation for $\frac{h}{H}(C_{ps}, C_{p2}; C_{pc})$ as given in equation II-21 was inverted numerically to determine the proper choice of C_{pc}. Having effected this, the remaining relations were evaluated by simply summing the indicated series or using a standard integration subroutine. Generally speaking, the complete solution was computed in a matter of two seconds of computer time.

The wall pressure distribution upstream of the step face was one of the main objectives of this investigation. To this effect, the solution obtained here was compared against the solutions for other flow models and is shown in Figure II-5 along with an experimentally measured wall pressure.[36] These other flow models were computed from known solutions (Model A) or from various limiting cases of the theory presented here (Models B and C).

It is evident from Figure II-5 that models A and B, which do not account for the upstream separated region, underestimate the magnitude and extent of the upstream influence in addition to being grossly in error in the separated region. Conversely, Model C which models the upstream separated region and models the wake region with an infinite and constant pressure cavity, overestimates the upstream influence. The model proposed herein (Model D) shows excellent agreement

with the measured data especially in the far field. The poor agreement near the separation point ($C_{ps} = 0.4$) was anticipated as mentioned earlier.

The theoretical solutions to Model D were then compared with experimental data taken for a series of step sizes in a constant height channel and are shown in Figure II-6. The abscissa for this graph is given directly in inches rather than step heights to more easily distinguish between the five cases shown. The input values of C_{ps} and C_{p2} were taken directly from the experimental data and agree closely with the values predicted by the methods discussed in Section II. 2.

The comparison between theory and experiment as shown in Figure II-6 is seen to be adequate in the "far-field" for all step sizes. For the larger step sizes, the theoretical wall pressure distribution is seen to be in excellent agreement with experiment up to a pressure coefficient near 0. 28. For step sizes less than the undisturbed boundary layer thickness ($h \leq 1''$) significant departures are noted when the pressure gradient increases rapidly. The important fact to be realized from the above comparison is that the flow model predicts the upstream flow field very well especially for $h/\delta \geq 2$. Admittedly, the pressure distribution near the separation point is in error or has been discussed and to account for this would require either a viscous solution or some form of inviscid rotational solution.

In Figure II-7 the upstream wall pressure is shown for the flows over a step both with cavitation and without cavitation. These are in turn compared with the experimental data for each of these situations. As can be seen, the model accounts for the effect of the downstream

flow field in addition to giving good quantitative agreement in the far field wall pressure.

The pressure distribution downstream of the step is shown in Figure II-8 along with the corresponding experimental data[36] for one specific case. The model obviously gives a lower base pressure, C_{pc}, than observed and also a faster recovery to the downstream pressure level, C_{p2}. This behavior is typical of the comparison at other values of the input parameters. It should be noted, however, that the theoretical curve shown is actually the pressure distribution along the theoretical dividing streamline rather than along the actual dividing streamline and is probably closer to the theoretical curve because of the pressure gradients caused by streamline curvature and a finite recirculating velocity in the separated region on top of the step.

In Figure II-9 the theoretical dividing streamline shapes for both non-cavitating and cavitating flows are shown along with the experimental observation[36] (from photographs of air or dye injected upstream of the step). The comparison for cavitating flow is considerably better than that for the non-cavitating flow. It should be remembered that it is not the purpose of the wake model to match the dividing streamline but to approximate the displacement effect of the wake. In the case of the non-cavitating flow, the far downstream displacement thickness of the wake is used as an input parameter to the solution and because of this the theoretical dividing streamline location is set. For the cavitating flow, on the other hand, the displacement thickness is primarily due to the cavity alone rather than to the viscous effects and thus good agreement between theory and experiment is expected.

With the good agreement between theory and experiment insofar as the upstream wall pressure distribution is concerned, the effect of the blockage ratio can now be assessed. In order to illustrate this clearly, the values of C_{ps} and h'/h were held constant at values of 0.50 and 1.23 respectively and the remaining parameter, h/H, varied between the limits of 1/5 and 1/10,000. The results of these calculations are shown in Figure II-10 where the pressure coefficient is depicted as a function of distance from the step face (in step heights). It is immediately apparent that the finite blockage ratio effects are not negligible as is occasionally assumed. For example, the distance to where the pressure coefficient is e^{-1} of the separated region value, C'_{ps}, differs by a factor of two for a blockage ratio of 20% and an infinitely high channel. For smaller values of the pressure coefficient this behavior is even more pronounced. It should also be noted that this blockage ratio effect is most predominant in the far field (say $x/h < -4$) which is where the theory and experiment are in best agreement.

Also shown in Figure II-10 is the effect of slight changes in the wake width parameter, h'/h, for the 10% blockage ratio flow field. The indicated limits of h'/h represent the upper and lower bounds of the experimentally observed values[36] (see also Table II-1). As can be seen, the effect of small changes in h'/h is slight and hence a nominal choice of this parameter gives a fairly accurate representation of the upstream wall pressure field.

Also indicated in Figure II-10 is the effect of blockage ratio in the length of the separated region (normalized by the value at $h/H = 0$)

and the distance to the stepface reattachment point, r/h. Both of these quantities are shown to be sensibly independent of blockage ratio for values less than, say, 5%. This indicates roughly that the finite channel height may have little effect on the geometry of the actual separated region which, by the reasoning discussed in Section II. 2, implies the value of C_{ps} is insensitive to the blockage ratio.

Comparing the predicted separation distance with experiment shows it to be about a factor of 2 too high. Similarly, the distance to the stepface reattachment point is also too high; values of about 0. 6h are observed whereas 0. 9h is predicted theoretically. Despite this poor agreement it is felt that the effect of blockage ratio on the actual values may be indicated by the curves shown in Figure II-10. No experimental data is available to confirm this, however.

The downstream pressure field for the cases computed in Figure II-10 is not shown because these are all very much like the situation depicted in Figure II-8.

The upstream wall pressure distribution has been shown predictable for a given blockage ratio h/H, a reasonable estimate of the wake width h'/h, and knowledge of the value of the separated region pressure coefficient. In order to increase the usefulness of the theory it would be advantageous that the precise value of C_{ps} not be required inasmuch as the details of the boundary layer may not be known. To accent this point, the parameter C_{ps} was varied while holding the blockage ratio and wake width parameter constant. The results of this calculation are shown in Figure II-11 for $C_{ps} = 0.5,\ 0.425,$ and 0.38 (this corresponds to $h/\delta \geq 1.5$) and it is seen that upstream of the

separation region, say $x/h < -4$, the three pressure distributions are almost identical. Again, this region is where the theory is in good agreement with experiment. Close to the theoretical separation point, where the three cases deviate from one another significantly is where the theory fails to give adequate information at any rate. Thus, it appears that in addition to a reasonable estimate of the wake width, h'/h, a reasonable estimate of the value of C_{p_s} is sufficient to determine the far upstream influence at a given blockage ratio. This finding, that the far field pressure distribution is predominantly affected by the geometry and not the boundary layer, was first determined experimentally and is verified theoretically here.

The insensitivity of upstream effects to the parameter h/δ is in contradiction to the findings of both Bradshaw[43] and Taulbee.[41] Bradshaw, in reaching the conclusion that the dominant scale for the upstream pressure field was δ, neglected completely the effects of blockage ratio which for his experiment was as high as 23% Taulbee, on the other hand, conducted experiments in an open jet to simulate an infinite flow field. Undoubtedly, blockage effects can also become significant even with the free surface effect. To show this theoretically would necessitate a solution including the additional free surface.

II.6 Conclusions

An inviscid flow model employing elements of free-streamline theory has been constructed on physical grounds to approximate the incompressible flow over a normal step in a channel.

The solution to this model depends on two experimentally evaluated parameters; the separated region pressure coefficient, C_{p_s}; and the effective displacement effect of the downstream wake, h'/h. Far more dominant in determining the upstream flow field is the geometry of the step and channel given by the parameter h/H. The comparison between theory and experiment for the upstream pressure field is seen to be quite good, especially for step sizes greater than two local undisturbed boundary layer thicknesses. Close to the separated region upstream of the step boundary layer effects are significant and are unaccounted for here except in a gross manner.

$\frac{h}{H}$	$\frac{h}{\delta}$	$Re_{\delta} \times 10^{-4}$	$\frac{h'}{h}$
0.2	2	7.5	1.21
	4	7.5	1.23
	4	1.2	1.22
0.1	1.54	5.0	1.27
	1.39	8.6	1.20
	2	7.5	1.25
	2	1.2	1.21
0.05	1	7.5	1.46
	1	1.2	1.30

Note: Data taken from Stevenson[36]

TABLE II-1. Effective Wake Widths from Experiment

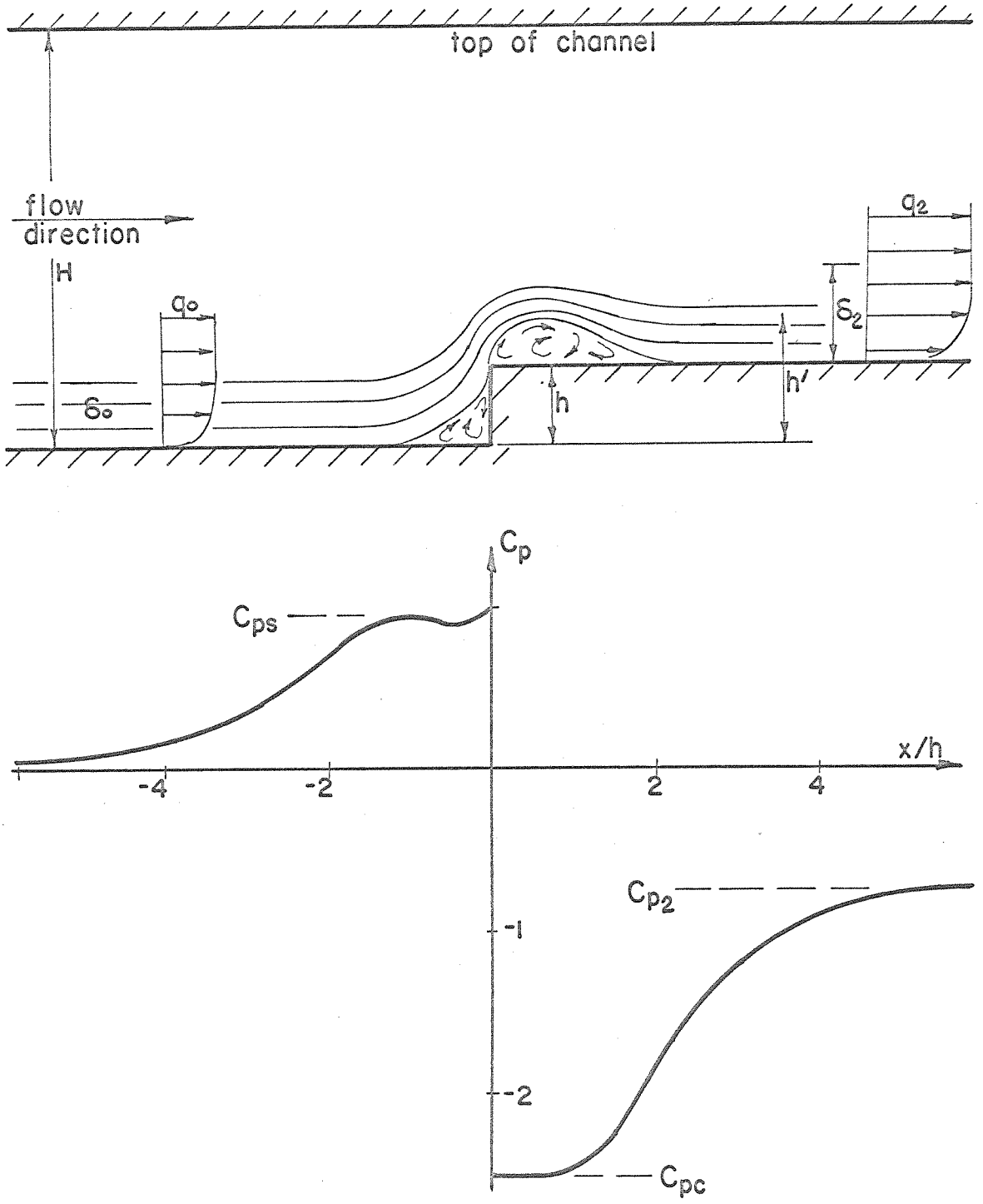

FIG. II-1 SCHEMATIC OF FLOW FIELD AND WALL PRESSURE DISTRIBUTION

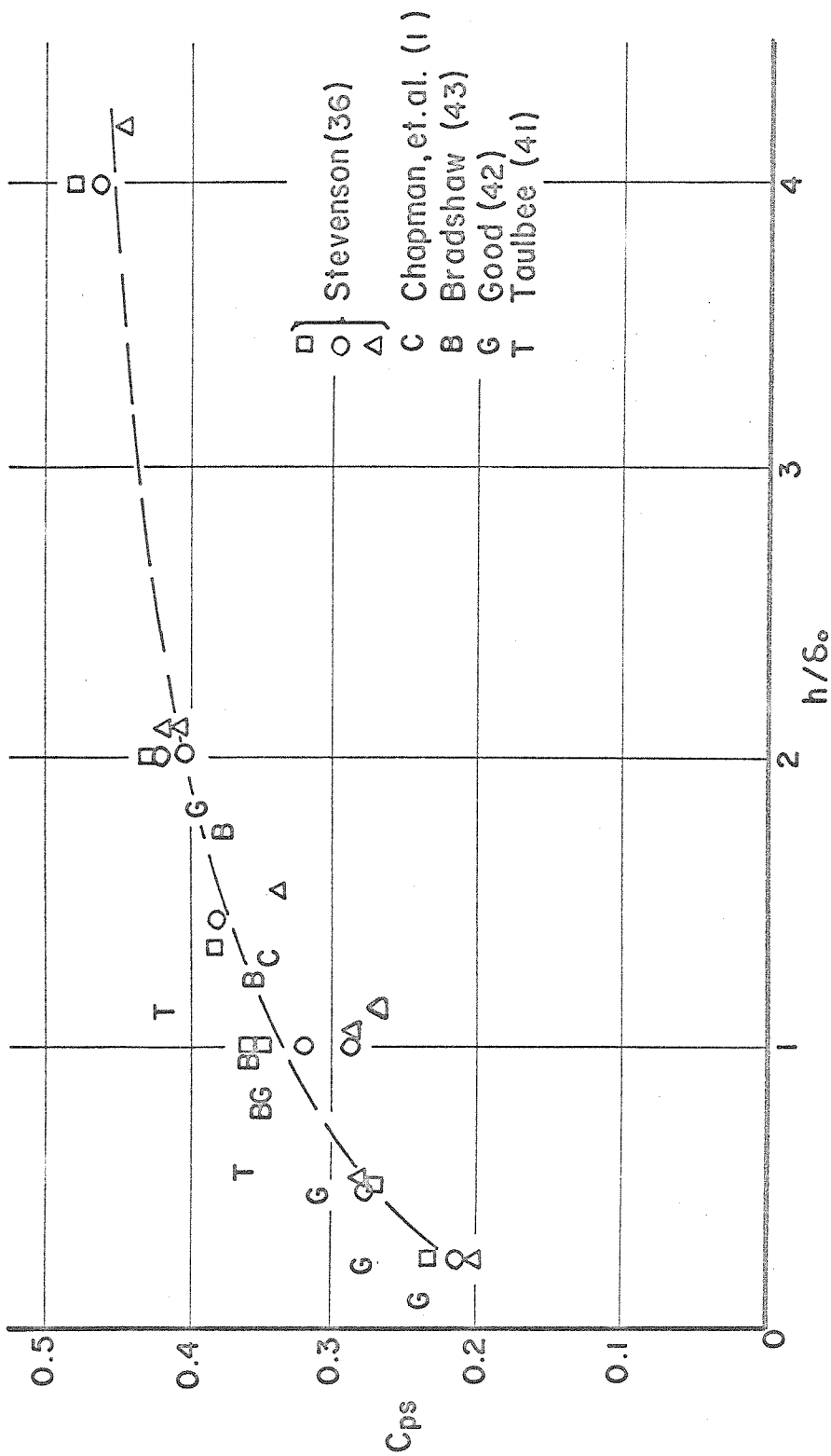

FIG. II-2 SEPARATED REGION PRESSURE COEFFICIENT

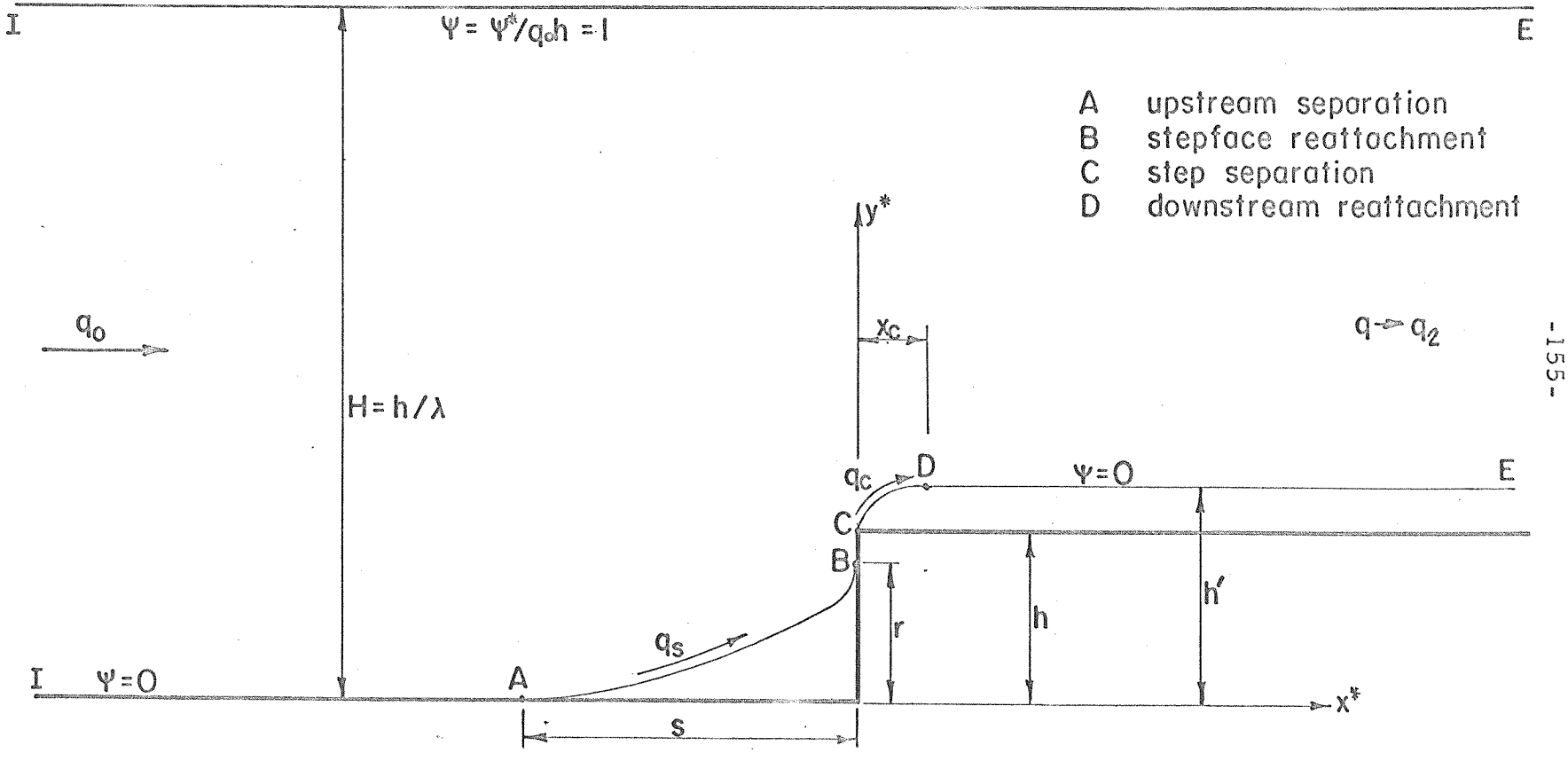

FIG. II-3 PHYSICAL PLANE ($z^* = x^* + iy^*$ plane)

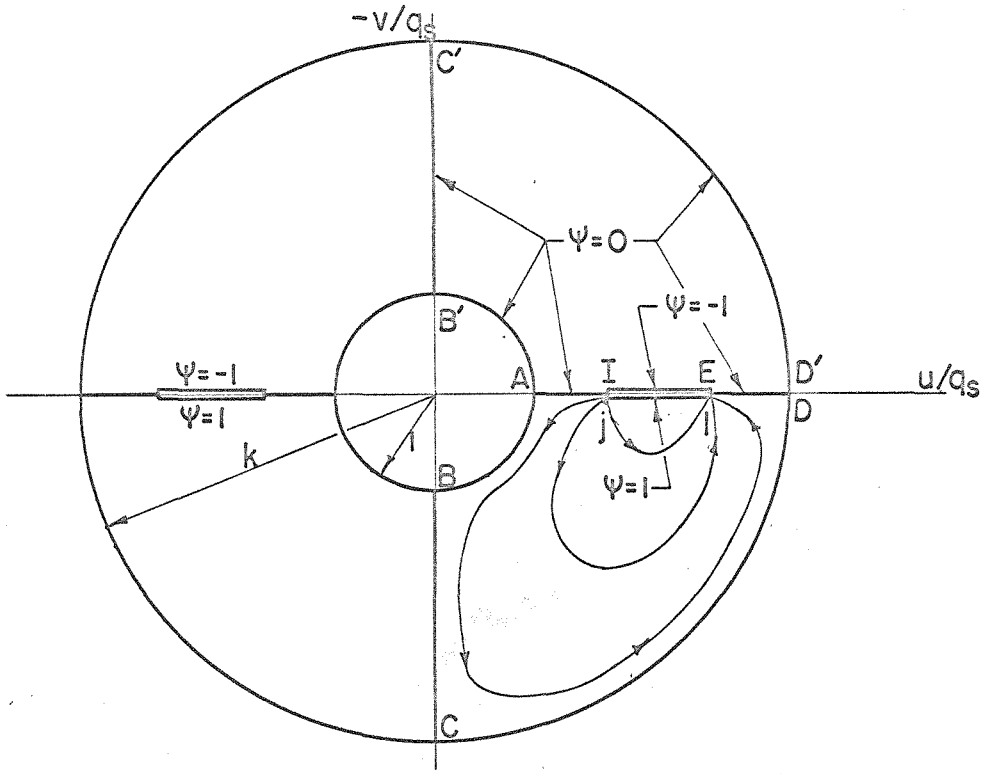

HODOGRAPH PLANE $w=(u-iv)/q_s$

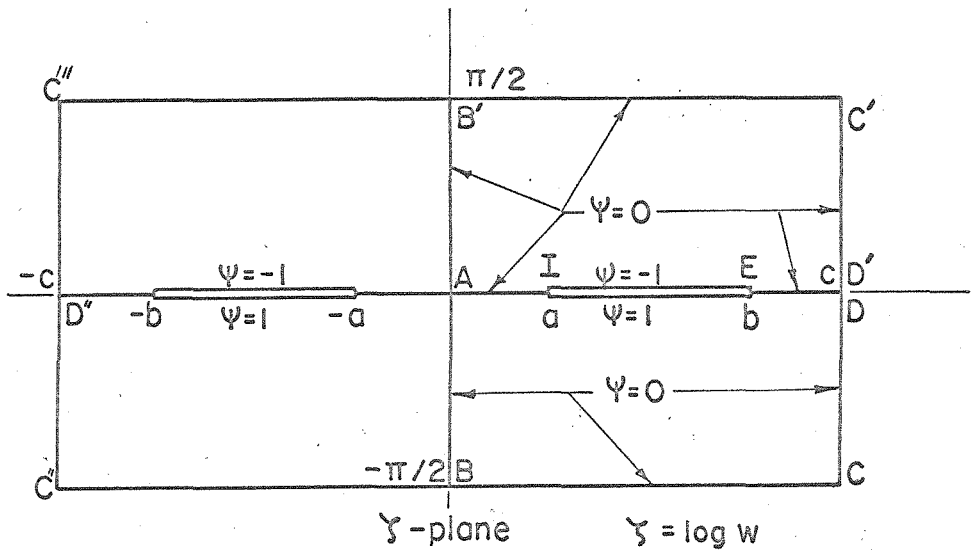

FIG. II-4 HODOGRAPH AND ζ PLANES

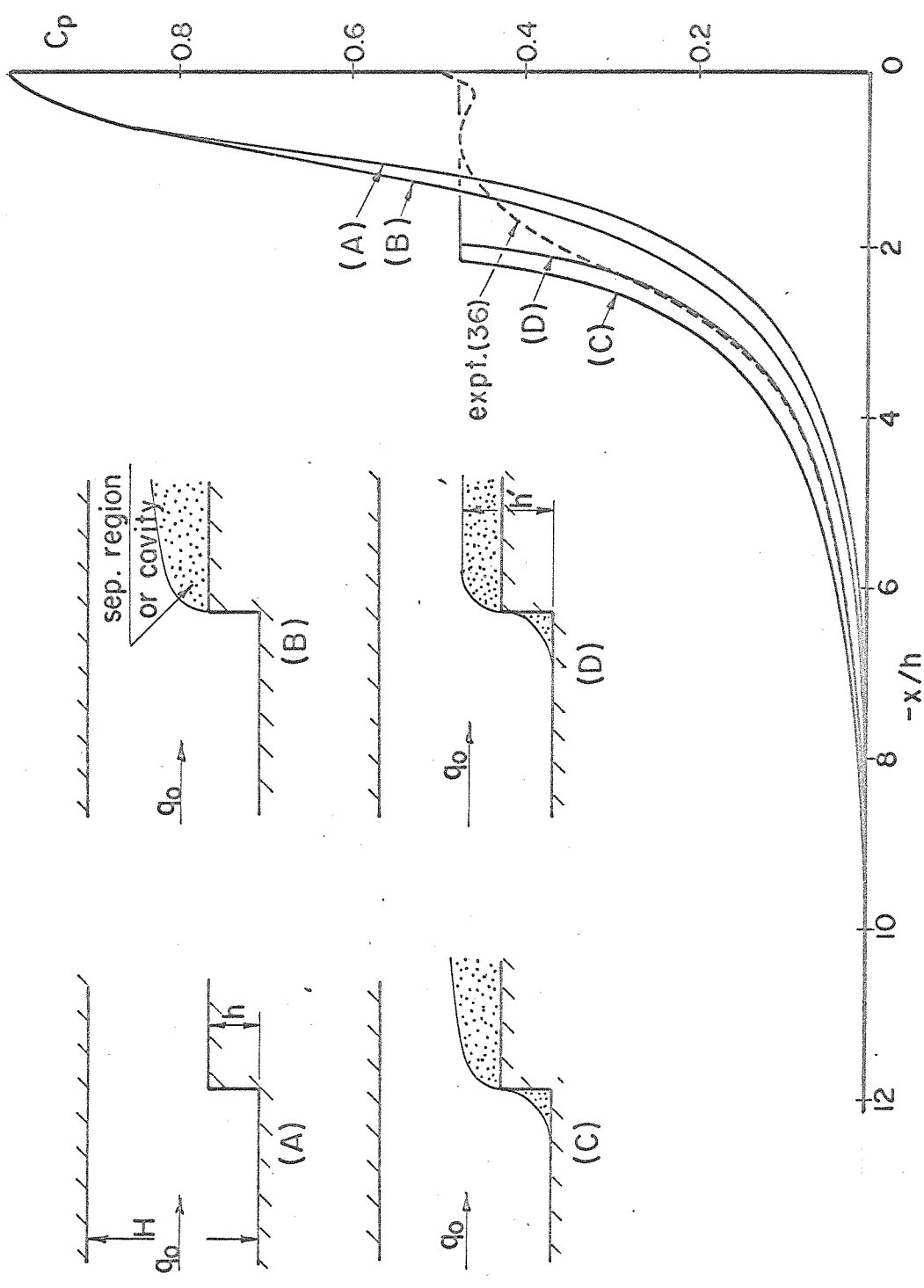

FIG. II-5 UPSTREAM PRESSURE DISTRIBUTION - COMPARISON OF VARIOUS MODELS WITH EXPERIMENT

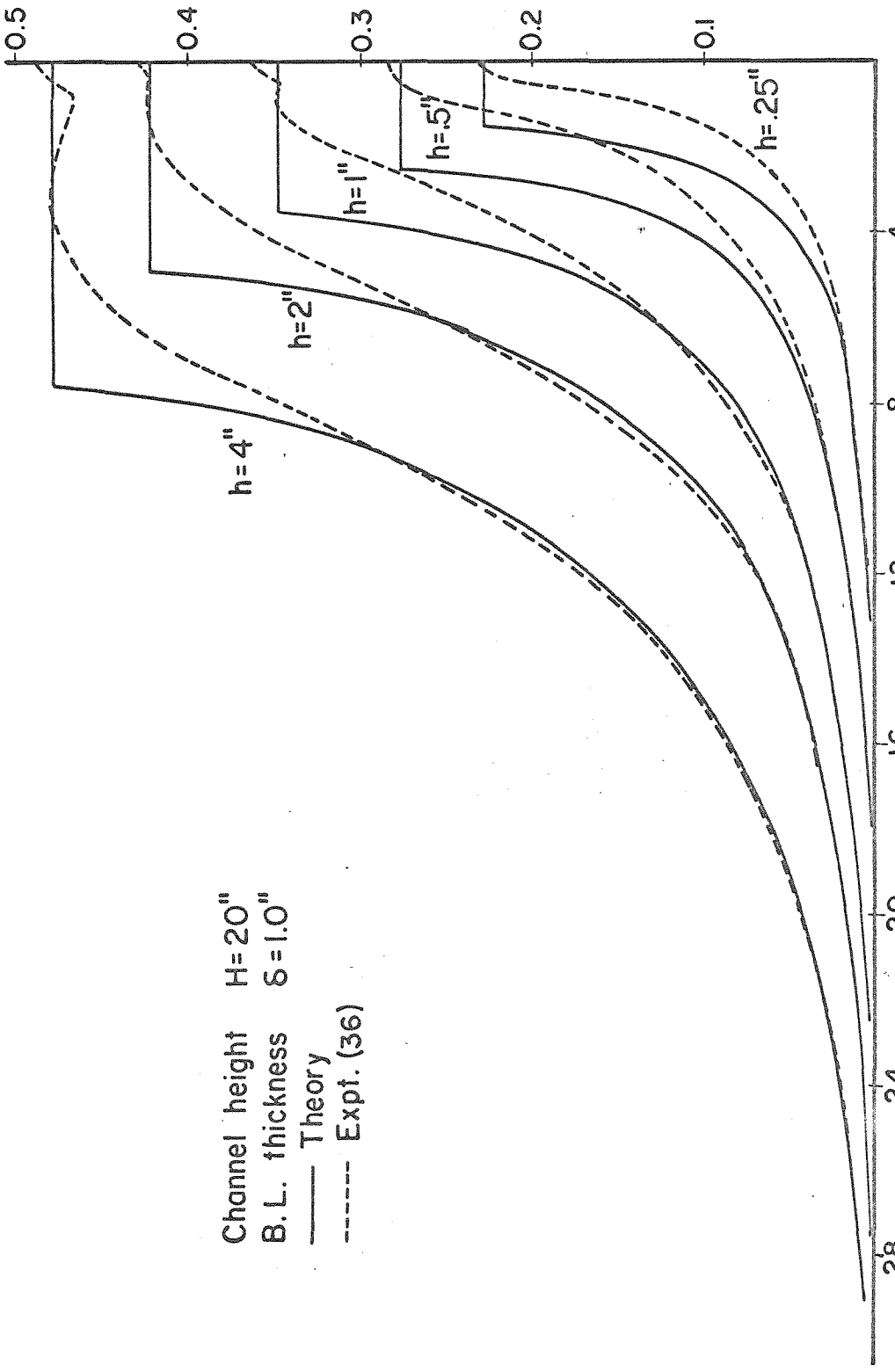

FIG. II-6 UPSTREAM PRESSURE DISTRIBUTION - EFFECT OF STEP SIZE

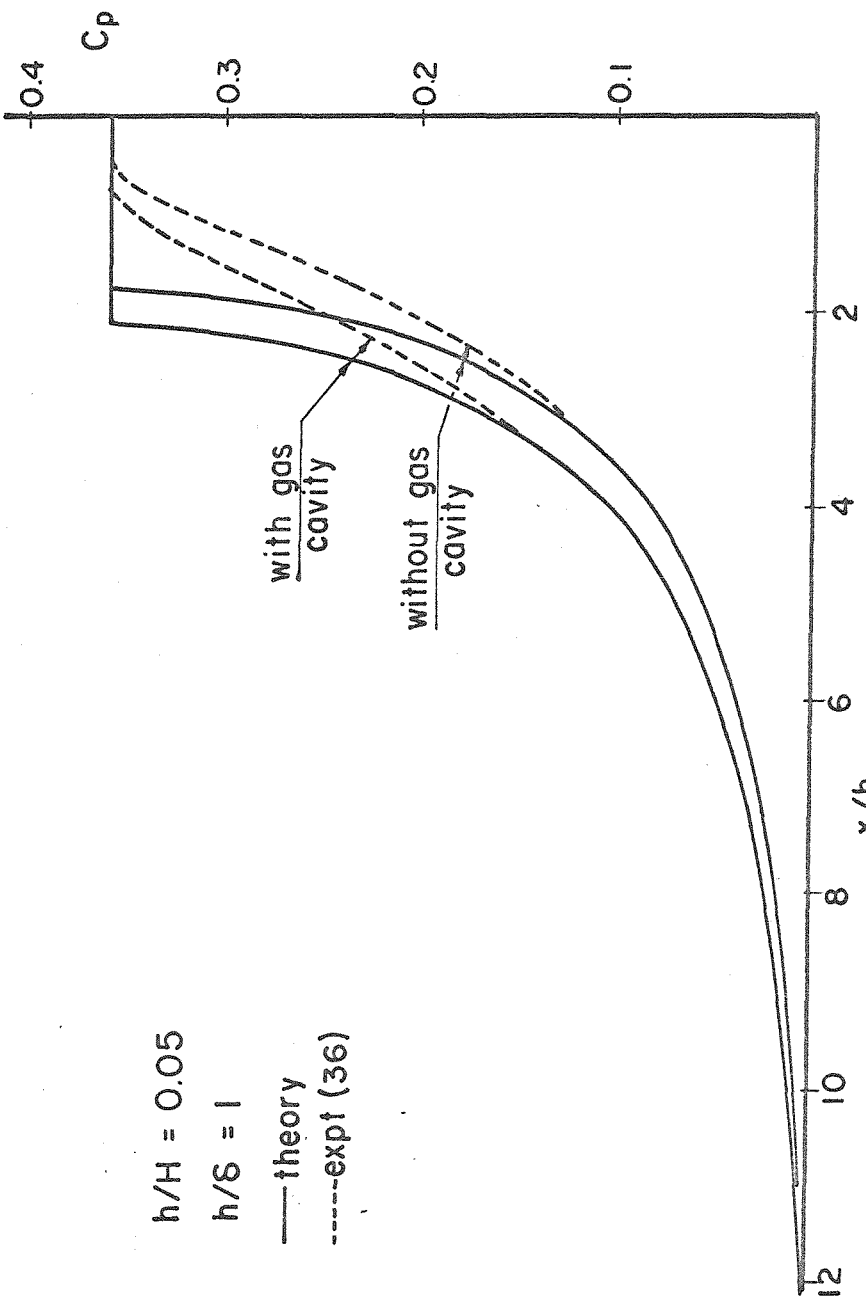

FIG. II-7 UPSTREAM PRESSURE DISTRIBUTION - EFFECT OF DOWNSTREAM FLOW FIELD

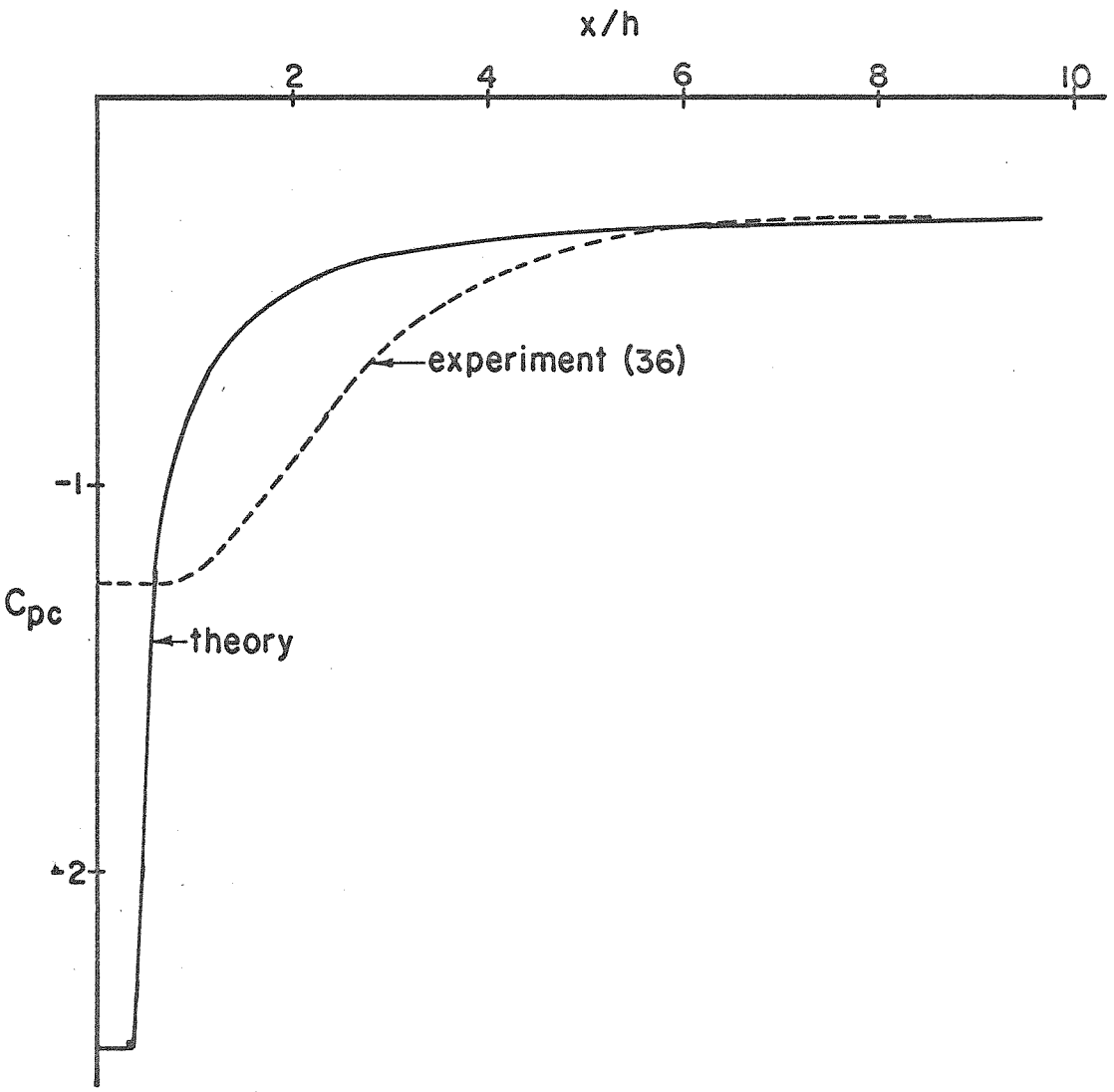

FIG. II-8 DOWNSTREAM PRESSURE DISTRIBUTION

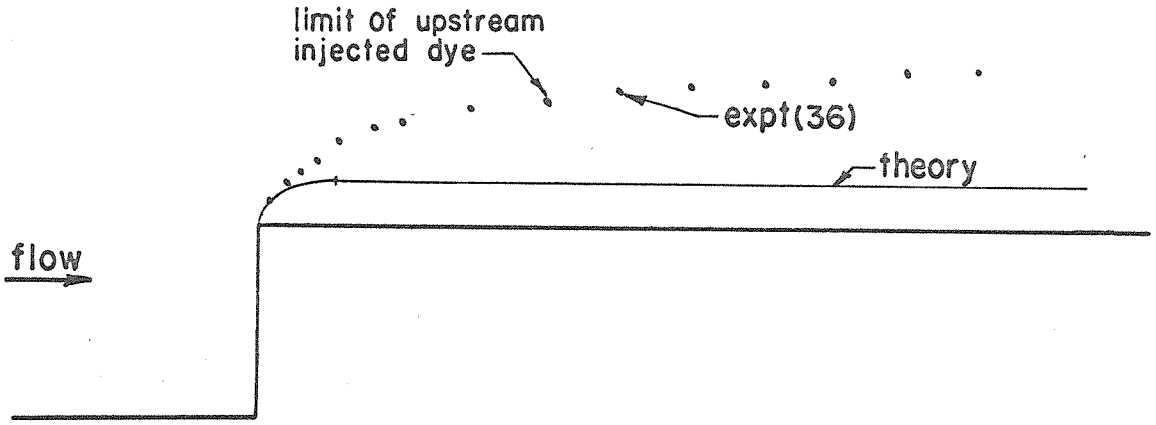

(a) Attached flow case h/H = 1/10

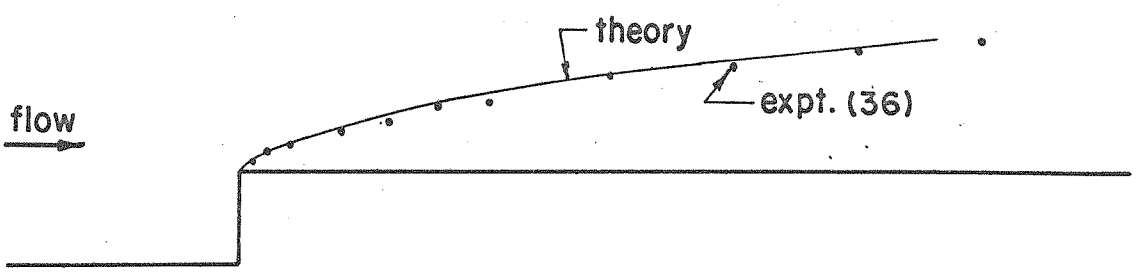

(b) Gas cavity flow case h/H = 1/20

FIG. II-9 DIVIDING STREAMLINE LOCATION DOWNSTREAM OF STEP

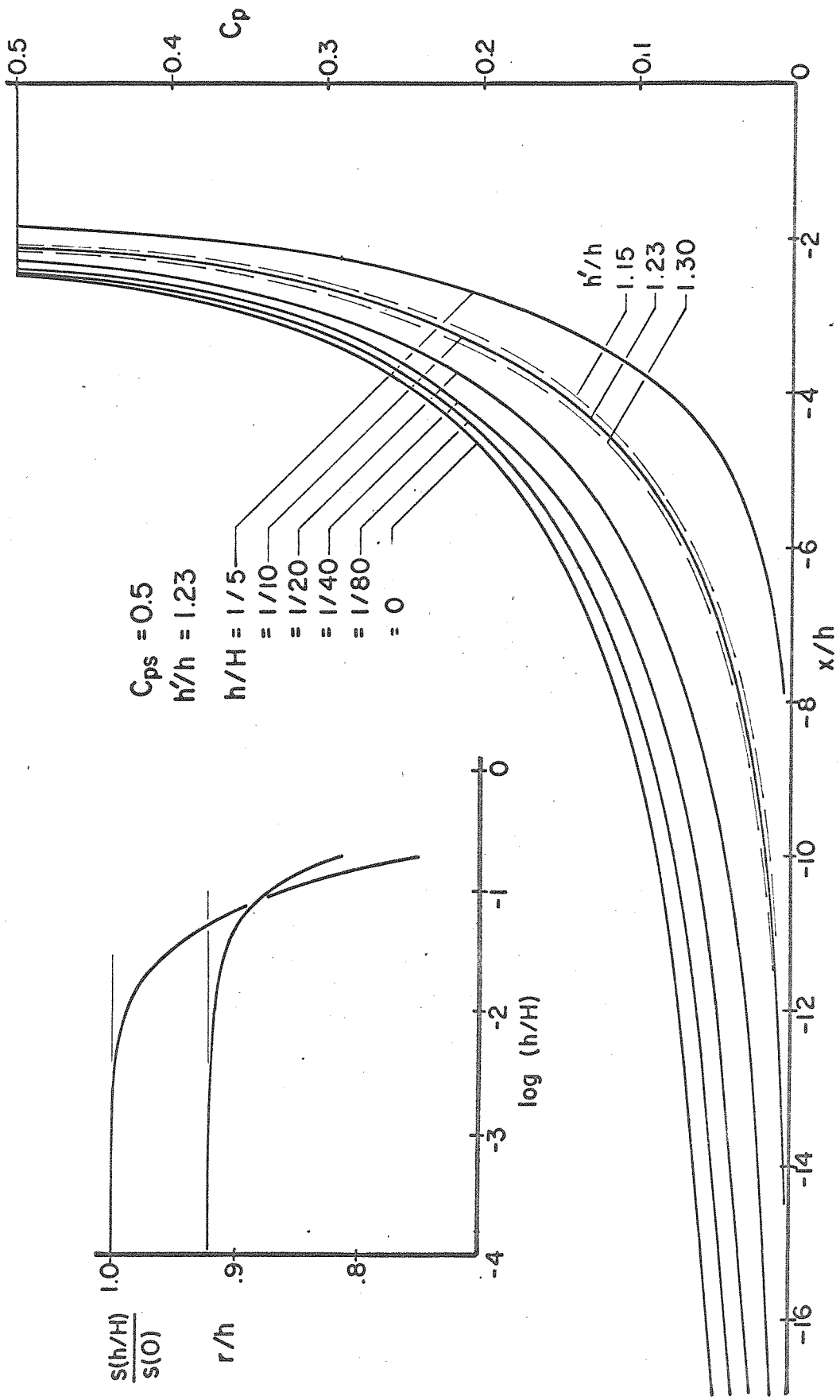

FIG. II-10 UPSTREAM PRESSURE DISTRIBUTION – EFFECT OF BLOCKAGE RATIO

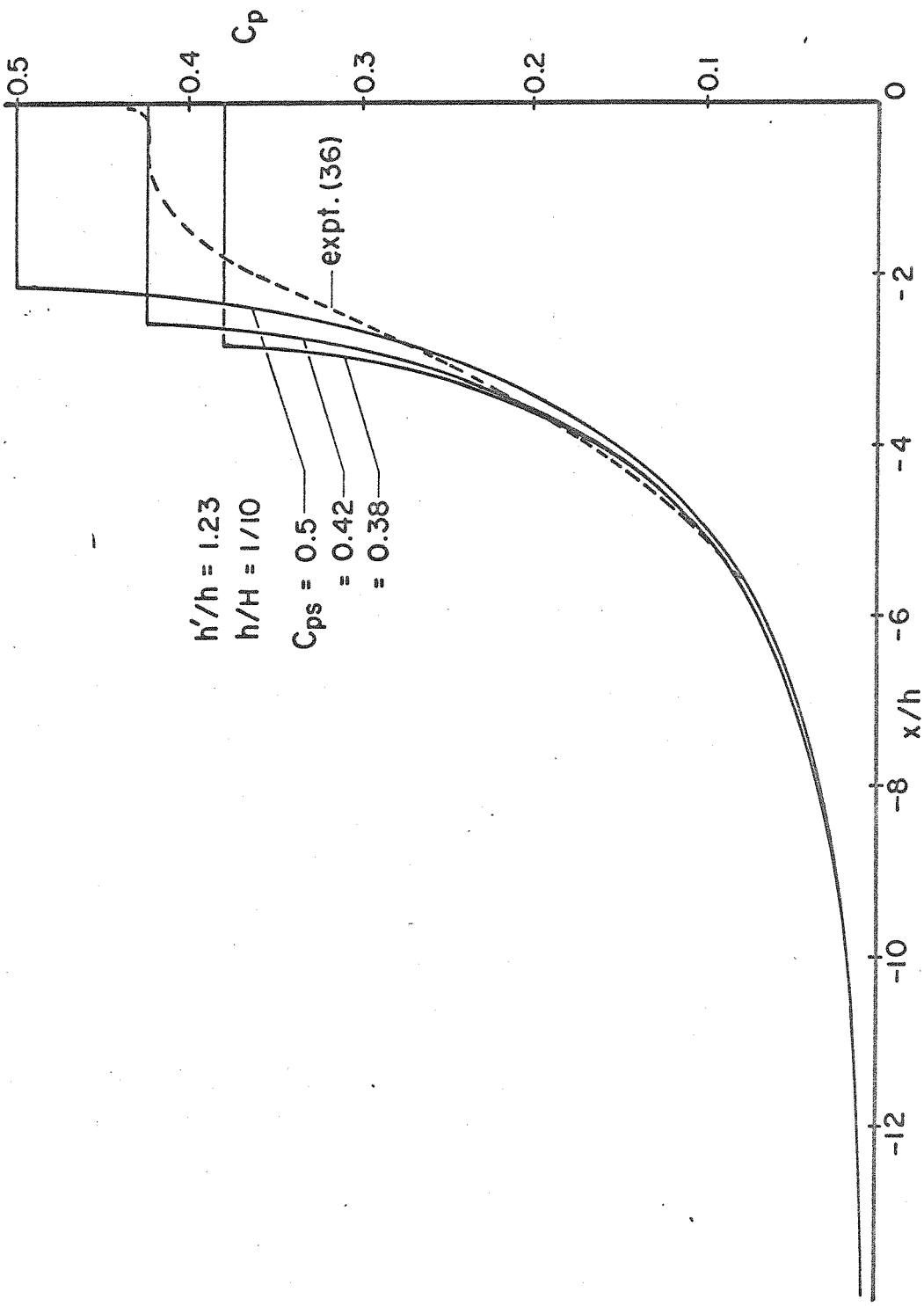

FIG. II-11 UPSTREAM PRESSURE DISTRIBUTION - EFFECT OF C_{ps}

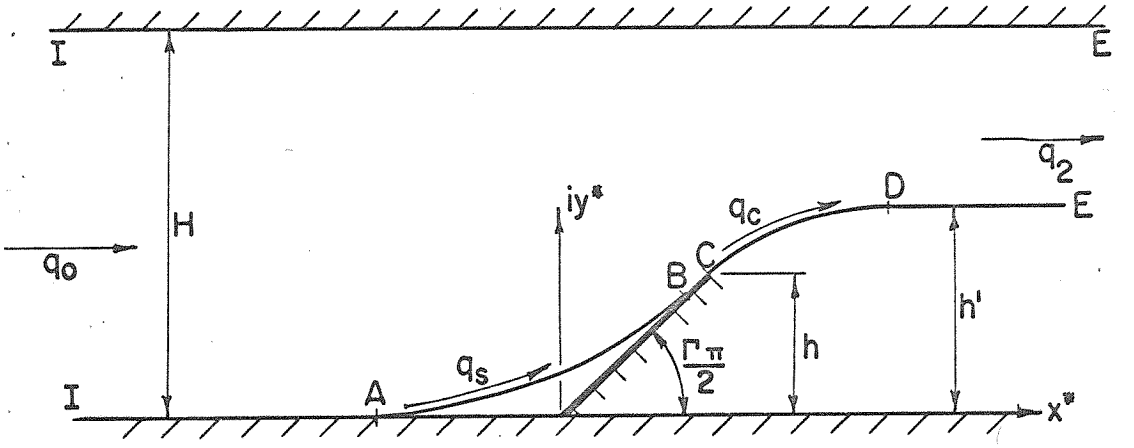

PHYSICAL PLANE $(z^* = x^* + iy^*)$

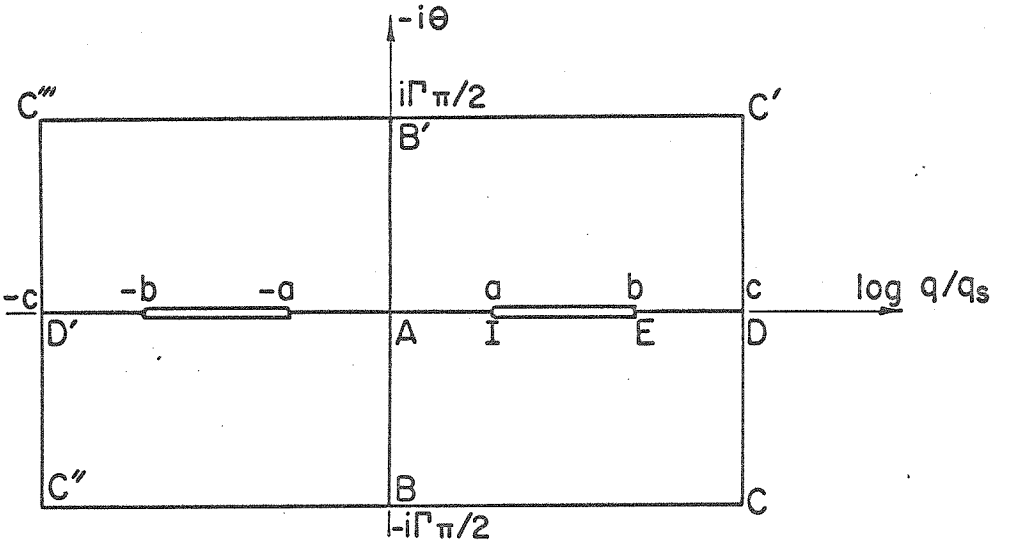

χ- PLANE

FIG. II-12 COMPLEX PLANES FOR FLOW OVER WEDGE IN CHANNEL

APPENDIX II-A

EXTENSION OF THEORY TO WEDGE SHAPED STEPS AND TYPICAL TRANSFORMATION TO THE PHYSICAL PLANE

This appendix is included to show the solution to the more general situation of flow over a wedge shaped obstacle as shown in Figure II-12. Moreover, included is an example of the mathematical manipulations necessary for the transformation to the z-plane.

For the case of flow over a wedge as depicted in Figure II-12 let the wedge angle be given by $\frac{\Gamma\pi}{2}$. The $\zeta \equiv \ell n(q/q_s) - i\theta$ plane is also shown in Figure II-12 and is identical to the ζ-plane shown in Figure II-4 except that the lines BC and B′C′ are at $-i\theta = -\frac{i\Gamma\pi}{2}$ and $\frac{i\Gamma\pi}{2}$ respectively. The derivation of the complex potential $f(\zeta;a, b, c) \equiv \varphi + i\psi$ is the same as given in Section II. 3 with the exception that the parameter q in the Theta Function argument is defined as

$$q \equiv \exp\left(-\frac{\pi^2\Gamma}{2c}\right) \qquad \text{(IIA. 1)}$$

Similarly, the transformation to the physical or z-plane is the same as indicated in equations II-14, II-15, and II-16 with the exception that the lower limit of integration is replaced by $c - \frac{i\Gamma\pi}{2}$. These equations will be shown here written in a notation necessary for this more general case being considered.

$$\frac{z^*(\zeta)-z_c^*}{j} = Z(\zeta;a)+Z(\zeta;-a)-Z(\zeta;b)-Z(\zeta;-b) \qquad \text{(IIA. 2)}$$

where

$$Z(\zeta;\alpha) \equiv \frac{1}{2c}\int_{c-\frac{i\Gamma\pi}{2}}^{\zeta} e^{-\tilde{\zeta}}\,\frac{\vartheta_1'\left[\frac{\pi}{2c}(\tilde{\zeta}-\alpha),\, q\right]}{\vartheta_1\left[\frac{\pi}{2c}(\tilde{\zeta}-\alpha),\, q\right]}\,d\tilde{\zeta} \quad , \qquad \text{(IIA. 3)}$$

$$z_c^* = \lambda\left[\operatorname{Cot}\frac{\pi\Gamma}{2} + i\right] \quad ,$$

$$\frac{\vartheta_1'(\zeta, q)}{\vartheta_1(\zeta, q)} = \operatorname{Cot}\zeta + 4\sum_{n=1}^{\infty}\frac{q^{2n}}{1-q^{2n}}\operatorname{Sin}2n\zeta \quad , \quad \text{and} \qquad \text{(II. A4)}$$

$$q \equiv \exp\left(-\frac{\pi^2\Gamma}{2c}\right)$$

As a typical example of the evaluation of the terms $Z(\zeta, \alpha)$ shown in equation IIA. 3, consider the integration along the path from C to D or $\zeta = C + i(\theta - \frac{\Gamma\pi}{2})$ for $0 \le \theta \le \frac{\Gamma\pi}{2}$.

The first problem encountered in simply evaluating equation IIA. 3 by means of equation IIA. 4 is that the series shown is only convergent in the interval $\theta < \frac{\pi^2\Gamma}{2c}$. The path of integration chosen is for $0 \le \theta \le \frac{\Gamma\pi}{2}$ which with the above requires $c < \pi$. This is rather restrictive since we will want to determine c from inverting the relation $\frac{h}{H} = \text{fcn}(a, b, c)$ as indicated in the text. Moreover, for numerical evaluation, many terms of the series might be required to assure accurate convergence. Thus, it is advantageous to transform the expression for $\vartheta_1'(\zeta;q)/\vartheta_1(\zeta;q)$ using the relations given in reference 49. After some algebra, it can be shown that

$$\frac{\vartheta_1'[\frac{\pi}{2c}(\zeta-\alpha)/q]}{\vartheta_1[\frac{\pi}{2c}(\zeta-\alpha)/q]} = \frac{1}{i}\left\{-1+\frac{2}{\pi}\frac{\theta+i\alpha}{\Gamma} + \frac{2c}{\Gamma\pi}\frac{\vartheta_3'[\frac{\theta+i\alpha}{\Gamma}/q']}{\vartheta_3[\frac{\theta+i\alpha}{\Gamma}/q']}\right\} \qquad \text{(IIA. 5)}$$

where $q' = e^{-\frac{2c}{\Gamma}} = 1/k^{2/\Gamma}$, and

$$\frac{\vartheta_3'(\zeta;q)}{\vartheta_3(\zeta;q)} = 4\sum_{n=1}^{\infty}\frac{(-1)^n q^n}{1-q^{2n}}\operatorname{Sin}2n\zeta \quad . \qquad \text{(IIA. 6)}$$

The infinite series shown in equation IIA. 6 is convergent for $|\text{IM}\,\zeta| < \ell n q^{-\frac{1}{2}}$ which, using the above definitions, is tantamount to $a, b < \Gamma c$. This is more in line with the flow model definitions. Thus,

substituting equations IIA. 6 and IIA. 5 into equation IIA. 3 gives;

$$Z(\theta;\alpha) + Z(\theta;-\alpha) = F(\theta) + \frac{8e^{\frac{i\Gamma\pi}{2}}}{\pi k} \sum_{n=1}^{\infty} \frac{(-1)^n k^{2n/\Gamma}}{k^{4n/\Gamma}-1} \cosh \frac{2n\alpha}{\Gamma} \times$$

$$\times \left[\frac{2n}{\Gamma} - e^{-i\theta}\left\{i \sin \frac{2n\theta}{\Gamma} + \frac{2n}{\Gamma} \cos \frac{2n\theta}{\Gamma}\right\}\right] \Big/ \left(\frac{4n^2}{\Gamma^2} - 1\right) \quad . \qquad \text{(IIA. 7)}$$

As was done in the text, define

$$g_n(k) \equiv \frac{k^{2n/\Gamma}}{k^{4n/\Gamma}-1} \quad , \qquad \text{and}$$

$$S_n(j, \ell) = \frac{2n/\Gamma}{4n^2/\Gamma^2 - 1} \ell^{2n/\Gamma} \left[1 - \left(\frac{j}{\ell}\right)^{\frac{2n}{\Gamma}}\right]\left[1 - \left(\frac{1}{\ell j}\right)^{\frac{2n}{\Gamma}}\right]. \qquad \text{(IIA. 8)}$$

Utilizing these relations along with equation IIA. 7 in equation IIA. 2 gives finally;

$$\frac{z-z_c}{j} = \frac{8e^{i\Gamma\pi/2}}{\pi k} \sum_{n=1}^{\infty} g_n(k) S_n(j, \ell)\left[1 - e^{-i\theta}\left\{\frac{i\Gamma}{2n} \sin \frac{2n\theta}{\Gamma} + \cos \frac{2n\theta}{\Gamma}\right\}\right] \times$$

$$\times \left(\cosh \frac{2na}{\Gamma} - \cosh \frac{2nb}{\Gamma}\right) \qquad \text{(IIA. 9)}$$

Evaluating this for $\theta = \frac{\Gamma\pi}{2}$ (i. e. point "D") gives;

$$\lambda \equiv \frac{h}{H} = 1 - \frac{j}{\ell} + \frac{4j}{\pi k} \sin \frac{\pi\Gamma}{2} \sum_{n=1}^{\infty} (-1)^n g_n(k) S_n(j, \ell)$$

$$\frac{x_D}{h} = \cot \frac{\pi\Gamma}{2} + \frac{4j}{\pi \lambda k} \sum_{n=1}^{\infty} g_n(k) S_n(j, \ell)\left[1 - (-1)^n \cos \frac{\pi\Gamma}{2}\right] \qquad \text{(IIA. 10)}$$

These formulae give, upon setting Γ=1 for a normal step, the same equations as derived in the text. Again, the proper value of k can be determined for the given input parameters, h/H, C_{ps}, C_{p2} (or equivalently, λ, a, c) as was discussed in the text.

Integrating along the other paths in the ζ-plane as was done in the text gives the following results;

1. step face reattachment point location

$$\frac{x_B}{h} = \text{Ctn}\,\frac{\pi\Gamma}{2} - \frac{8j}{\lambda ck}\,\text{Cos}\,\frac{\pi\Gamma}{2}\sum_{n=1}^{\infty} T_n\left[k-(-1)^n\right]$$

$$\frac{y_B}{h} = 1 - \frac{8j}{\lambda ck}\,\text{Sin}\,\frac{\Gamma\pi}{2}\sum_{n=1}^{\infty} T_n\left[k-(-1)^n\right] \qquad \text{(IIA. 11)}$$

where

$$T_n \equiv \frac{q^n}{1-q^{2n}}\,\frac{\left(\frac{n\pi}{c}\right)}{\left(\frac{n\pi}{c}\right)^2+1}\,\text{Sin}\,\frac{n\pi}{2c}(a+b)\,\text{Sin}\,\frac{n\pi}{2c}(b-a) \quad ;$$

2. separation streamline

$$z(\theta)-z_B = \frac{2j}{\lambda\pi}\,e^{\frac{i\Gamma\pi}{2}}\left\{f_2(\theta;b)-f_2(\theta;a) + i\left[f_1(\theta;a) - f_1(\theta;b)\right]\right.$$
$$\left. -2\sum_{n=1}^{\infty}\frac{(-1)^n}{k^{2n/\Gamma}}\,g_n(k)S_n(j,k)\left[1-e^{-i\theta}\left[\frac{i\Gamma}{2n}\,\text{Sin}\,\frac{2n}{\Gamma}\theta+\text{Cos}\,\frac{2n}{\Gamma}\theta\right]\right]\right\}$$

$$0 \le \theta \le \frac{\pi\Gamma}{2} \qquad \text{(IIA. 12)}$$

where; $f_1(\theta;\alpha) = \text{Sin}\theta + \frac{1}{2}\,\text{Cosh}\,\alpha\,\log\left\{\frac{\text{Cosh}\,\alpha+\text{Sin}\theta}{\text{Cosh}\,\alpha-\text{Sin}\theta}\right\}$

$$f_2(\theta;\alpha) = 1-\text{Cos}\,\theta - \text{Sinh}\,\alpha\,\tan^{-1}\left\{\text{Sinh}\,\alpha\,\frac{1-\text{Cos}\theta}{\text{Sinh}^2\alpha+\text{Cos}\theta}\right\} \quad ,$$

Setting $\theta = \frac{\pi\Gamma}{2}$ in the above gives the separation point $z_A = x_A + io$;

3. wall pressure distribution upstream of separation and pressure recovery in wake.

These are identical to the formula given in the text (equations II-30 through II-33, inclusive) except for using the new definition of the parameter q as given in equation IIA. 1.

The limiting forms given in Section II. 4. 5 for the extension to other flow models are also valid for the equations derived here.

REFERENCES

1. Chapman, D. R., Kuehn, D. M., and Larson, H. K., "Investigation of Separated Flows in Supersonic and Subsonic Streams with Emphasis on the Effect of Transition," NACA TN 3869 (1957).

2. Sigal, A., Calif. Inst. of Tech., Private Communication.

3. Bogdonoff, S. M. and Kepler, C. E., "Separation of a Supersonic Turbulent Boundary Layer," Journal of the Aeronautical Sciences, Vol. 22, Page 414, 1955.

4. Bogdonoff, S. M., "Some Experimental Studies of the Separation of Supersonic Turbulent Boundary Layers," Princeton Univ. Rept. 336 (June 1955).

5. Vas, I. E. and Bogdonoff, S. M., "Interaction of a Turbulent Boundary Layer with a Step at M = 3.85," Princeton Univ. Rept. 295 (April 1955).

6. Fernandez, F. L. and Zukoski, E. E., "Experiments in Supersonic Turbulent Flow with Large Distributed Surface Injection," AIAA 6th Aerospace Sciences Meeting, 1968, Preprint No. AIAA 68-129.

7. Fernandez, F. L., "Two-dimensional Viscous Flows with Large Distributed Surface Injection," Ph.D. Thesis, Calif. Inst. of Tech., 1969.

8. Demetriades, A., "Turbulence Measurements in an Axisymmetric Compressible Wake," Philco-Ford Corp. Publication UG-4118, 1967.

9. Kovásznay, L. S. G., "Turbulence in Supersonic Flow," Journal of the Aeronautical Sciences, Vol. 20, No. 10, Oct. 1953.

10. Morkovin, M. V., "Fluctuations and Hot Wire Anemometry in Compressible Flows, AGARD-ograph 24, November 1956.

11. Behrens, W., "Flow Field and Stability of the Far Wake Behind Cylinders at Hypersonic Speeds," Ph. D. Thesis, Calif. Inst. of Tech., 1966.

12. Behrens, W., Calif. Inst. of Tech., unpublished report.

13. Kistler, A. L., "Fluctuating Wall Pressure Under a Separated Supersonic Flow," Journal of the Acoustical Society of America, Vol. 36, No. 3, 543-550, March 1964.

14. Coe, C. F., Ames Research Center, unpublished data.

15. Speaker, W. V. and Ailman, C. M., "Static and Fluctuating Pressures in Regions of Separated Flow," AIAA Paper 66-456, 4th Aerospace Sciences Meeting, June 1966.

16. Zukoski, E. E., "Turbulent Boundary Layer Separation in Front of a Forward Facing Step," AIAA Journal, Vol. 5, No. 10, Oct. 1967.

17. Hahn, J. S., "Experimental Investigation of Turbulent Step-induced Boundary Layer Separation at Mach Numbers 2.5, 3, and 4," AEDC-TR-69-1, Nov. 1968.

18. Czarnecki, Langley Research Center, personal communication.

19. Krishnamurty, K., "Acoustic Radiation from Two-dimensional Rectangular Cut-outs in Aerodynamic Surfaces," NACA TN 3487 (1955).

20. Thomke, G. J. and Roshko, A., "Incipient Separation of a Turbulent Boundary Layer at High Reynolds Number in Two-dimensional Supersonic Flow over a Compression Corner," McDonnell Douglas Astronautics Co., Santa Monica, Calif., Report DAC 59819, Jan. 31, 1969.

21. Paynter, G. C., "On the Prediction of Separation and Reattachment Flow Characteristics for Two-dimensional Supersonic Turbulent Boundary Layers," Ph. D. Thesis, University of Washington, 1965.

22. Lees, L., Calif. Inst. of Tech., unpublished report.

23. Todisco, A. and Reeves, B. L., "Turbulent Boundary Layer Separation and Reattachment at Supersonic and Hypersonic Speeds," AVCO Systems Div., July 1969.

24. Korst, H. H. and Chow, W. L., "Compressible Non-isoenergetic Two-dimensional Turbulent ($P_{R_T} = 1$) Jet Mixing at Constant Pressure," University of Illinois, Engineering Experimental Station, M. E. Technical Note 392-4, Jan. 1959.

25. Kistler, A. L., "Fluctuation Measurements in a Supersonic Turbulent Boundary Layer," Physics of Fluids, Vol. 2, No. 3, May-June, 1959.

26. Igawa, H., Calif. Inst. of Tech., private communication.

27. Ames Res. Center, "Equations, Charts, and Tables for Compressible Flow," NACA Rept. 1135.

28. Kovásznay, L. S. G., "Physical Measurements in Gas Dynamics and Combustion," High Speed Aerodynamics and Jet Propulsion, Vol. IX, Princeton University Press, 1954.

29. Laufer, J. and McClellan, R., "Measurements of Heat Transfer from Fine Wires in Supersonic Flows," Journal of Fluid Mechanics, Vol. 1, p. 256 (1956).

30. Laufer, J. and Vrebalovich, T., "Stability and Transition of a Supersonic Laminar Boundary Layer in an Insulated Flat Plate," Journal of Fluid Mechanics, Vol. 9, p. 257, (1961).

31. Bull, M. K., "Wall Pressure Fluctuations Associated with Subsonic Turbulent Boundary Layer Flow," Journal of Fluid Mechanics, Vol. 28, part 4, pp. 719-754, 1967.

32. Graham, E. W. and Graham, B. B., "The Effect of a Shear Layer on Plane Waves of Sound in a Fluid," Boeing Scientific Research Laboratories Document D1-82-0823, Nov. 1968.

33. Mellor, G. L. and Gibson, D. M., "Equilibrium Turbulent Boundary Layers," Vol. 24, part 2, p. 225 (1966).

34. Trilling, L., "Oscillating Shock Boundary-Layer Interaction," Journal of the Aeronautical Sciences, May 1958.

35. Clayton, F. I. and Wuerer, J. E., "Flow Separation in High-Speed Flight - A Report Bibliography," Douglas Missile and Space Systems Div. Report DAC 59101, Sept. 1966.

36. Stevenson, R. G., "Experimental Study of the Flow of a Subsonic and Turbulent Boundary Layer Over a Forward-Facing Step," Engineer's Thesis, Calif. Inst. of Tech., 1969.

37. Stratford, B. S., "The Prediction of Separation of the Turbulent Boundary Layer," Journal of Fluid Mech., Vol. 5, pp. 1-16, 1959.

38. Townsend, A. A., "The Behavior of a Turbulent Boundary Layer Near Separation," J. Fluid Mech., Vol. 12, pp. 536-554, 1962.

39. Lighthill, M. J., "On Boundary Layers on Upstream Influence. I. A Comparison Between Subsonic and Supersonic Flows," Proc. Roy. Soc. A, Vol. 217, pp. 344-357, 1953.

40. Barrows, J. F., "Upstream Separation Point for an Internal Corner in a Two-dimensional Channel Flow," J. of Appl. Mech., Vol. 30, No. 4, p. 505, 1963.

41. Taulbee, D. B., "Separation of a Turbulent Shear Flow Ahead of a Normal Step," Ph.D. Thesis, Univ. of Ill., 1964.

42. Good, M. C. and Joubert, P. N., "The Form Drag of Two-dimensional Bluff Plates Immersed in Turbulent Boundary Layers," J. Fluid Mech., Vol. 31, part 3, pp. 547-582, 1968.

43. Bradshaw, P. and Galea, P. V., "Step-induced Separation of a Turbulent Boundary Layer in Incompressible Flow," J. Fluid Mech. (1967), Vol. 27, part 1, pp. 111-130.

44. Roshko, A., "A Review of Concepts in Separated Flow," Canadian Congress of Appl. Mech. (1967), Proceedings - Vol. 3.

45. Roshko, A. "A New Hodograph for Free Streamline Theory," NACA TN 3168, July 1954.

46. Wu, T. Y., "A Free Streamline Theory for Two-dimensional Fully Cavitating Hydrofoils," Hydrodynamics Lab., Calif. Inst. of Tech., Report 21-17, July 1955.

47. Wu, T. Y., Whitney, A. K. and Lin, J. D., "Wall Effects in Cavity Flows," Div. of Engr. and Appl. Science, Calif. Inst. of Tech., Rept. E-111A.5, August 1969.

48. Roshko, A. and Lau, J. C., "Some Observations on Transition and Reattachment of a Free Shear Layer in Incompressible Flow," Proceedings of the 1965 Heat Transfer and Fluid Mech. Inst., Stanford Univ. Press, 1965.

49. Whittaker, E. T. and Watson, G. N., "A Course in Modern Analysis," 4th Ed. Cambridge Univ. Press, 1965.